CUKUROVA UNIVERSITY
INSTITUTE OF NATURAL AND APPLIED SCIENCES

MSc THESIS

Alper KUNİ

THE DESIGN OF HIGH PRESSURE WATER-JET CUTTING MACHINE, INTENSIFIER UNIT

DEPARTMENT OF MECHANICAL ENGINEERING

ADANA, 2008

INSTITUTE OF NATURAL AND APPLIED SCIENCES

UNIVERSITY OF CUKUROVA

THE DESIGN OF HIGH PRESSURE WATER-JET CUTTING MACHINE, INTENSIFIER UNIT

By Alper KUNİ

A MASTER OF SCIENCE THESIS

DEPARTMENT OF MECHANICAL ENGINEERING

We certify that the thesis titled above was reviewed and approved for the award of degree of the Master of Science by the board of jury on 15/02/2008.

Signature: ……..	Signature:……	Signature:……..
Prof. Dr. Necdet GEREN	Prof. Dr. Melih BAYRAMOĞLU	Assist. Prof. Dr Ali KOKANGÜL
Supervisor	Member	Member

This MSc Thesis is performed in Department of Mechanical Engineering of Institute of Natural and Applied Sciences of Cukurova University.
Registration Number:

Prof. Dr. Aziz ERTUNÇ
Director
Institute of Natural and Applied Sciences

ÖZ

YÜKSEK LİSANS TEZİ

SU JETİ İLE KESME MAKİNESİNİN YOĞUNLAŞTIRICI TASARIMI

Alper KUNİ

ÇUKUROVA UNİVERSİTESİ
FEN BİLİMLERİ ENSTİTÜSÜ
MAKİNA MÜHENDİSLİĞİ ANABİLİM DALI

Danışman : Prof. Dr. Necdet GEREN
Yıl : 2008, Sayfa: 107
Jüri : Prof. Dr. Necdet GEREN
Prof. Dr. Melih BAYRAMOĞLU
Yrd. Doç. Dr. Ali KOKANGÜL

Su jeti sistemlerinin, özellikle endüstriyel alanda sağladıkları avantajlardan bazıları söyle sıralanabilir: kesim yelpazesinin çok geniş olması, istenen şeklin kolayca oluşturulabilmesi, takım aşınması probleminin olmaması, ısıl gerilmelere sebebiyet vermemesi. Bu avantajlardan dolayı, su jeti kesme sistemleri endüstriyel alanda giderek yaygınlaşmakta. Su jeti ile kesme işlemi için su basıncının yükseltilmesinde kullanılan araç yoğunlaştırıcıdır. Yoğunlaştırıcılar tek katlı olabildiği gibi çok katlı da olabilir. Tek katlı yoğunlaştırıcılarda malzeme sınırları dolayısıyla ekonomik bir şekilde 180 MPa basıncın üzerine çıkılamazken, çok katlılarda iç ve dış bölgelerde farklı nitelikteki malzemeleri kullanarak ultra-yüksek basınçlara çıkılabilmektedir. Çukurova Üniversitesi Makine Mühendisliği Bölümü laboratuarında öncelikle tek katlı ve 180 MPa çalışma basıncına sahip bir ilk örnek üretilmiştir. Ardından iki katlı bir ilk örnek üretilerek çalışma basıncın 300 MPa değerine çekilmek istenmiştir. Bu çalışmada bu son tasarlanan iki katlı yoğunlaştırıcının kontrollü şekilde seçilmiş malzeme cinslerine göre tasarın sınırları Mathematica® gibi matematiksel araçlar kullanılarak incelenmiş, cidar kalınlığı boyunca gerilmelerin dağılımı grafiklerle açıklanmış, temel kontrol parametrelerinin diğer parametrelerle ilişkileri incelenmiş, ve cidar kalınlıkları minimum malzeme kullanımı temel alınarak optimize edilmiş ve bu optimizasyon yöntemi de açıklanmıştır.

Anahtar Kelimeler: Basınç Yükselticisi, Yoğunlaştırıcı, Tasarım, Sıkı Geçme.

ABSTRACT

MSc THESIS

THE DESIGN OF THE WATER JET CUTTING MACHINE, INTENSIFIER UNIT

Alper KUNİ

ÇUKUROVA UNIVERSİTY
INSTITUTE OF THE NATURAL AND APPLIED SCIENCES
DEPARTMENT OF MECHANICAL ENGINEERING

Supervisor : Prof. Dr. Necdet GEREN

Year : 2008, Pages: 107

Jury : Prof. Dr. Necdet GEREN

Prof. Dr. Melih BAYRAMOĞLU

Assist. Prof. Dr. Ali KOKANGÜL

Some of the advantages that the water-jet cutting systems provide in industrial area are: wide scale of cutting materials, any form can be cut easily, no tool change or wear, no thermal distortion. For these advantages water-jet cutting technology is getting spread in the industrial usage. The main part to intensify the water to the high pressures is the intensifier unit. Intensifier can be single layered as they can be double- layered or multi-layered. As 180 MPa is the upper pressure limit for the single layer intensifier due to the material properties based on material strength, the multi-layered intensifiers can withstand ultra high pressures. A single-layer prototype was produced in Mechanical Engineering Department Laboratory in The University of Çukurova which has the operating pressure of 180 MPa. Later a double-layer intensifier was produced to increase the operating pressure up to the 300 MPa. In this study, the design limits of the last prototype of intensifier was investigated according to the material, and optimum design criteria was found. Optimum design parameters and stress distributions along the radial axis were shown in graphs by using mathematical tools like Mathematica®. And the optimization method was explained briefly.

Keywords: Intensifier, Design, Shrink fit.

ACKNOWLEDGEMENTS

I am very grateful to my supervisor Prof. Dr. Necdet GEREN for his guidance and supports from beginning to the end of this study.

CONTENT PAGE

LIST OF FIGURES PAGE

LIST OF TABLES PAGE

NOMENCLATURE

$P_{h\max}$: The Maximum Hydraulic Pressure.

S_1 : Piston Area of the Hydraulic Cylinder.

S_2 : Plunger Area.

rat : Intensification Ratio.

x : Displacement of the Piston.

$comp$: Compressibility of the Liquid.

M_{pis} : Mass of the Piston.

M_{pl} : Mass of the Plunger.

ρ_{oil} : Density of the Oil.

L : Length of the Cylinder

H : Width of the Piston

p_i : Inlet Pressure

σ : Stress

σ_r : Radial Stress

σ_t : Tangential Stress

σ_l : Longitudinal Stress

ε : Strain

$\sigma_{\min}$: Minimum Stress

$\sigma_{1\min}$: Minimum Stress Acting on Inner Cylinder

$\sigma_{2\min}$: Minimum Stress Acting on Outer Cylinder

$\sigma_{\max}$: Maximum Stress

$\sigma_{1\max}$: Maximum Stress Acting on Inner Cylinder

$\sigma_{2\max}$: Maximum Stress Acting on Outer Cylinder

σ_{mean} : Mean Stress

σ_{ampl} : Amplitude Stress

σ' : Von Mises Stress

ΔT : Temperature difference between inner and outer cylinders

a : Inner Radius of the Inner Cylinder before Shrink Fit

b : Outer Radius of the Inner Cylinder before Shrink Fit

c : Inner Radius of the Outer Cylinder before Shrink Fit

d : Outer Radius of the Outer Cylinder before Shrink Fit

t_1 : Inner Cylinder Wall Thickness before Shrink Fit

t_2 : Outer Cylinder Wall Thickness before Shrink Fit

p_i : Internal Pressure (Operating pressure)

p_o : Outer Pressure (Relative Ambient Pressure)

p : Interface Pressure

S_Y : Yield Strength

S_{Y1} : Yield Strength of the Inner Cylinder

S_{Y2} : Yield Strength of the Outer Cylinder

S_{ut} : Ultimate Tensile Strength

S_{ut1} : Ultimate Tensile Strength of the Inner Cylinder

S_{ut2} : Ultimate Tensile Strength of the Outer Cylinder

S_{uc} : Ultimate Compressive Strength

S_{uc1} : Ultimate Compressive Strength of the Inner Cylinder

S_{uc2} : Ultimate Compressive Strength of the Outer Cylinder

S_{ep} : Endurance Limit of the Test Specimen

S_{ep1} : Endurance Limit of the Test Specimen made by the same material with inner cylinder

S_{ep2} : Endurance Limit of the Test Specimen Made by the same material with inner cylinder

S_e : Endurance Limit

S_{e1} : Endurance Limit of the Inner cylinder

S_{e2} : Endurance Limit of the Inner cylinder

E : Modulus of Elasticity

E_1 : Modulus of Elasticity of inner cylinder

E_2 : Modulus of Elasticity of outer cylinder

μ : Poisson's Ratio

μ_1 : Poisson's Ratio of the Inner Cylinder

μ_2 : Poisson's Ratio of the Outer Cylinder

R : Inner radius of the Inner cylinder After Shrink Fit

G : Interface Radius

M : Outer radius of the Outer Cylinder After Shrink Fit

δ : Radial Displacement

δ_1 : Radial Displacement at the Inner Surface of the Inner Cylinder

δ_2 : Radial Displacement at the Outer Surface of the Inner Cylinder

δ_3 : Radial Displacement at the Inner Surface of the Outer Cylinder

δ_4 : Radial Displacement at the Outer Surface of the Outer Cylinder

δ_T : Total Interface Displacement

C_1, C_2 : Stress Constants of the Inner Cylinder for Pre-Shrink Fit

C_3, C_4 : Stress Constants of the Outer Cylinder for Pre-Shrink Fit

C_{1s}, C_{2s} : Stress Constants of the Inner Cylinder under Interface Pressure

C_{3s}, C_{4s} : Stress Constants of the Outer Cylinder under Interface Pressure

C_{1ss}, C_{2ss} : Stress Constants of the Inner Cylinder under Operating Pressure

C_{3ss}, C_{4ss} : Stress Constants of the Outer Cylinder under Operating Pressure

α : Thermal Expansion Coefficient

$\sigma_{r11}, \sigma_{t11}$: Radial and Tangential Stresses for the Inner Cylinder under Interface Pressure

$\sigma_{r11}, \sigma_{t11}$: Radial and Tangential Stresses for the Inner Cylinder under Interface Pressure

$\sigma_{r21}, \sigma_{t21}$: Radial and Tangential Stresses for the Outer Cylinder under Interface Pressure

$\sigma_{r12}, \sigma_{t12}$: Radial and Tangential Stresses for the Inner Cylinder under Operating Pressure

$\sigma_{r22}, \sigma_{t22}$: Radial and Tangential Stresses for the Outer Cylinder under Operating Pressure

σ_{l1}, σ_{l2} : Longitudinal Stresses for the Inner and Outer Cylinders

SF : Factor of Safety

$SF1$: Factor of Safety for Inner Cylinder

$SF2$: Factor of Safety for Outer Cylinder

k_a : Surface Factor

k_b : Size Factor

k_c : Reliability Factor

k_d : Temperature Factor

k_e : Stress Concentration Factor

k_f : Miscellaneous Factor

1. INTRODUCTION

Plasma, laser and (abrasive)-water-jet cutting are some of the most important techniques that are used in modern industrial cutting processes. Water-jet cutting (WJC) is a unique, 'cold' cutting process. The process uses a fine-bore jewel nozzle to form a coherent, high velocity water jet which has a pressure up to 400MPa at rest and a velocity of up to 1000 ms^{-1} after leaving nozzle (See Figure 1.1.). Abrasive water-jet cutting is the modified method of WJC by adding some erosive materials to the streaming jet.

1.1. Water-Jet Cutting (WJC)

Water-jet cutting, also referred to as hydrodynamic machining, is an advanced technology cutting tool that uses stream of ultra-high pressure (UHP) water forced through a jewel nozzle. The water-jet removes work piece material and produces a narrow kerf by the cutting action of a fine diameter (Tunç, 2000).

As a potential tool of machining, the high pressure water-jet is excellent for cutting special shapes, even in tough materials. Superior to more conventional cutting methods, water-jet cutting avoids the heat effected zones and distortion created by laser and plasma-arc systems. Because the cutting head does not contact the work piece, water-jet cutting is highly maneuverable and easy cutting in precise right angles. Since the size of the jet is small, the water-jet can cut small holes, narrow slots, etc., which minimize material use (Min Jou, 1999).

Along with all these advantages, there are some disadvantages too with water-jet cutting. From the characteristics of the water-jet, the water flow will grow naturally along the axis, which makes the cutting effect different when the work pieces touch the different parts of the jet. Furthermore, if it is used to cut several layers of composites, the consequences of cutting vary from layer to layer. Moreover, when the work piece is not cut through, the water-jet may splash, which is very dangerous. Also in some cases WJC can cause the depth of cut variation on cut edge

along the stream direction. So the traverse rate must be adjusted according to the stream radius, material thickness, stream velocity and content.

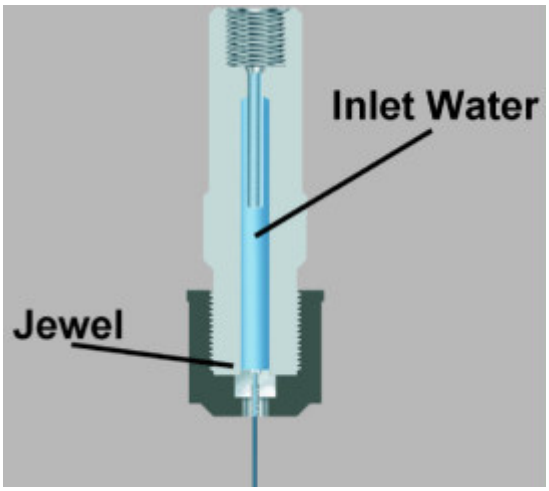

Figure 1.1.The water-jet cutting nozzle system (Courtesy of OMAX)

1.2. Abrasive Water-Jet Cutting (AWJ)

Abrasive water-jet (AWJ) is the improved process of water-jet cutting by means of adding some abrasive particles to the streaming water jet. This increases the cutting ability of the jet. On the basis of jet generation, abrasive water-jets can generally be categorized as injection jets (AIJ) or suspension jets (ASJ). For practical applications, AIJs are more commonly used. For this type of jet, the pump pressure ranges between 100 and 400 MPa. An AIJ is formed by accelerating small particles (garnet, aluminum oxide, silicon carbide, olivine, glass bead and zirconium) through contact with a high velocity plain water jet. A typical abrasive grain diameter is 400 μm. The high pressure water is converted into a high velocity water-jet as it flows through an orifice on the top of the abrasive cutting head (See Figure1.2.). The abrasives enter the cutting head through a separate inlet. The mixing between abrasives, water and air takes place in a mixing chamber. Beside this ASJ uses mixed liquid-abrasive solid suspension which is hard to pump inject at high pressures. So this is a pressure limitation for this technique. This type of system appears to be more

efficient than previously developed abrasive water-jet systems. The intended use of this system is for micro machining (see figure 1.2.).

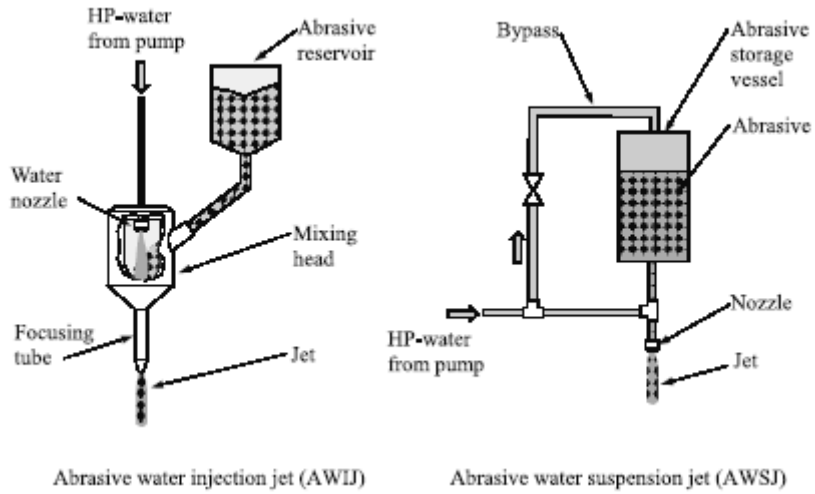

Figure 1.2. Schematic view of Abrasive water jet and abrasive water suspension jets [Cadavid and Wüstenberg, 2005]

The intensity and efficiency of the cutting process depend on several process parameters, such as pump pressure, orifice diameter, traverse rate, standoff distance. The water-jet is a stream-like tool, similar to laser and electron beams, which is characterized by an unsteady material removal process. The most pronounced characteristic of WJ-generated surfaces is the presence of striation marks which transpire below a region relatively smooth surface finish (Momber, Kovacevic, Kwak, 1995).

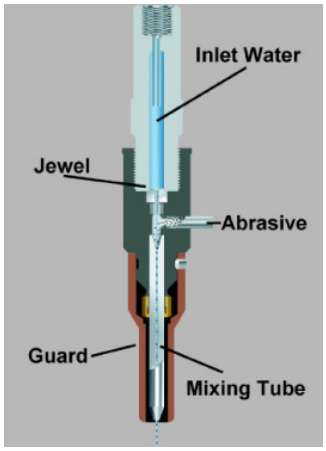

Figure 1.3. Abrasive Water-Jet (AWJ mixing chamber and nozzle. (Courtesy of OMAX)

1.3. Water-jet Cutting and Abrasive Water-jet Cutting Applications

1.3.1. Common Industrial Machining

The table 1.1 shows below the full list of work-proof materials by using the AWJ and WJC cutting techniques. And the table 1.2 shows the list of work-proof materials for only AWJ system. Examples can be increased by testing.

Table1.1 Processed Materials Using WJC Methods

Soft Rubber	Soft Gasket Material
Foam	Food Industry
Foils	Diapers
Carpet	Wood
Paper	All sorts of Soft Materials
Cardboard	--

Table1.2. Processed Materials Using AWJ

All Alloy Steels	Expanded Metal	Teflon	Nylon
Alumina 95	Hastalloy	Mild Steel	Tile Bonded Metals
Alumina 99	Hot Rolled Steel	Molybdenum	Tin
Armor Plate Boron	Limestone	Mylar Laminates	Tool Steel
Bullet Proof Glass	Linoleum	Neoprene	Tungsten
Cobalt	Magnesium	Nickel Alloys	Hardened Tool Steel
Exotic Alloys	Tantalum	Niobium	Titanium

1.3.2. Printed Circuit Boards

For circuit boards, water-jet cutting is mostly used to cut out smaller boards from a large piece of stock. This is a desired method, since it has a very small kerf, or cutting width, and does not waste a lot of material. Because the stream is so concentrated, it can also cut very close to the given tolerances for parts mounted on the circuit board without damaging them. Another benefit is that water-jet cutting

does not produce the vibrations and forces on the board that a saw would, and thus components would be less likely to be damaged.

1.3.3. Wire Stripping

Wire stripping is another application that can be used effectively in water-jet cutting. If no abrasives are used, the stream is powerful enough to remove any insulation from wires, without damaging the wires themselves. It is also much faster and efficient than using human power to strip wires.

1.3.4. Food Preparation

The cutting of certain foods such as bread can also be easily done with water-jet cutting. Since the water-jet exerts such a small force on the food, it does not crush it, and with a small kerf width, very little is wasted.

1.3.5. Tool Steel

For abrasive water-jet cutting, tool steels are one application, although a limited one. It can be very useful though because tool steel is generally very difficult to cut with conventional machining methods, and may cause an unwanted by product: heat. Abrasive water-jets, however, do not produce heat that could alter the structure of the material being cut, and thus the strength of the tool is retained.

1.3.6. Wood Cutting

Woodworking is another application that abrasive water-jet machining can be used for. Since wood is a softer material compared to steel, almost all wood can be cut, and the abrasive particles sand the surface, leaving a smooth finish that doesn’t require sanding.

1.3.7. Composite Material Cutting

Today's advanced composites can be as hard and rigid as steel. The same properties that make these materials so tough also make them difficult to cut without deteriorating their quality. Composition technologists continue to introduce new material combinations that defy the capabilities of traditional machining methods. The nature of metal, ceramics, and carbon matrix composites slows down cutting speeds and rapidly dulls conventional cutting tools.

Until recently, conventional cutting methods were used to cut these new materials. Because of the composition and the fiber orientation of these composites, they have often damaged by the heat of the operation or by having their edges frayed or delaminated. Much of these damage could not be determined before assembly and use. AWJ cuts 10 times faster and generally without damage.

1.3.8. Aeronautical Applications

An Ingersoll-Rand hydro-abrasive nozzle was used by North American Aircraft to cut components for the B-1B bomber. The parts were cut from titanium sheet 0,32 cm thick. The operating pressure was 69 MPa. One of the main reasons for using AWJ on these titanium sheets is that the cuts were almost burr-free. This helped raise production by factor of 10 to 1 in favor of AWJ over the previous conventional method.

1.3.9. Space Industry

Flow Corp. has joined with ASI, a developer of advanced gantry robots, to install water-jet systems for Boeing, McDonnell Douglas, Lockheed, and others. These projects were to provide the capability of cutting very large work pieces.

1.3.10. Cleaning

The NLB Corp. of Wixam manufactures water-jet cleaning systems. Their machinery harnesses the power of the water for cleaning industrial plants. Whatever the buildup, rust, scale, resins, chemical residues, paint, or epoxies, an NLB waterblast system is much faster than manual cleaning.

1.4. History

Dr. Norman Franz is regarded as the father of the water-jet. He was the first person who studied the use of ultrahigh-pressure (UHP) water as a cutting tool. The term UHP is defined as more than 2000 bar (200 MPa). Dr. Franz, a forestry engineer, wanted to find new ways to slice thick trees into lumber. In the 1950's, Franz first dropped heavy weights onto columns of water, forcing that water through a tiny orifice. He obtained short bursts of very high pressures (often many times higher than are currently in use), and was able to cut wood and other materials. His later studies involved more continuous streams of water, but he found it difficult to obtain high pressures continually. Also, component life was measured in minutes, not weeks or months as it is today.

Dr. Franz never made a production lumber cutter. Ironically, today wood cutting is a very minor application for UHP technology. But Franz proved that a focused beam of water at very high velocity had enormous cutting power.

In 1979, Dr. Mohamed Hashish working at Flow Research began researching methods to increase the cutting power of the water-jet so it could cut metals, and other hard materials. Dr. Hashish invented the process of adding abrasives to the plain water-jet. He used garnet abrasives, a material commonly used on sandpaper. With this method, the water-jet (containing abrasives) could cut virtually any material. In 1980, abrasive water-jets were used for the first time to cut steel, glass, and concrete. In 1983, the world's first commercial abrasive water-jet cutting system was sold for cutting automotive glass. The first adopters of the technology were primarily in the aviation and space industries which found the water-jet a perfect tool for cutting high strength materials such as Inconel, stainless steel, and titanium as

well as high strength light-weight composites such as carbon fiber composites used on military aircraft and now used on commercial airplanes. Since then, abrasive water-jets have been introduced into many other industries such as job-shop, stone, tile, glass, jet engine, construction, nuclear, and shipyard, to name a few (FlowCorp).

1.5. Main Components and Working Principles of Water-Jet System Developed in University of Çukurova

The first prototype water-jet cutting system was designed and manufactured in Mechanical Engineering Department of University of Çukurova in 1999. The first prototype had single layer intensifier. So the pressure was limited to 140 MPa. The developed system has been able to cut the soft metals like aluminum and brass.

As seen in Figure 1.4., the water-jet cutting system consists of an intensifier, check valves for low and high pressures, a hydraulic pressure generation system, a programmable logic controller, a cutting nozzle, two proximity sensors, oil hoses and high pressure water hoses. The intensifier is simply a hydraulically driven reciprocating plunger pump. It is driven by a hydraulic actuator, located in the middle of two cylinders. As shown in Figure 1.4., the oil piston and two water piston rods carrying water pistons are coupled together as one piece. The hydraulic actuator is reciprocated by pressurized oil (up to 250 bars) through the use of hydraulic direction control valve under programmable logic controller supervision and feedback received from proximity sensors at the stroke ends. The reciprocating action intakes low-pressure water into one cylinder while the other cylinder compresses the previously taken low-pressure water. As a result, ultra-high-pressure can be generated by the intensifier. The intensification ratio depends on the area ratio of the oil and water pistons. [GEREN N., BAYRAMOĞLU M., EŞME U., 2007]

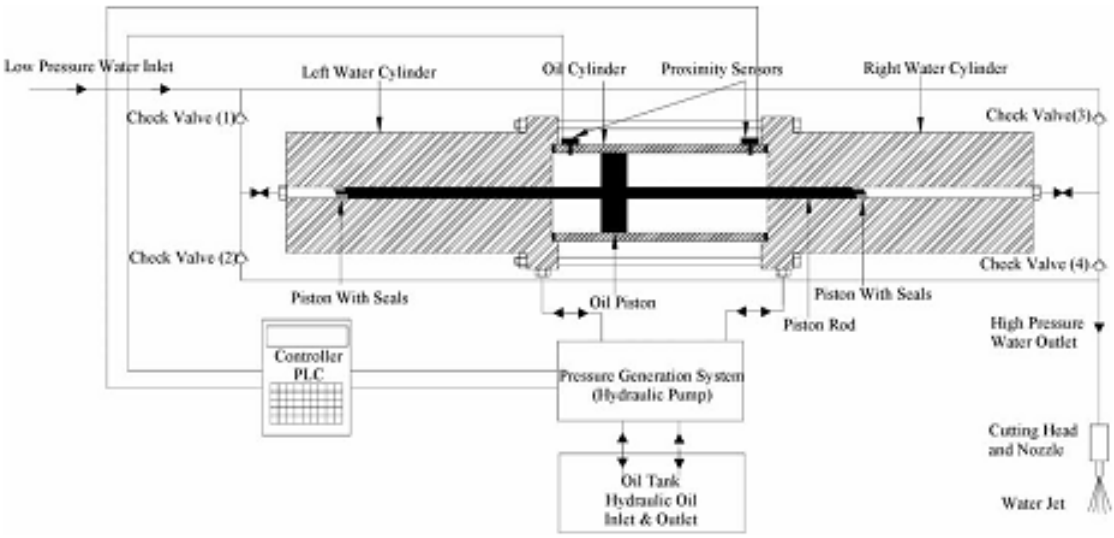

Figure 1.4. Abrasive Water-Jet Pressure generation, liquid distribution and nozzle systems

1.5.1. Intensifier Unit (Pressure Generation System)

1.5.1.1. Reciprocating Plunger (Oil-Water Piston)

This part is the main pressure generator system of the intensifier unit. A double plunger connected to large area oil piston intensifies the input oil pressure to ultra high water pressure by reciprocating action controlled by a controller PLC. Two capacitive proximity sensors located near the end of the water cylinder senses the oil piston existence and sends a signal to PLC unit. The solenoid valve connected to PLC unit changes its switching position by the signal generated by the PLC. Thus a reciprocating motion is obtained. The principle of pressure increase is based on the Pascal Law. In any fluid, the pressure acting on any surface will be the same. So the perpendicular force is F=PA where F is force, P is pressure and A is the area exposed to pressure. Thus the big force produced by the large area oil piston is directly transmitted to the water piston by the mechanical means. Same force must be balanced by producing greater counter-pressure on a smaller area. The pressure is inversely proportional with the area ratio. As example, an intensifier which has 20:1 oil-water piston area ratio will produce 20 times greater pressure in water piston

neglecting loses. Therefore, water output pressure can be regulated by adjustment of the oil pump pressure.

1.5.1.2. Water Cylinders

Water cylinders are the essential parts of the intensifier unit. It has two layers to obtain high strength and toughness at the same time. Inner cylinder, which is made of AISI 4340 steel, has high tensile strength, high yield strength and high hardness value to withstand to exposure of ultra high pressure. Both of the water cylinders could be made by AISI 4340 steel. But AISI 4340 have poor ductility and impact resistance. The economy and the cost of the first intensifier could increase drastically as well. So outer shell is made of AISI 4140 steel which has tolerably low tensile strength, yield strength and hardness, but superior ductility, impact resistance and economy.

1.5.1.3. Sensors

The sensors that are used for sensing the oil piston is capacitive type. When the plunger unit reaches to the left or right side of the oil piston, sensors send the signal to the plc unit which changes the moving direction of the oil piston.

The capacitive sensors are widely used sensors in modern industry due to their short response time and some other important sensing characteristics.

2. PREVIOUS STUDIES

2.1 High Pressure Generation Methods

There are two types of pressure generators (pumps) which are commonly used in the water-jet industry, and a number of other, experimental units which have been tried. At lower pressures, pumps are normally piston driven, with a three pistons and triplex pump being the most common. Where the pressures are higher, and flow rates normally lower, then an intensifier system can be used. Each has its own advantages and disadvantages. The normal type of pump which one encounters the lower pressure levels, i.e., below 140MPa, is one in which the water is delivered to the supply line by the oscillating pistons (see figure 2.1. at next page). These pumps are called positive displacement, reciprocating pumps because the pistons normally move backwards and forwards at a constant speed. On each stroke a fixed volume of water is drawn into the cylinder above the piston, and then pumped out into the line. Thus, if the pump is operated at constant speed, then each piston, and therefore the total pump, will provide a constant flow of water into the delivery line.

2.1.1. Triplex and Positive Displacement Pumps

There are several ways to control the volume of the water which the pump will supply. It is possible, though not common, to vary the speed of the drive motor to the pump. This can change the oscillation speed of the pistons, and thus controls the amount of water each pumps out every minute. An alternate method of achieving the same goal is to place a gearbox between the drive motor and the pump drive shaft. Thus by changing gears, the speed of the pump drive shaft may be changed, and the volume coming from the pump altered accordingly.

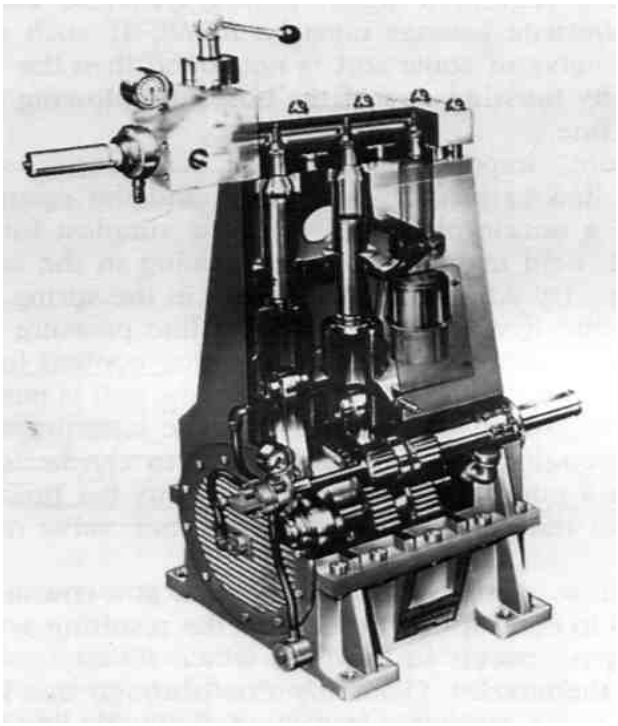

Figure 2.1. Sectioned view of the piston area of a triplex high pressure pump (courtesy of Paul Hammelmann Maschinenfabrik GmbH)

This fixed volume of water flowing into the pump outlet manifold has both advantages and disadvantages to high pressure pump operations. The advantage lies the steadiness of flow generated. However, there is a disadvantage in that if the nozzle should be blocked or partially blocked, then the water must still find a way out of the line. This will occur by either the water speeding up to get through the remaining area of the orifice, which will require a higher pressure exerted back on the pump pistons, or an alternate passage must be found. If such a passage in the form of a relief of some sort is not found then the water may make its own passage by bursting one of the hoses, or blowing apart one of the couplings in the line.

It is therefore, important to ensure that proper safety valves be included in the line to protect the system and the operator against the consequences of a nozzle blockage. In their simplest form safety valves consist of a ball, held in place over an opening in the supply line, by a spring.

By adjusting the pressure in the spring, it is possible to set the valve so that it will open, when the line pressure exceeds a given level.

Because the flow coming from the pump is constant volume, there are several ways to control the pressure of the resulting water. The first is to provide a bypass circuit in the line, which diverts some of the water flow away from the nozzle. Generally flow through this line is controlled by an adjustable valve, and the water going down this line is returned to the pump reservoir for reuse (Figure 2.3.). The alternative method is to except all the water into the delivery line to the nozzle and to size the nozzle according to pressure required from the jet.

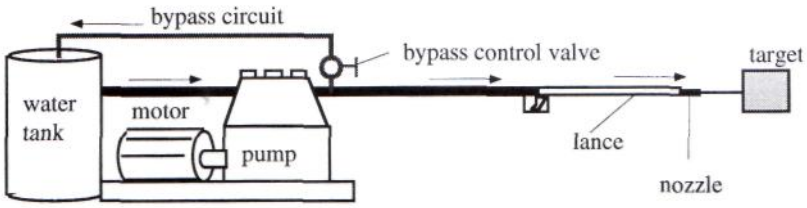

Figure 2.2. Typical arrangement of a bypass circuit (Summers, 1995)

Piston pump designs follow much the same basic designs, with only one or two exceptions. One such variation is to change the driving mechanism which moves the piston from a rotating crankshaft, as in the pumps described above, to a swinging swash plate.

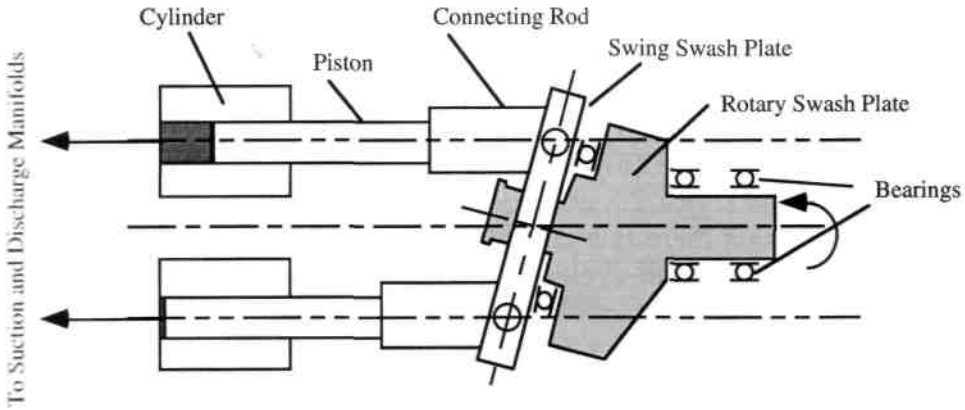

Figure 2.3. Schematic of a pump using a swash plate drive (Summer, 1995)

As the Rotary Swash Plate turns it also turns the Swinging Swash Plate, causing the connecting rods to oscillate back and forth, sequentially pulling in and discharging fluid through the pistons and cylinders as seen in the figure 2.4.

As materials and sealing technologies improve, so the capabilities of these systems have grown with them, to current working pressures which have reached 1,500 bar.

The second point relates to the first but is not quite as obvious. In a typical triplex pump the pistons are equally arranged about a crankshaft at 120 degrees apart. This will not give an absolutely steady flow, since, as the pistons move backward and forward in the cylinders, water is drawn in, the inlet valve is closed, then the water is compressed by the piston motion, and it is only when it reaches a set pressure, that the delivery valve will open to push the water out to the manifold, and thence down the line to the nozzle (see Fig. 2.5.).

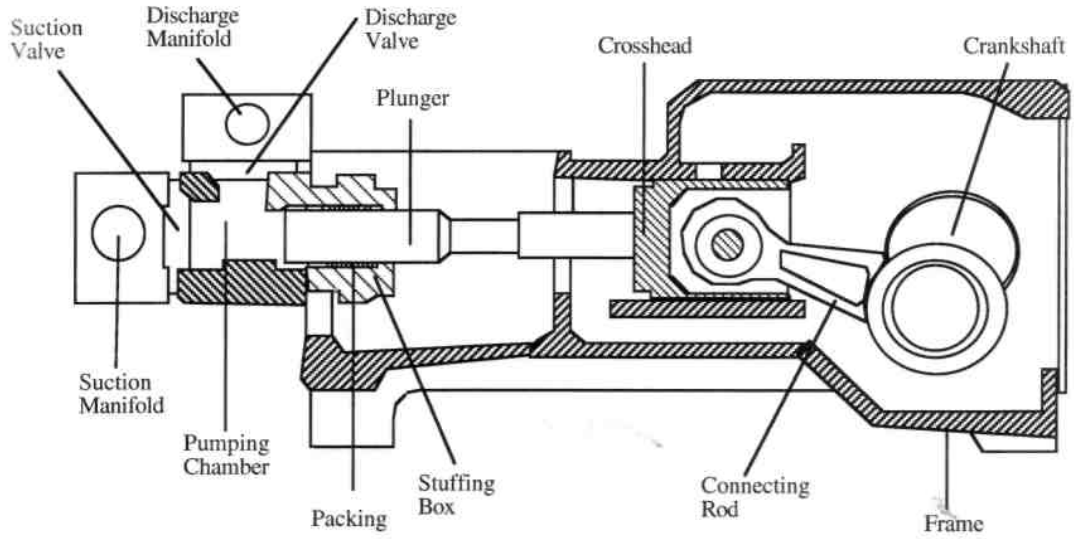

Figure 2.4. Sectioned view of a triplex pump, showing the valve locations (Summers, 1995)

2.1.2. Intensifiers

In a conventional high pressure pump the power is transmitted, through a crankshaft which forces the reciprocal motion of each piston, and in this way generates pressure in the fluid drawn into the space above the piston. This type of

system works well at intermediate pressures, but as the pressure levels required mount, it becomes less reliable. An alternative approach has, therefore, been developed in which an intensifier design is used as a pumping unit.

In the basic design of such a unit, (see fig. 2.6) oil is supplied at normal hydraulic operating pressures (in the range from 200 - 350 bars). The oil flows into a cylinder and applies pressure to the large surface area of the reciprocating piston within that cylinder. The pressure causes the piston to move, and in so doing, it drives water out of the volume ahead of its motion. This volume is however, held in a vessel of smaller diameter, so that with relative equal forces across the piston, much higher pressures can be generated in the delivery water.

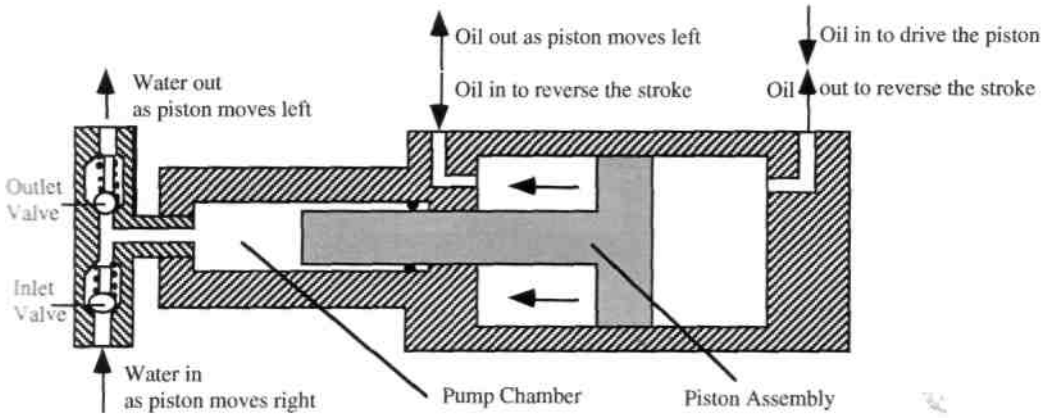

Figure 2.5. Schematic of the operation of an intensifier pump

This can, perhaps, be most easily illustrated by example. If a piston is used where the oil pushes against a piston face with a 5 cm radius, then at a pressure of 350 bar, the oil will exert a force (= pressure x area) of (350 x pi x 52) = 27,500 kg. If the piston size on the water side is only 1.58 cm in radius, then the pressure that will be exerted on the water is given by force/ area = 27500/ (pi x 1.582) = 3,500 bar. Thus by reducing the size of the piston from 10.0 cm in diameter on the low pressure side, to 3.16 cm diameter on the high pressure side, the pressure delivered can be increased by a factor of 10 (Summers, 1995).

In order for the intensifier to give a quasi-continuous flow the units are generally made double acting (see fig. 2.7) so that, at the end of each stroke the cylinder is caused to change direction and then acts to pressurize the fluid in the opposing chamber, while allowing the inactive chamber to recharge. This alternate cycling can be achieved by alternately directing the flow of fluid to either side of the low pressure piston (Summers, 1995).

High pressure intensifiers have found a significant market, particularly in industrial cutting. They operate, however, most frequently at pressures at which metal behavior becomes of significant importance. Thus these pumps require that particular care be taken in the choice of material components, and in monitoring the quality of the water, or other fluid, which is used as the cutting fluid on the delivery size of the intensifier.

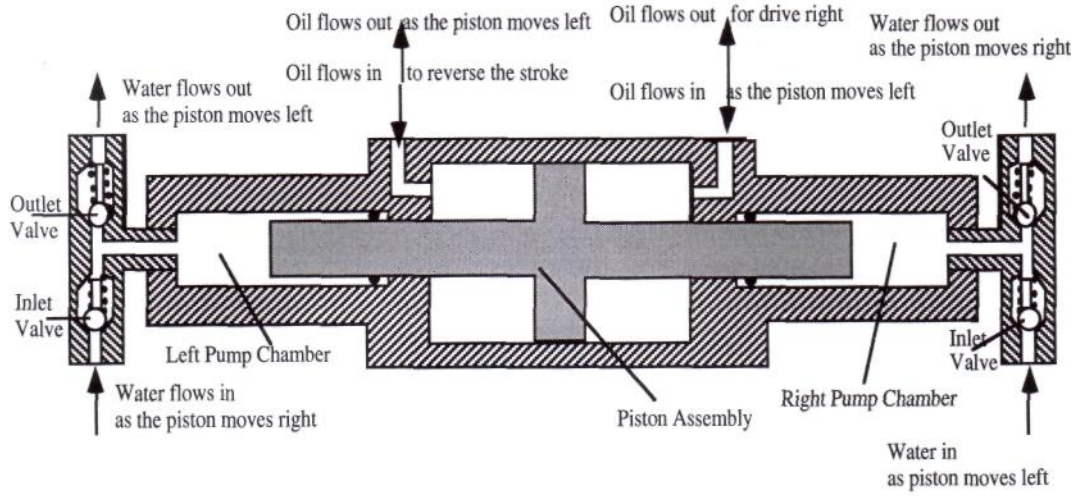

Figure 2.6. Schematic of the operational parts of a double acting intensifier

An additional problem which arises with their use comes from the need to compress the fluid before pumping will begin on each stroke, given that the pump must also change direction before fluid delivery can start again. There are two approaches which can be taken to solving this problem. The traditional one has been to include an accumulator or attenuator in the system (Fig. 2.8.), (Summers, 1995).

Pressure and flow variations are highly undesirable in intensifier operations particularly in the high precision cutting applications for which they have been found

very effective. Any variations in the jet stream can show up as a change in the contour of the cut and can lead to an unacceptable surface. Sizing the attenuator to effectively reduce pressure fluctuations is critical to its effectiveness. Because the attenuator stores a volume of water at pressure, which it releases into the system as the pump pressure falls; it can even out some of the fluctuations (Fig. 2.9) (Summers, 1995).

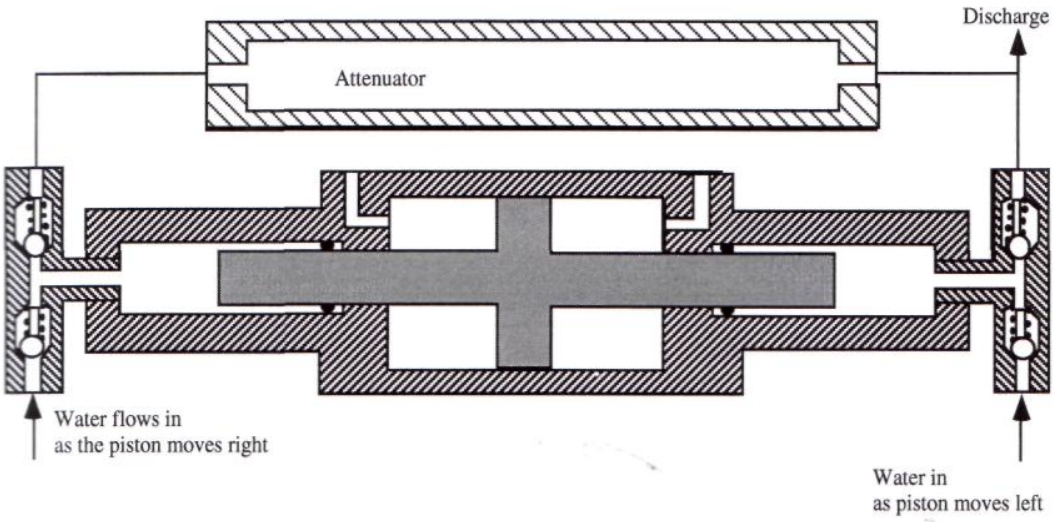

Figure 2.7. Hydraulic intensifier circuit fitted with an intensifier

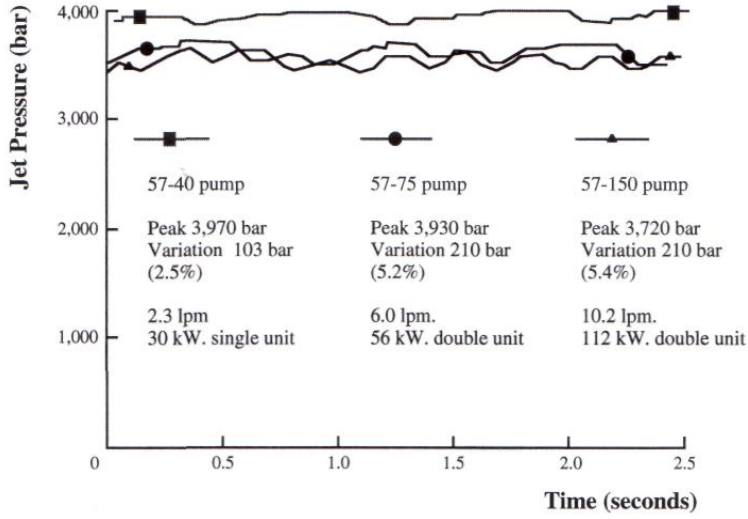

Figure 2.8. Variations in intensifier pressure output with an attenuator and for different pump sizes

However the capacity of the attenuator must be sized to the delivery volume of the pump (Figure 2.10.). It is important to note that this system affects the overall efficiency of the operation.

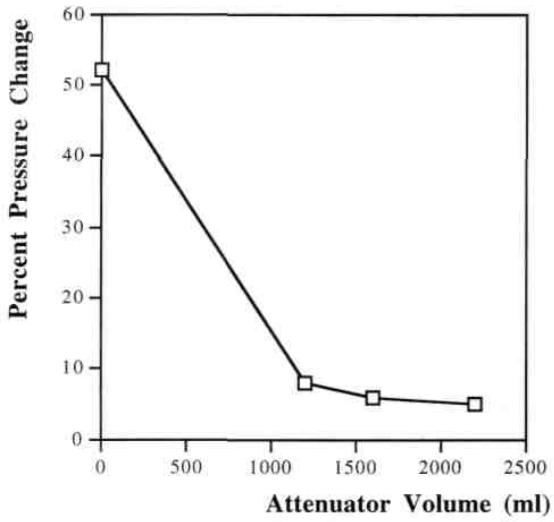

Figure 2.9. Effect of attenuator size on intensifier pressure fluctuations

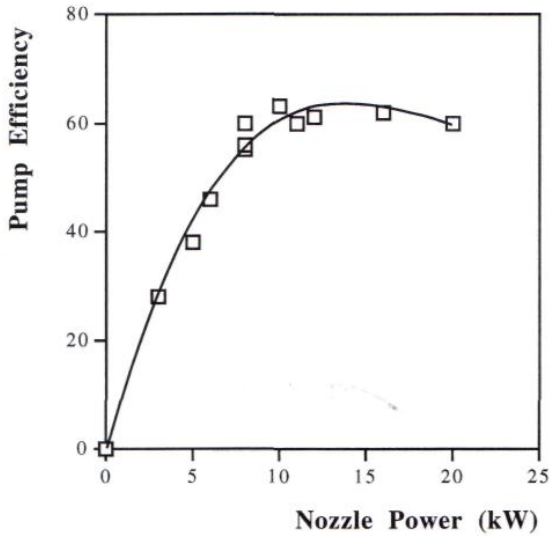

Figure 2.10. Intensifier efficiency as a function of nozzle power

The alternative approach is to run two single intensifier pistons so that one has started its compression stroke, before the second has completed its delivery.

Thus, as one piston stops, the other is already at pressure and continues the delivery (Fig. 2.12., Figure 2.13.)

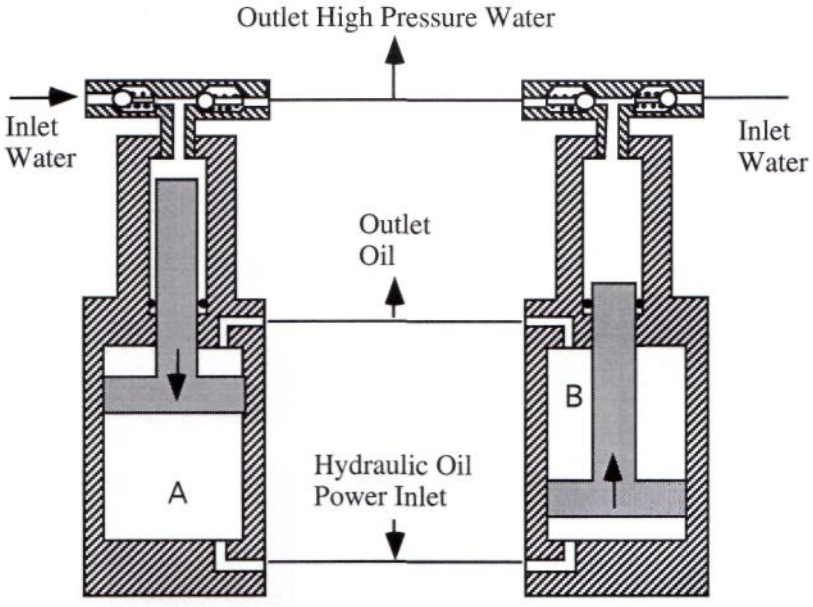

Figure 2.11. Sequential operation of a phased intensifier system. Pistons A and B are independently controlled and at this stage A has started to retract, drawing water into the cylinder, while B is discharging high pressure water

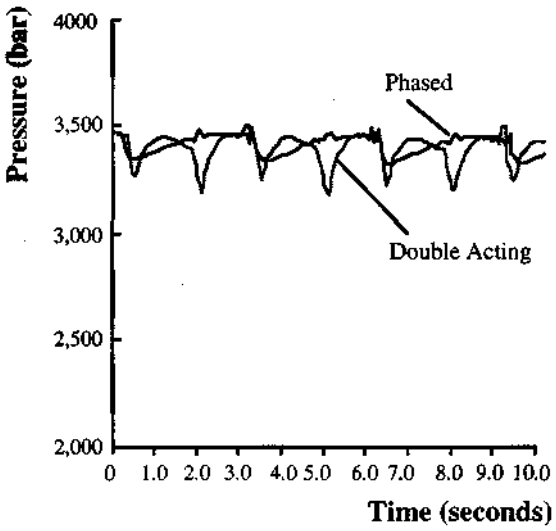

Figure 2.12. Reduction in pressure pulsation with a phased intensifier

The increasing use of high pressure water-jets in industrial plants has led to a perception that intensifiers are large, heavy and expensive units. This need not be the case, and, for example, the phased systems discussed above are both smaller and lighter than their earlier counterparts. However, for very small and precise applications there is another alternative particularly then only relatively small water flows may be required. For these low flow applications it is possible to obtain air driven intensifiers which use a compressed air feed to provide the power supply to the low pressure side of the intensifier. While such units may individually only generate flow rates on the order of 260 cc/min, they do this at pressure of 2,000 bar and above, and can be connected in parallel to provide greater flow volumes. With an initial cost of under $2,000 they provide a relatively inexpensive and small solution to some industrial application problems (Summers, 1995).

Other high pressure generation techniques are Airhydropump, Belfast Intensifier and Harwood Intensifier.

Airhydropump was developed by Charles Madan & Co. Ltd. In airhydropump, compressed air is used to intensify the liquid. Airhydropump can reach up to the operating pressure f 7000 bar. The compressed air in air cylinder is used to power the plunger of high pressure cylinder. The intensification ratio can take values as high as 1000. A differential plunger is used. The continuity is maintained by operation of valves. Valves operate as a rod passes through a gland at the back of the low pressure cylinder. In this way, when the plungers reach the end of their stroke, they are drawn back and the supply of supply of working fluid then refills the high-pressure space for the next stroke, which is automatically begun as soon as the withdrawal is complete (Manning, 1971).

Belfast intensifier is developed at the Queen's University of Belfast. It can reach operation pressures of 16000 bar.

Harwood intensifier is developed for a double acting injector for introducing catalyst into the reaction space of high-pressure polyethylene plants. The Harwood intensifier can reach operating pressure of 15000 bar. It is normally operated by pressurized water in the catalyst injectors, is provided with parts at each end r double acting if a second high pressure cylinder is connected to the other side.

2.2. The First Prototype of Water-Jet Machine System Designed in Çukurova University

A simple prototype WJM system has been developed in the University of Çukurova (Geren, Bayramoğlu, and Eşme) previously to meet the demand for a low-cost WJM system. A schematic of the water jet cutting system showing main system components is given in figure 3.1. As shown in figure 3.1., the oil piston and two water piston rods carrying water pistons are coupled together as one piece. The hydraulic actuator is reciprocated by pressurized oil (up to 250 bars) through the use of hydraulic direction control valve under programmable logic controller supervision and feedback received from proximity sensors at the stroke ends. The reciprocating action intakes low-pressure water into one cylinder while the other cylinder compresses the previously taken low-pressure water. As a result, ultra-high-pressure can be generated by the intensifier. The intensification ratio depends on the area ratio of the oil and water pistons.

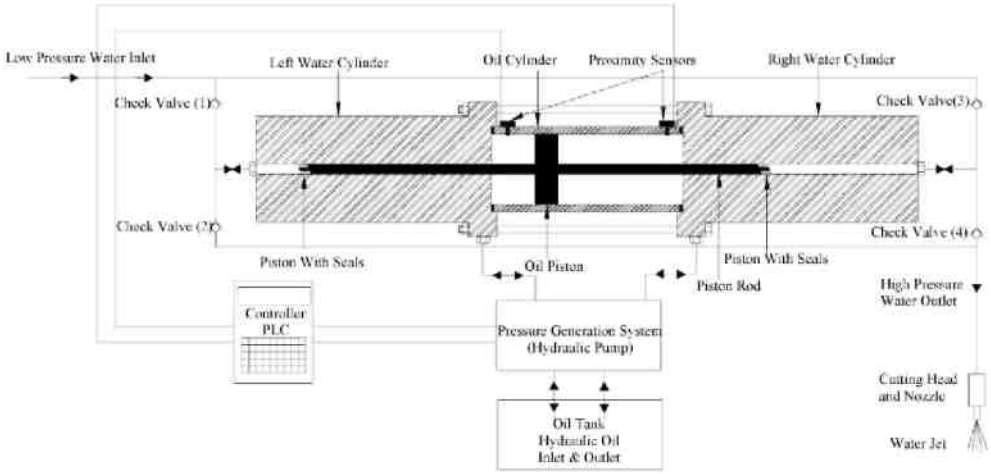

Figure 2.13. Main components of the WJM system

The double-acting intensifier used in this machine was designed for a maximum operating pressure of 1400 bar in order to use a single-layer cost-effective intensifier. But, the other components of the first alpha-prototype WJM system were designed for a 4000 bar operating pressure. The intensifier of the system was designed as simply as possible, using well-known or standard sealing techniques (see figure 3.2). The main components of the intensifier are an oil cylinder and two water

cylinders. Adapters and check valves located in 'T'-connections are the auxiliary parts of the system. The oil (low-pressure) piston and the water (high-pressure) piston have diameters of 160 and 40 mm, respectively, which gives an area ratio of 16:1. This means that the water pressure can be increased 16 times the incoming oil pressure. The stroke is 390 mm. The intensifier is activated by manually adjustable (up to 250 bar) oil pressure acting against the large piston to confine the high-pressure water to a small portion of the intensifier.

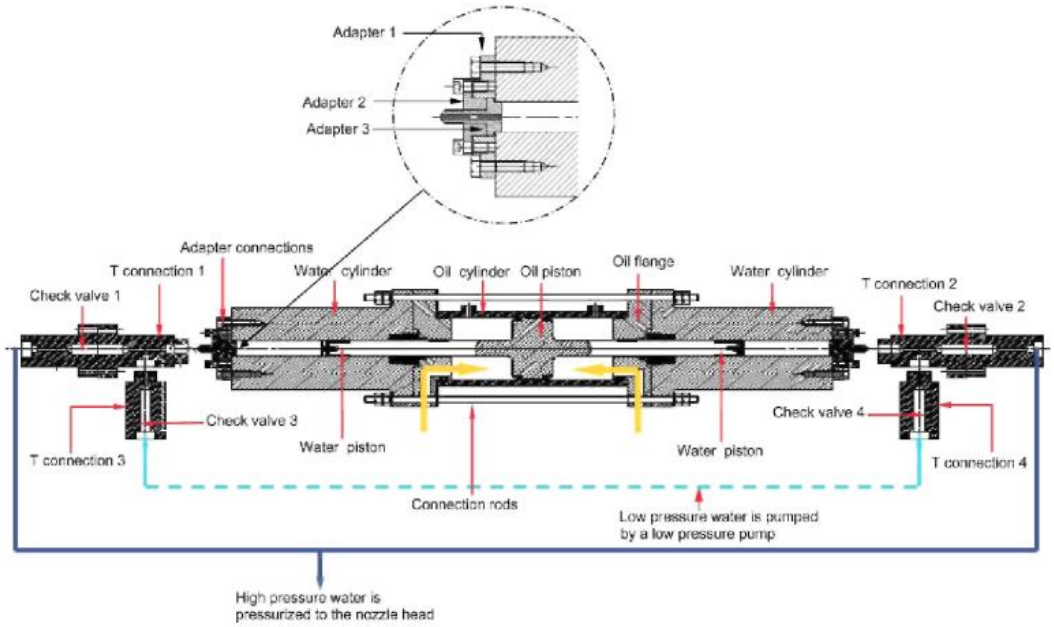

Figure 2.14. First alpha-prototype WJM system intensifier and auxiliary parts.

2.3. Fretting Analysis

Fretting may arise in engineering applications where cyclic tangential loads are transferred through contacts. The cyclic load leads to local repeated relative displacements of low amplitude between the contact surfaces, known as *slip*. Slip usually covers a part of the contact, the rest of which is characterized by no relative motion, denoted as *stick*. When the slip distance is small, only limited wear is observed on the contact surfaces and the fretting phenomenon mainly leads to early crack nucleation within the contact. In this case, the damage mechanism is normally

referred to as *fretting fatigue*. It is reported in the literature that fretting considerably reduces crack initiation life compared to ordinary fatigue conditions (Hattori, Watanabe, 2006)

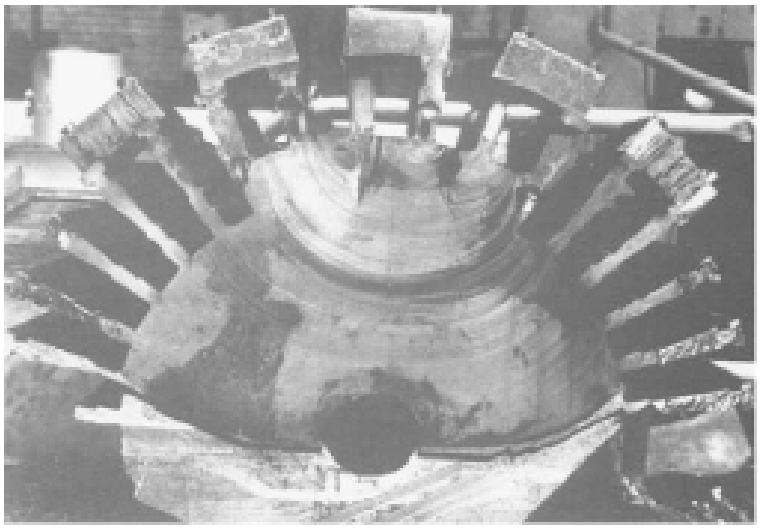

Figure 2.15. Fretting fatigue failure example of turbogenerator rotor (Lindley and Nix, 1991)

Fretting can occur when a pair of structural elements are in contact under a normal load while cyclic stress and relative displacement are forced along the contact surface. This condition can be seen in bolted or riveted joints, in shrink-fitted shafts, in the blade dovetail region of turbo machinery, etc. During fretting the fatigue strength decreases to less than one-third of that without fretting. The strength is reduced because of concentrations of contact stresses such as contact pressure and tangential stress at the contact edge, where fretting fatigue cracks initiate and propagate. This concentration of stress can be calculated using the finite element method or boundary element method. Methods for estimating the strength of fretting fatigue have been developed that use values of this stress concentration on a contact surface. However, the stress fields near the contact edges show singularity behavior, where the stress at contact edges is infinite. Thus, maximum stresses cannot be used to evaluate fretting fatigue strength (Cadario and Alfredsson, 2007).

A number of studies have been conducted in order to quantify the influence of fretting on crack nucleation. The nucleated small cracks are also largely affected by fretting since they are located in the highly stressed region under the contact. The

growth of the long cracks, on the other hand, does not differ from plain fatigue if the complex contact loads are taken into consideration. Thus, classical fatigue crack growth analyses can be performed when the crack is long.

During the last decades, increased knowledge about the fretting phenomenon has resulted in a number of solutions and palliatives against fretting. Shot peening is one of the most common techniques for improving fretting life. In shot peening the surface is repeatedly exposed to blasts of small, hard particles. At each impact the material deforms plastically giving rise to compressive residual stresses in a thin surface layer. The compressive stresses primarily reduce the fatigue growth rate of small cracks. The crack initiation phase may, in fact, decrease or even disappear due to the increased surface roughness and introduction of small surface cracks. However, the residual stress state is not always stable and may relax during component operation. The operating temperature and the mechanical load levels are factors that may affect relaxation. High temperature leads to annealing of the residual stresses with time. For static loading, the stresses can relax due to creep effects.

A mechanical load can cause relaxation when the yield limit is locally exceeded. For cyclic loading, relaxation is possible at even lower stresses. The fact that fretting damage is located within contacts, in regions not easily accessible, increases the danger. Thus, reliable estimates of the fretting fatigue lives are of great importance. With accurate estimates, the intervals between expensive and time-consuming inspections can be extended without lowering the safety demands. In this framework, it is desirable to include residual stresses into the fatigue life models. However, a consequence of the difficulties in quantifying the redistribution of residual stresses is that these are usually neglected in the life calculations. They are solely considered as an additional safety factor. The purpose of the present investigation was to simulate and predict the life improvements observed in the experiments by Hansson and Clevfors,15 when comparing fretting fatigue lives of shot peened and unpeened specimens. Fretting relaxation of the residual stresses from peening was measured after experiments and analyzed numerically. The fretting fatigue lives were simulated taking into consideration the stress distributions after relaxation. Three numerical fatigue growth models based on linear elastic fracture

mechanics were compared in order to give a recommendation for an engineering method to estimate fretting fatigue life including the beneficial effect of shot peening. The total fatigue life is usually divided into two phases: crack initiation and crack propagation. In fretting fatigue, the time to crack initiation often represents only a small part of the total life. This is especially true in peened specimens, where small surface cracks may exist before the experiment start. Moreover, slip locally increases the surface roughness, as in the experiments reported by Alfredsson and Cadario, introducing surface defects that could be considered as very small nucleated cracks (Cadario and Alfredsson, 2007).

2.3.1. Fretting Experiments

The test rig and the bridge type indenter in Figure 2.16. were used in Hansson and Clevfors (2001) to investigate the effect of shot peening on the total fretting fatigue life. The sharp edges of the indenter were slightly smoothed by hand with emery paper. The specimen had a rectangular cross section of size 10 mm × 3.18 mm with rounded corners of radius 0.5 mm. Two bridges were put into contact with the specimen and the total normal contact force, P, was applied through the load ring in Fig. 1a. The load ring was very compliant and P was therefore constant during the test. The value of P was chosen to give an average contact pressure of 250 MPa. The specimen was mounted in a servo-hydraulic test machine and loaded by a longitudinal cyclic bulk stress with amplitude σ a and mean value σ m.

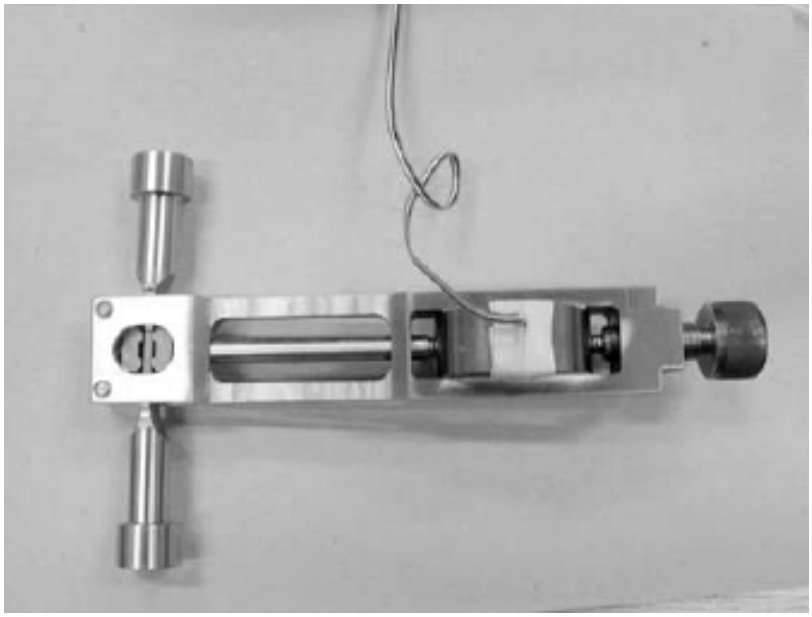

Figure 2.16. Photograph of the fretting rig. The flat specimen and the two bridge type pads are visible on the left-hand side. The compliant ring used to apply a constant normal contact force to the bridge pads is found on the right-hand side (See fig. 2.17.)

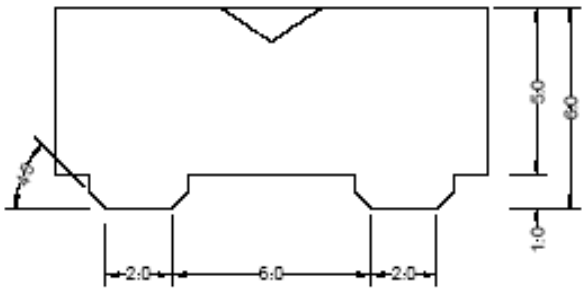

Figure 2.17. Schematic view of the bridge type pad.

2.3.2. Fretting Fatigue Process

Hattori and Watanabe (2006) present fretting fatigue process model as illustrated in figure 2.18. Cracking due to fretting fatigue starts very early in fretting fatigue life. They used stress singularity parameters at the contact edge to estimate the initiation of these cracks. During this early period, fretting fatigue cracks tend to close and propagate very slow, due to the high contact pressure acting near this contact edge. But wear on the contact surface reduces the contact pressure near the contact edge, and cracks gradually start to propagate. Hence, fretting fatigue life will be dominated by the propagation of this small cracks initiated at the contact edge. So to estimate the fretting fatigue strength or life, the precise estimation of the fretting wear progress is indispensable. The propagation life in long crack length region can be estimate using ordinal fracture mechanics. The estimation method of wear extension on contact surfaces near the contact edge, and present the fretting fatigue crack propagation estimation method considering fretting wear extension is discussed (Hattori and Watanabe, 2006).

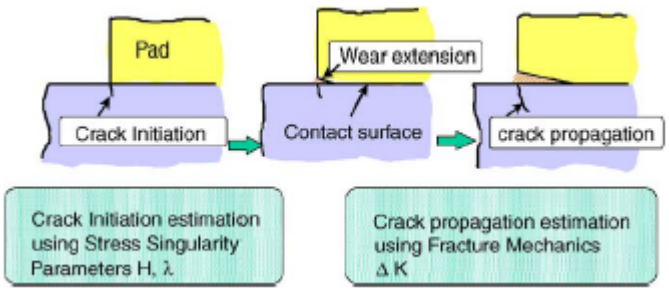

Figure 2.18. Fretting fatigue mechanisms in various processes.

2.3.3. Fretting Fatigue Life Analysis Considering Fretting Wear

In Fig.2.19. the flow of fretting fatigue life analysis considering the extension of fretting wear. Firstly the fretting wear amount is estimated using contact pressure and relative slippage on each loading condition. Then the shapes of contact surfaces are modified following the fretting wear amount. And finally fretting crack extension

or arrest evaluation is performed using fracture mechanics, if the operating ΔK is higher than the threshold stress intensity factor range ΔK_{th} we can estimate this load cycle as fretting life, and if the operating ΔK is lower than the threshold stress intensity factor range ΔK_{th} fretting wear amount is estimated using new contact pressure and new relative slippage and repeat these process until operating ΔK reach to the threshold stress intensity factor range ΔK_{th}.

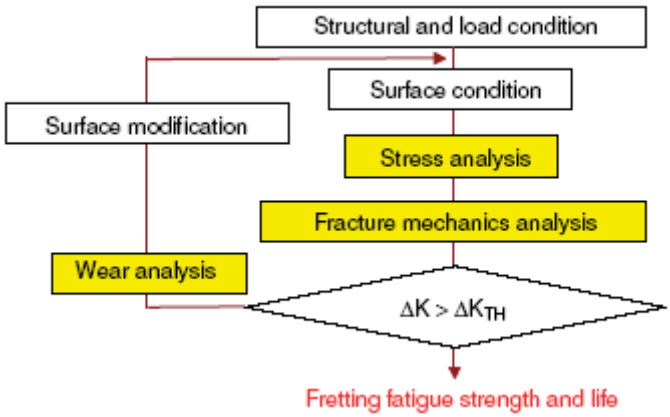

Figure 2.19. Flow chart of fretting fatigue life analysis.

2.3.4. Fatigue Crack Growth Analysis

An engineering structure and design may contain irregularities. These are geometric discontinuities in the structural members which yields stress concentrated points. Irregularities are usually called stress raisers or stress concentrators.

Presence of irregularities require special attention as they reduce the resistance of a component to fatigue failure and brittle fracture which are very dangerous as they usually occur at nominal stress level below the yield strength. Many catastrophic structural failures (n bridges, ships, towers, storage tanks, and high pressure vessels, etc.) maybe be good examples for the important role of the notches in engineering design and structures. As a general point of view, 90% of fractures occur due to stress concentration caused by irregularities (Davadandipour and Toth, 1996)

The structural design philosophy based on durability and damage tolerance requires prediction of the fatigue crack growth due to anticipated service loads. The essential elements of the analysis are: service load histories (random spectrum loads); characterization of constant amplitude data for material in question; and fatigue model (Sih and Faria, 1984)

2.3.5. Endurance limit calculation

Threshold condition

Fatigue crack growth thresholds are usually expressed in terms of the range of the stress intensity factor, ΔK_{th}. In the case of a completely opened crack it is more convenient to apply the closure-free range, $\Delta K_{eff,th}$. It is evident that an accurate value for the stress intensity factor is hard to extract from the finite element calculations. In the vicinity of the crack tip, the material behavior is elastic–plastic, and therefore a crack tip parameter defined via elastic strain and stress fields cannot be calculated. A detour via far field stresses and the J-integral might be suggested. However, from basic physical understanding, it is not clear how to deal with crack closure. The requirements for a path independent result are violated.

A crack tip parameter chosen from the proposals of the elastic–plastic fracture mechanics might be considered, e.g. the crack tip opening displacement or the J-integral. Arguments against the use of the latter are given above. The present finite element investigation only yields crack tip opening displacements afflicted by plastic elongations of crack wake elements, previously caught when they were crack tip elements. Those values cannot be compared to values converted from $\Delta K_{eff,th}$ applying the assumptions of fracture mechanics for monotonic loading. Therefore, it seems inevitable to break the straightforward analysis by calculating stress intensity factors by a simple linear elastic approach. The threshold condition is given in the equation 2.1.

$$\Delta K_{eff} \leq \Delta K_{eff;th} \qquad 2.1.$$

In order to facilitate the computation, the stress intensity factors have been calculated applying the integration of a weight function solution. Note that both the elastic circumferential stress distribution in the uncracked tube due to internal pressure and the pressure on the crack faces (effective ranges only) contribute to ΔK_{eff}.

The evolution of ΔK_{eff} over the crack length is shown in Fig. 2.20.

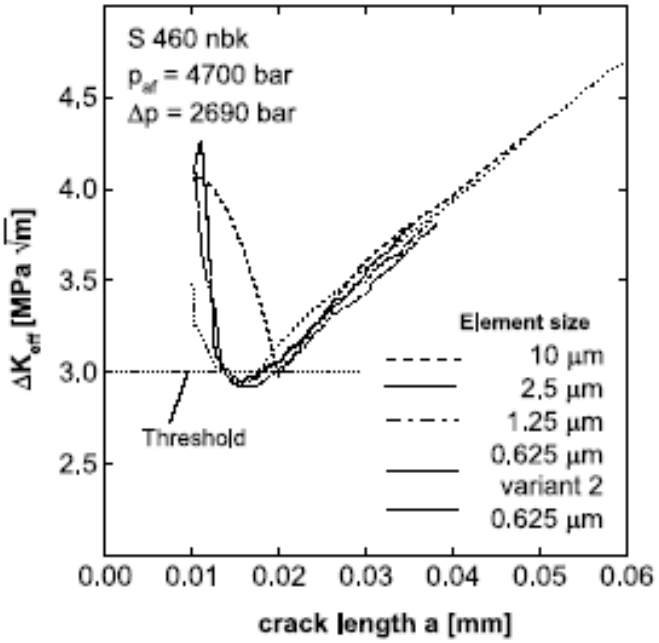

Figure 2.20. ΔK_{eff} over crack length for S 460, node release after 10 intermediate cycles, initial defect length 10 µm

2.3.6. Autofrettage

The autofrettage process is a practical method for increasing the elastic-carrying capacity and the fatigue life of a thick-walled cylinder such as a cannon or a high-pressure tubular reactor. The essence of the autofrettage technique is the introduction and utilization of residual stresses. These residual stresses are generated after pressurizing to cause yielding partway through the cylinder wall. The reliable prediction of the influence of residual stresses on the elastic-carrying capacity,

fatigue crack growth, and fracture in a thick-walled cylinder requires accurate estimation of the residual stress field. Residual stress distributions can be determined by experiment or calculation. The calculation procedures usually involve making simplifying assumptions about the material behavior, which may limit their accuracies. The basic autofrettage model proposed by Hill (1950) is an elastic–perfectly plastic model, shown in Fig. 2.20.(a). Because of the Bauschinger effect and strain-hardening, most materials do not satisfy the elastic–perfectly plastic assumption, and consequently alternative autofrettage models, based on various simplified material strain hardening characteristics, have been proposed. These are an unloading linear strain-hardening model, a bilinear strain-hardening model, a loading elastic–perfectly plastic and unloading power strain hardening model, a loading and unloading power strain-hardening model, and a loading linear and unloading power strain-hardening model, shown in Fig. 2.20. These models give more accurate solutions than the elastic–perfectly plastic model and each of them suits different strain-hardening materials.

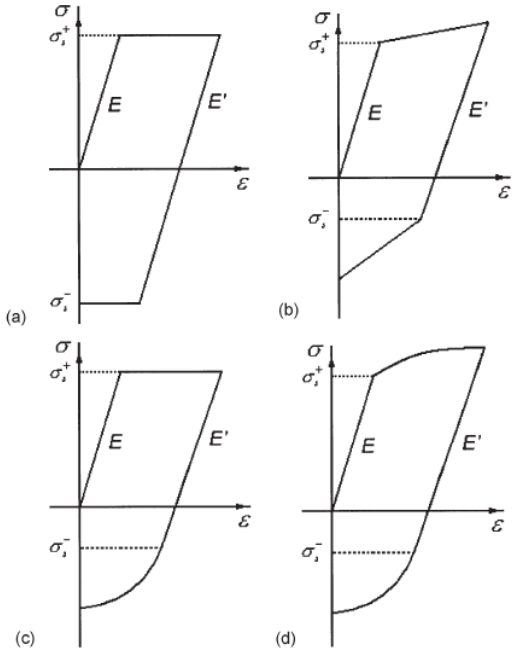

Figure 2.21. Four typical autofrettage models: (a) elastic-perfectly plastic model; (b) linear strain-hardening model; (c) unloading power function strain-hardening model; (d) power function strain-hardening model

2.4. Available Commercial WJC Design and Its Specifications

Jet Edge ultra high pressure intensifier pumps incorporate pressure compensation so the water flow is tailored to the specific job thus providing steady flow rates when operating multiple tools. Various features of some models are given below (www.jetedge.com).

X-Stream xP90-100 Intensifier Pump

Construction

- Heavy gauge sheet metal covers
- Rugged all-steel welded framework
- Hinged cover and removable access panels for convenient machine inspection and maintenance
- Integral hydraulic reservoir
- Sound insulated for quiet operation
- NEMA 12/13 rated electrical enclosure

Standard Features

- High efficiency TEFC motor
- 1,500 or 1,800 nominal motor speed (rpm)
- Electronically shifted intensifiers
- Wye-Delta soft start with disconnect

- Fail-safe high-pressure attenuator
- Safety shutdown systems
- Automatic safety pressure bleed-down valve
- Thermostatically controlled cooling system
- Programmable Logic Controller (PLC) for operation and safety monitoring
- Axial piston, variable displacement, pressure-compensated hydraulic pump
- Liquid-filled pressure gauges
- UHP safety shielded tubing

Product Specifications

Physical Size

- Length: 218 cm
- Width: 102 cm
- Height: 140 cm
- Approximate Weight with Fluid: 2,222 kg

Electric Motor

- Motor Output: 100 hp (75 kw)
- Motor Type: High Efficiency TEFC electric motor
- Full load amps @ 460vac: (60Hz) 119
- Full load amps @ 230vac: (60Hz) 238

Intensifier

- Type: Single piston, dual plunger, reciprocating
- Number of Intensifiers: Two
- Maximum Pressure: 90,000 static psi (6,200 bar)
- Intensification Ratio: 25:1
- Flow Rate: 1.45 gpm (5.49 lpm)
- Maximum Rated Orifice Size: 0.017" (0.43mm)
- 100,000 PSI-rated fittings and tubing

- Supports 75K+ continuous operating pressure

Low-Pressure Water/Intensification Water

- Type: Pretreated, <100 TDS, PH 6-8, Silica <15PPM
- Supply Requirements: 2.0 gpm @ 20 psi (1.4 bar) min. / 75°F (24°C) max
- Filtration: 10, 1, .45 Micron

Coolant Water

- Maximum Temperature: 70°F (21°C)
- Minimum: 0-10.0 gpm (0-37.9 lpm) @ Minimum 20 psi (1.3 bar)
- Ability to Remove: 95,000 BTU's / Hour
- Heat Exchanger: Shell and Tube (2)

Hydraulics

- Reservoir Capacity: 55 gallons (209 liters)
- Filtration: Full Flow 10 Micron

Environmental

- Ambient Room Temperature: 50°-100°F (10°-37°C)
- Relative Humidity: Noncondensing, Maximum 95% @ 100°F

2.5. Future Studies

2.5.1. Water-Jet Guided Laser

The laser-microjet, in which a hair thin jet of water guides the laser beam much like an optical fiber, yielding a combination that rules out of the thermal damage familiar from conventional lasers. Water-jet guided laser beam is bale to cut silicon wafer of 25 to 5000 micrometer at speed of up to 120 mm/sec, with the cutting width of 50 microns and in any conceivable contour. This method can

justifiable be called force-free, due to the low pressure of the actual water-jet. It is also non-abrasive, as there is no mechanical contact between material and the tool. The water jet is essentially transparent for the laser beam. However, if the laser beam encounters a body which absorbs it, the surface of the material is heated to such an extend that plasma is created that separates the water-jet and the material from another. The plasma shields the water, but the laser is able to penetrate. The plasma only remains as long as the laser beam is activated. Because the pulse laser was used, this continuous water-jet was able to immediately re-cool the cut. Resulting in only a very slight depth of penetration (Synova, 1998).

Synova (1998) has reported that the water-jet guider laser in the field of the wafer dicing have shown that the semiconductor industry and this technology was decisive advantages over the classical cutting processes. It was able to fulfill all these in expectations in this technology with regard to kerf width, cutting speed and edge quality.

2.5.2. Water-Jet Cutting in the Helium Atmospheres

The coherence of cutting pure water jets can be enhanced by shooting them into low-density atmospheres. Coherent cutting water jets produce deeper and narrower kerfs and cuts, produce fewer noise and sprinkle less; they also operate with longer stand-off distances (distance between the nozzle and the piece to be cut) and cut with greater efficiency. Pure water jets surrounded by low-density atmospheres are more coherent than jets shot into regular atmospheres (air at 990 hPa). Abrasive water jets have wide use in industry. For some applications it is desired that they have a more coherent structure. In the study here presented the effectiveness of the low-density atmosphere technique on abrasive cutting water jets was tested.

Jet coherence

A jet loses its coherence when disturbances on its surface grow until such a size that the jet breaks up into drops. The disturbances are usually due to turbulence in the fluid stream and vibrations of the system. The turbulence depends on variables like nozzle geometry, working pressure, mechanic and hydraulic characteristics of the system, and jet-fluid properties. These variables are associated with facts like velocity-profile relaxation, cavitation, radial-inertial forces and capillary forces, all of them considered as breakup mechanisms. The interaction of the jet and its surroundings can also play an important role on the jet coherence. The shearing drag force is a product of the relative movement between the jet and its surroundings, as well as the entrainment of atmospheric fluid into the jet, assist the growth of the jet disturbances, and therefore the loss of coherence of the jet.

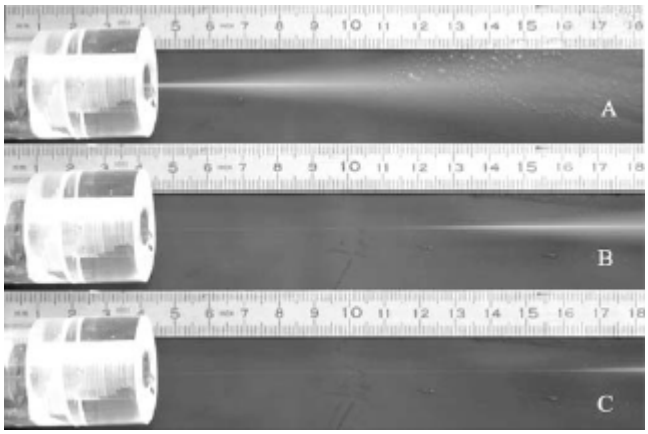

Figure 2.22. Jet surrounded by helium stream (Cadavid and Wüstenberg, 2002)

3. MATERIAL AND METHOD

This chapter will deal with the stress modeling of the double-layer intensifier. The modeling will be based on the first proto has a prototype which has been manufactured in the laboratory of Mechanical Engineering Department at the University of Çukurova. To carry out modeling study, first, the general stress equations were derived based on the equations provided by Harvey. Firstly, these equations were used for the boundary conditions of pre-shrink fit situation. Pre-shrink fit stress constants were calculated for the derivation of the relationship between δ_1 and p. After that the interface pressure and the displacement of the inner surface of the inner cylinder were calculated. These are the key values for the derivation of the other values. Then stress constants were obtained for post-shrink fit case. And using these relationships, radial, longitudinal and tangential stress components were obtained. Using suitable yield criterion (distortion energy for this situation), safety factors were calculated for both inner and outer cylinders. After these calculations, a Mathematica® program was used to derive expressions to find free radii's of the inner and outer cylinders before shrink fit. After completing the above, all calculations are performed by the Mathematica® v5.2 Algebraic Computation Toolbox. The following section provides the details of the modeling studies.

3.1. Stress Analysis in Multi-Layer Intensifiers.

When the thickness of the cylinder is relatively large in the case that we are working on it, the stress variation from inside to outside surfaces will not obey the stress models that were made for thin walled cylinders anymore. If a cylinder of constant wall thickness is subjected to an internal pressure p_i and external pressure p_o, the deformation will be symmetrical about its longitudinal axis and it is constant. It may be thought of as being composed of a series of concentric cylinders.

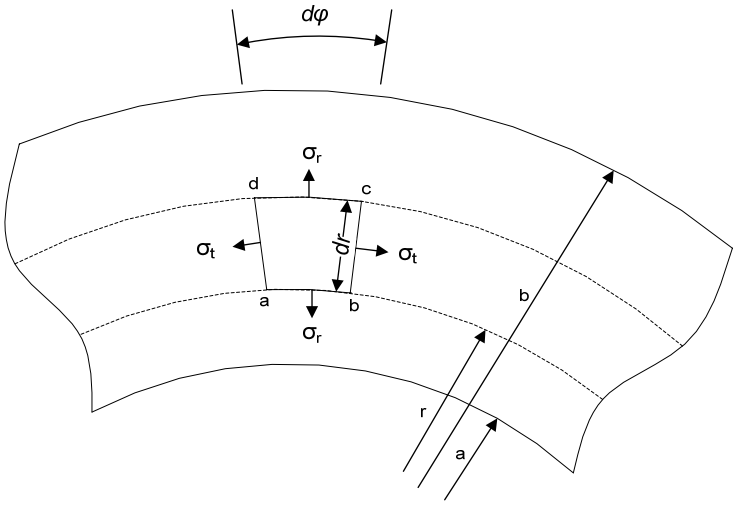

Figure 3.1. The cross-section of the cylinder perpendicular to the longitudinal axis

If a ring is cut by two planes perpendicular to the axis at unit distance apart, it will be seen that symmetrical and no shear stresses exist on the sides of the element *abcd*.

Considering the element *abcd*, the hoop stress acting on the sides *ad* and *bc* is σ_t as seen in figure 3.1. The radial stress normal to the side *ab* is σ_r, and this stress varies with the radius *r* is amount of $\frac{d\sigma_r}{dr}dr$ over a distance *dr*. So, the normal radial stress on the side *dc* is:

$$\sigma_r + \frac{d\sigma_r}{dr}dr \tag{3.1.}$$

The equilibrium equation for this infinitesimal element is obtained by summing up the forces in the direction of the bisector of angle $d\phi$, knowing that for small angles, sine function approaches the angle value:

$$\sigma_r \cdot r \cdot d\phi + \sigma_t \cdot dr \cdot d\phi - \left(\sigma_r + \frac{d\sigma_r}{dr}dr\right)\cdot(r+dr)\cdot d\phi = 0 \tag{3.2.}$$

If higher order derivatives are neglected,

$$\sigma_t - \sigma_r - r\frac{d\sigma_r}{dr} = 0 \qquad (3.3.)$$

Equation 3.3. is the relationship between radial and tangential stresses existing on cylinder.

Another relation can be obtained by using the strain relations. Assuming the longitudinal fibers are uniform. So the problem can be reduced to planar from space. Hence the displacement is equal in circumferential direction but varying along radial direction (directly proportional). "u" denotes here, the circumferential displacement. At the radial displacement of $r + dr$, the circumferential displacement will be:

$$u + \frac{du}{dr}dr \qquad (3.4.)$$

Therefore, an element abcd undergoes a total elongation in a radial direction of $(du/dr)dr$, a unit elongation of:

$$e_r = \frac{du}{dr} \qquad (3.5.)$$

Then from generalized Hook's Law equations (Beer and Johnson, 1992) for radial and tangential stresses in terms of elongation will be:

$$\sigma_r = \frac{E}{1-\mu^2}\left(\frac{du}{dr} + \mu\frac{u}{r}\right) \qquad (3.6.)$$

$$\sigma_t = \frac{E}{1-\mu^2}\left(\frac{u}{r} + \mu\frac{du}{dr}\right) \qquad (3.7.)$$

These stresses are only dependent to u value. So substituting equations (3.6.) and (3.7.) into (3.3.) gives:

$$\frac{d^2u}{dr^2}+\frac{1}{r}\frac{du}{dr}-\frac{u}{r^2}=0 \qquad (3.8.)$$

There is one general solution of this differential equation:

$$u=C_1r+\frac{C_2}{r} \qquad (3.9.)$$

Substituting u and *du/dr* into equations (3.6.) and (3.7.) gives:

$$\sigma_r=\frac{E}{1-\mu^2}\left(C_1(1+\mu)-C_2\frac{1-\mu}{r^2}\right) \qquad (3.10.)$$

$$\sigma_t=\frac{E}{1-\mu^2}\left(C_1(1+\mu)+C_2\frac{1-\mu}{r^2}\right) \qquad (3.11.)$$

The constants C_1 and C_2 can be found using boundary conditions.

At ultra-high pressures, single layer intensifiers shows poor characteristics to withstand high operating pressure. The feasible solution to this is to shrink-fit another shell outside. Shrink fitting is one of the methods doing this job. To shrink fit two cylinders, outer diameter of the inner cylinder must a little bit larger than the inner hole radius of the outer shell. Then the outer cylinder would be heated and hole diameter increases above the outer diameter of inner cylinder. After assembling the cylinders, the assembly is cooled and the outer shell grabs the inner cylinder and the contact pressure p is obtained between the two. Obviously, outer cylinder has a temperature limit. It must not be heated over 200 ^{o}C. Since overheating will produce morphological deformation on its microstructure. If the thermal expansion is not

enough to compensate this little difference, inner cylinder can be cooled to shrink too.

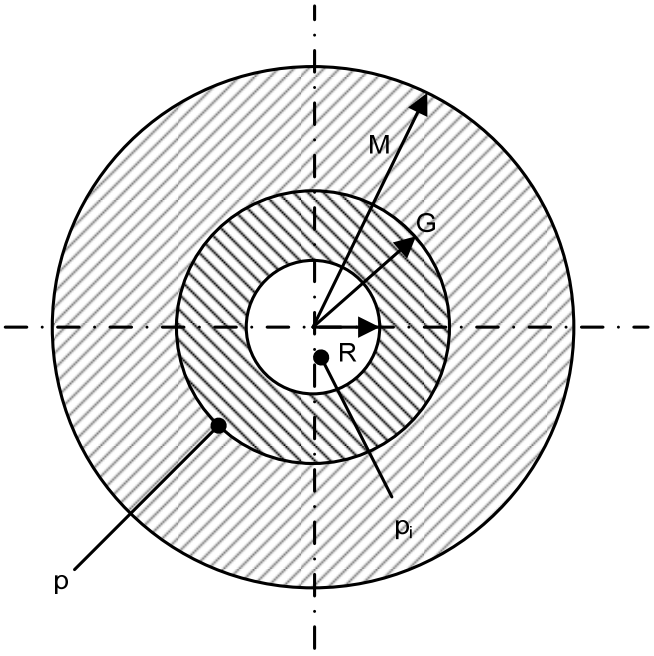

Figure 3.2. Shrink fit under interference pressure

A contact pressure *p* is developed after cooling dependent upon the initial interference of the two cylinders as shown in figure 3.2.

If such built up cylinder is subjected to internal pressure, the stresses produced by this pressure are the same as those in a solid-wall cylinder of thickness equal to sum of those of the individual cylinders. These stresses are superposed on the shrink fit stresses.

So far, how the stresses created in thick walled single layer cylinder walls are calculated have been considered. Now those formulas will be used for multi-layer structures to calculate interface pressures, factor of safety and deformations after shrink fit. Figure 3.3. shows inner and outer cylinder parts before shrink fitting.

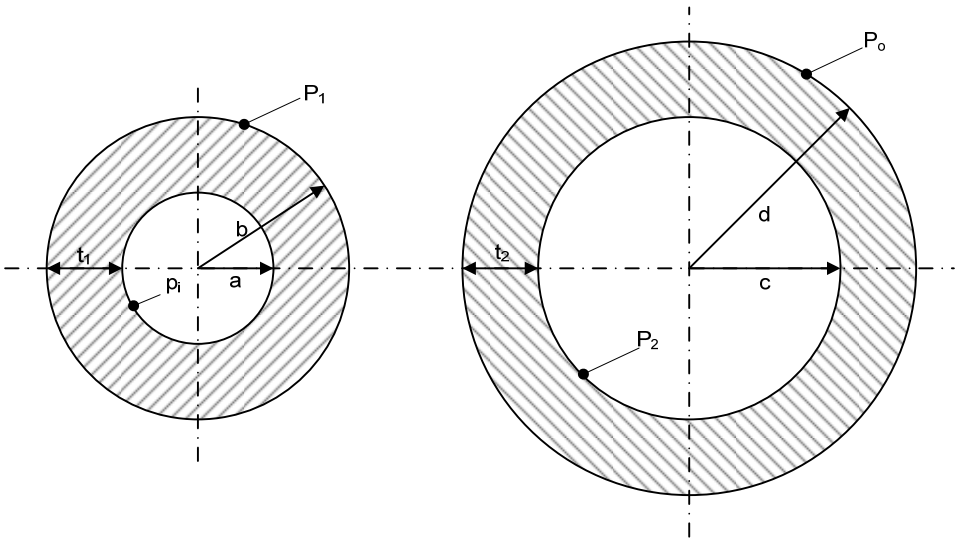

Figure 3.3. Inner and outer cylinder pairs

3.1.1. Calculation of the Stress Equations for Pre-Shrink Fit Case

But before the calculations, some assumptions about environmental conditions and material properties must be made:

- Formulas are derived for pre-shrink fit situation.
- Inner cylinder is under operating pressure of p_i on inner surface and interface pressure of p_1 on the outer surface.
- Outer cylinder is under interface pressure of p_2 on inner surface and outside pressure of p_o on the outer surface.
- Inner and outer cylinder materials are different. But both are isotropic and homogeneous in all direction.
- The elasticity modulus and Poisson's ratio of the inner cylinder is E_1, and μ_1 respectively.
- The elasticity modulus and Poisson's ratio of the outer cylinder is E_2, and μ_2 respectively.
- Cylinders are disposed to normal atmospheric conditions (room temperature).

According to the circumstances above, the boundary conditions of the stress equations for both inner and outer cylinders are expressed below.

a) The radial stress at the inner surface of the cylinder is:

$$-p_i = \sigma_r \ @ \ r = a$$

So;

$$-p_i = \frac{E_1}{1-\mu_1^2}\left(C_1(1+\mu_1) - C_2\frac{1-\mu_1}{a^2}\right) \tag{3.12.}$$

b) The radial stress equation for outer surface of the inner cylinder is:

$$-p_1 = \sigma_r \ @ \ r = b$$

$$-p_1 = \frac{E_1}{1-\mu_1^2}\left(C_1(1+\mu_1) - C_2\frac{1-\mu_1}{b^2}\right) \tag{3.13.}$$

c) The radial stress equation for inner surface of the outer cylinder is:

$$-p_2 = \sigma_r \ @ \ r = c$$

$$-p_2 = \frac{E_2}{1-\mu_2^2}\left(C_3(1+\mu_2) - C_4\frac{1-\mu_2}{c^2}\right) \tag{3.14.}$$

d) The radial stress equation for outer surface of the outer cylinder is:

$$-p_o = \sigma_r \ @ \ r = d$$

$$-p_o = \frac{E_2}{1-\mu_2^2}\left(C_3(1+\mu_2) - C_4\frac{1-\mu_2}{d^2}\right) \tag{3.15.}$$

Each cylinder has two surfaces. Inner and outer cylinder has 4 surfaces totally. And there are four boundary conditions and equations derived from them. By using the Mathematica mathematics editor, the unknown constants C_1, C_2, C_3, and C_4 are obtained using the equations (3.12.), (3.13.), (3.14.), (3.15.). The output of the Mathematica is:

$$\left\{\left\{C1 \to \frac{(-b^2\,p1 + a^2\,pi)\,(-1+\mu 1)}{(a^2-b^2)\,E1},\ C2 \to \frac{a^2\,b^2\,(p1-pi)\,(1+\mu 1)}{(a^2-b^2)\,E1},\right.\right.$$
$$\left.\left.C3 \to \frac{(c^2\,p2 - d^2\,po)\,(-1+\mu 2)}{(c^2-d^2)\,E2},\ C4 \to -\frac{c^2\,d^2\,(p2-po)\,(1+\mu 2)}{(c^2-d^2)\,E2}\right\}\right\}$$

$$C_1 = \frac{\mu_1 - 1}{E_1} \cdot \frac{a^2 p_i - b^2 p_1}{a^2 - b^2} \tag{3.16.}$$

$$C_2 = -\frac{\mu_1 + 1}{E_1} \cdot \frac{a^2 b^2 (p_i - p_1)}{a^2 - b^2} \tag{3.17.}$$

$$C_3 = \frac{\mu_2 - 1}{E_2} \cdot \frac{c^2 p_2 - d^2 p_o}{c^2 - d^2} \tag{3.18.}$$

$$C_4 = -\frac{\mu_2 + 1}{E_2} \cdot \frac{c^2 d^2 (p_2 - p_o)}{c^2 - d^2} \tag{3.19.}$$

If the interface pressures p_1 and p_2 are equal to p ; operating pressure and outer pressure p_i=p_o=0, then the constants C_1, C_2, C_3, C_4, will be calculated as C_{1w}, C_{2w}, C_{3w}, C_{4w}. They are:

$$C_{1w} = -\frac{\mu_1 - 1}{E_1} \cdot \frac{b^2 p}{a^2 - b^2} \tag{3.20.}$$

$$C_{2w} = \frac{\mu_1 + 1}{E_1} \cdot \frac{a^2 b^2 p}{a^2 - b^2} \tag{3.21.}$$

$$C_{3w} = \frac{\mu_2 - 1}{E_2} \cdot \frac{d^2 p}{c^2 - d^2} \tag{3.22.}$$

$$C_{4w} = -\frac{\mu_2 + 1}{E_2} \cdot \frac{c^2 d^2 p}{c^2 - d^2} \tag{3.23.}$$

The cylinder displacements δ_1, δ_2, δ_3, δ_4 are shown in figure 3.4., are derived from Equation (3.9.)

$$\delta_1 = C_1 a + \frac{C_2}{a} \tag{3.24.}$$

$$\delta_2 = C_1 b + \frac{C_2}{b} \tag{3.25.}$$

$$\delta_3 = C_3 c + \frac{C_4}{c} \tag{3.26.}$$

$$\delta_4 = C_3 d + \frac{C_4}{d} \tag{3.27.}$$

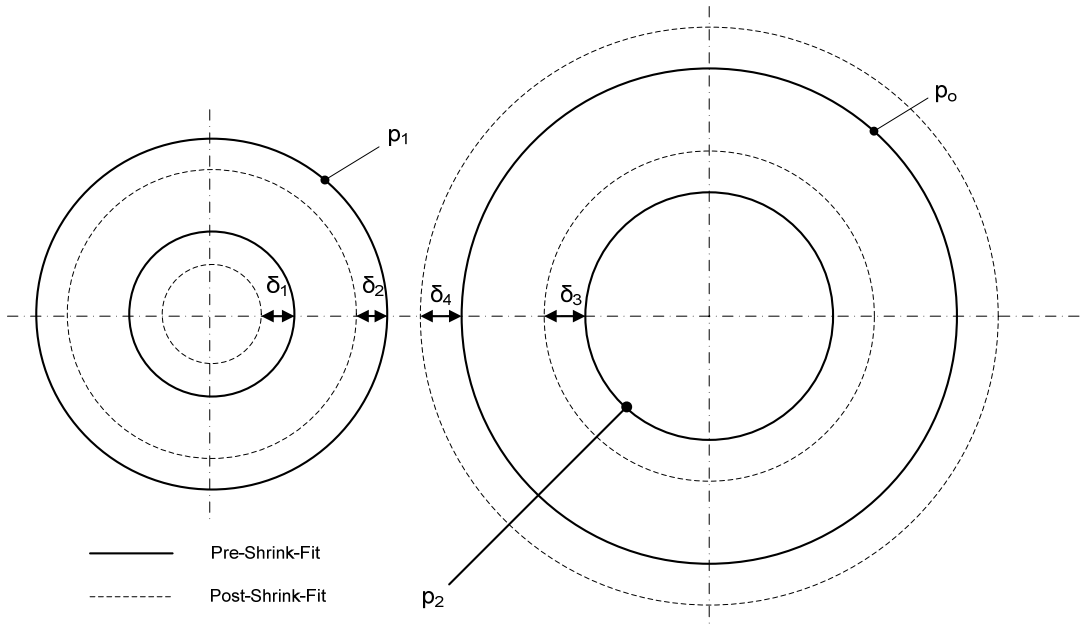

Figure 3.4. The deformation of cylinders under interface pressure

Total interface displacement is:

$$\delta_T = \delta_2 + \delta_3 = C_1 b + \frac{C_2}{b} + C_3 c + \frac{C_4}{c} \tag{3.28.}$$

And the pre-shrink fit dimensions, in terms of post-shrink fit radial dimension R:

$$a = R - \delta_1 \tag{3.29.}$$

$$b = a + t_1 \tag{3.30.}$$

$$c = b - \delta_T \tag{3.31.}$$

$$d = c + t_2 \tag{3.32.}$$

3.1.2. Calculation of the Stress Equations for Post-Shrink Fit Case (Superposition Principle)

So far, it was dealt with the stresses and deformations under only interface pressure caused by the shrink-fit. Now stress constants and stress equations were investigated in the situation that both interface and operating pressures are exerted on the cylinder pairs. The superposition method will be used to perform the calculation. Based on this method, the stresses caused by interface pressure and operating pressure will be superposed to find the resultant stress components.

I. Boundary Conditions and Calculation of Stress Constants for Post-Shrink Fit under only Interface Pressure

Now, it will be assumed that, the cylinders are on only interface pressure, p, the boundary conditions are:

a) Radial stress at the inner surface of the inner cylinder.

$$\sigma_r = 0 \ @ \ r = R$$

$$0 = \frac{E_1}{1-\mu_1^2}\left(C_{1s}(1+\mu_1) - C_{2s}\frac{1-\mu_1}{R^2} \right) \qquad (3.33.)$$

b) Radial stress at the outer surface of the inner cylinder and inner surface of the outer cylinder.

$$-p = \sigma_r \ @ \ r = G$$

$$-p = \frac{E_1}{1-\mu_1^2}\left(C_{1s}(1+\mu_1) - C_{2s}\frac{1-\mu_1}{G^2} \right) \qquad (3.34.)$$

$$-p = \frac{E_2}{1-\mu_2^2}\left(C_{3s}(1+\mu_2) - C_{4s}\frac{1-\mu_2}{G^2} \right) \qquad (3.35.)$$

c) Radial stress at the outer surface of the outer cylinder.

$$\sigma_r = 0 \ @ \ r = M$$

$$0 = \frac{E_2}{1-\mu_2^2}\left(C_{3s}(1+\mu_2) - C_{4s}\frac{1-\mu_2}{M^2} \right) \tag{3.36.}$$

Using equations 3.33., 3.34., 3.35., 3.36.; C_{1s}, C_{2s}, C_{3s}, C_{4s}, can be obtained:

$$\left\{\left\{C1s \to \frac{G^2\, p\, (-1+\mu 1)}{E1\, (G^2-R^2)},\ C2s \to -\frac{G^2\, p\, R^2\, (1+\mu 1)}{E1\, (G^2-R^2)},\ C3s \to \frac{G^2\, p\, (-1+\mu 2)}{E2\, (G^2-M^2)},\ C4s \to -\frac{G^2\, M^2\, p\, (1+\mu 2)}{E2\, (G^2-M^2)}\right\}\right\}$$

In pretty form:

$$C_{1s} = \frac{\mu_1 - 1}{E_1} \cdot \frac{G^2 p}{(G^2 - R^2)} \tag{3.37.}$$

$$C_{2s} = -\frac{\mu_1 + 1}{E_1} \cdot \frac{G^2 R^2 p}{(G^2 - R^2)} \tag{3.38.}$$

$$C_{3s} = \frac{\mu_2 - 1}{E_2} \cdot \frac{G^2 p}{(G^2 - M^2)} \tag{3.39.}$$

$$C_{4s} = -\frac{\mu_2 + 1}{E_2} \cdot \frac{G^2 M^2 p}{(G^2 - M^2)} \tag{3.40.}$$

Then only under interface pressure, the radial and tangential stress equations for inner and outer cylinders are:

$$\sigma_{r11} = \frac{E_1}{1-\mu_1^2}\left(C_{1s}(1+\mu_1) - C_{2s}\frac{1-\mu_1}{r^2} \right) \tag{3.41.}$$

$$\sigma_{t11} = \frac{E_1}{1-\mu_1^2}\left(C_{1s}(1+\mu_1) + C_{2s}\frac{1-\mu_1}{r^2} \right) \quad (3.42.)$$

$$\sigma_{r21} = \frac{E_2}{1-\mu_2^2}\left(C_{3s}(1+\mu_2) - C_{4s}\frac{1-\mu_2}{r^2} \right) \quad (3.43.)$$

$$\sigma_{t21} = \frac{E_2}{1-\mu_2^2}\left(C_{3s}(1+\mu_2) + C_{4s}\frac{1-\mu_2}{r^2} \right) \quad (3.44.)$$

II. Boundary Conditions and Calculation of Stress Constants for Post-Shrink Fit Under only Operating Pressure

Now the same assumptions are made for the only inner and outer pressures:

a) Radial Stress for inner surface of inner cylinder is:

$$\sigma_r = -p_i \ @ \ r = R$$

$$-p_i = \frac{E_1}{1-\mu_1^2}\left(C_{1ss}(1+\mu_1) - C_{2ss}\frac{1-\mu_1}{R^2} \right) \quad (3.45.)$$

b) Radial stresses at the interface of the cylinders are:

$$\sigma_r^1 = \sigma_r^2 \ @ \ r = G$$

$$\frac{E_1}{1-\mu_1^2}\left(C_{1ss}(1+\mu_1) - C_{2ss}\frac{1-\mu_1}{G^2} \right) = \frac{E_2}{1-\mu_2^2}\left(C_{3ss}(1+\mu_2) - C_{4ss}\frac{1-\mu_2}{G^2} \right) \quad (3.46.)$$

c) Radial displacement at the interface of the cylinders are equal and:

$$u^1 = u^2 \ @ \ r = G$$

$$C_{1ss}G + \frac{C_{2ss}}{G} = C_{3ss}G + \frac{C_{4ss}}{G} \quad (3.47.)$$

d) Radial stress at the outer surface of the outer cylinder:

$$\sigma_r = p_o \ @ \ r = M$$

$$p_o = \frac{E_2}{1-\mu_2^2}\left(C_{3ss}(1+\mu_2) - C_{4ss}\frac{1-\mu_2}{M^2} \right) \tag{3.48.}$$

And using the equations (3.45.), (3.46.), (3.47.), (3.48.),

$$\left\{\left\{ C1ss \to \frac{(-1+\mu1)\ (E2\ (G-M)\ (G+M)\ pi\ R^2\ (1+\mu1) + E1\ (G^2\ (2\ M^2\ po - pi\ R^2\ (-1+\mu2)) + M^2\ pi\ R^2\ (1+\mu2)))}{E1\ (E2\ (G-M)\ (G+M)\ (-G^2\ (-1+\mu1) + R^2\ (1+\mu1)) + E1\ (G-R)\ (G+R)\ (G^2\ (-1+\mu2) - M^2\ (1+\mu2)))},\right.$$

$$C2ss \to -\frac{G^2\ R^2\ (1+\mu1)\ (E2\ (G-M)\ (G+M)\ pi\ (-1+\mu1) + E1\ (G^2\ (pi - pi\ \mu2) + M^2\ (pi + 2\ po + pi\ \mu2)))}{E1\ (E2\ (G-M)\ (G+M)\ (-G^2\ (-1+\mu1) + R^2\ (1+\mu1)) + E1\ (G-R)\ (G+R)\ (G^2\ (-1+\mu2) - M^2\ (1+\mu2)))},$$

$$C3ss \to \frac{(-1+\mu2)\ (E2\ (G^2\ (2\ pi\ R^2 - M^2\ po\ (-1+\mu1)) + M^2\ po\ R^2\ (1+\mu1)) + E1\ M^2\ po\ (G-R)\ (G+R)\ (1+\mu2))}{E2\ (E2\ (G-M)\ (G+M)\ (-G^2\ (-1+\mu1) + R^2\ (1+\mu1)) + E1\ (G-R)\ (G+R)\ (G^2\ (-1+\mu2) - M^2\ (1+\mu2)))},$$

$$\left. C4ss \to -\frac{G^2\ M^2\ (E2\ (G^2\ (po - po\ \mu1) + R^2\ (2\ pi + po + po\ \mu1)) + E1\ po\ (G-R)\ (G+R)\ (-1+\mu2))\ (1+\mu2)}{E2\ (E2\ (G-M)\ (G+M)\ (-G^2\ (-1+\mu1) + R^2\ (1+\mu1)) + E1\ (G-R)\ (G+R)\ (G^2\ (-1+\mu2) - M^2\ (1+\mu2)))} \right\}\right\}$$

As seen from the output of the Mathematica, solutions have too many parameters which will be a trouble in programming. So root reduction must be made:

$$X_1 = \frac{E_1}{1-\mu_1^2} \quad X_2 = 1+\mu_1 \quad X_3 = 1-\mu_1 \tag{3.49.}$$

$$Y_1 = \frac{E_2}{1-\mu_2^2} \quad Y_2 = 1+\mu_2 \quad Y_3 = 1-\mu_2 \tag{3.50.}$$

So the equations (3.45.), (3.46.) and (3.48.) will become:

$$-p_i = X_1\left(C_{1ss}(X_2) - C_{2ss}\frac{X_3}{R^2} \right) \tag{3.51.}$$

$$X_1\left(C_{1ss}(X_2) - C_{2ss}\frac{X_3}{G^2} \right) = Y_1\left(C_{3ss}(Y_2) - C_{4ss}\frac{Y_3}{G^2} \right) \tag{3.52.}$$

$$p_o = Y_1\left(C_{3ss}(Y_2) - C_{4ss}\frac{Y_3}{M^2} \right) \tag{3.53.}$$

Then the following solution is obtained:

$$\left\{\left\{C1ss \to \frac{M^2\,pi\,R^2\,Y2\,(X1X3 - Y1Y3) + G^2\,(pi\,R^2\,(X1X3 + Y1Y2)\,Y3 + M^2\,po\,X1X3\,(Y2 + Y3))}{X1\,(M^2\,(G-R)\,(G+R)\,X1X2X3Y2 + (G^2\,(G-R)\,(G+R)\,X1X2X3 - (G-M)\,(G+M)\,(R^2X2 + G^2X3)\,Y1Y2)\,Y3)},\right.\right.$$

$$C2ss \to \frac{G^2R^2\,(G^2\,pi\,(X1X2 - Y1Y2)\,Y3 + M^2\,(po\,X1X2\,(Y2 + Y3) + pi\,Y2\,(X1X2 + Y1Y3)))}{X1\,(M^2\,(G-R)\,(G+R)\,X1X2X3Y2 + (G^2\,(G-R)\,(G+R)\,X1X2X3 - (G-M)\,(G+M)\,(R^2X2 + G^2X3)\,Y1Y2)\,Y3)},$$

$$C3ss \to \frac{M^2\,po\,R^2X2\,(-X1X3 + Y1Y3) + G^2\,(pi\,R^2\,(X2 + X3)\,Y1Y3 + M^2\,po\,X3\,(X1X2 + Y1Y3))}{M^2\,(G-R)\,(G+R)\,X1X2X3Y1Y2 - Y1\,(-G^2\,(G-R)\,(G+R)\,X1X2X3 + (G-M)\,(G+M)\,(R^2X2 + G^2X3)\,Y1Y2)\,Y3},$$

$$\left.\left.C4ss \to \frac{G^2M^2\,(G^2\,po\,X3\,(-X1X2 + Y1Y2) + R^2\,(pi\,(X2 + X3)\,Y1Y2 + po\,X2\,(X1X3 + Y1Y2)))}{M^2\,(G-R)\,(G+R)\,X1X2X3Y1Y2 - Y1\,(-G^2\,(G-R)\,(G+R)\,X1X2X3 + (G-M)\,(G+M)\,(R^2X2 + G^2X3)\,Y1Y2)\,Y3}\right\}\right\}$$

Then the radial and tangential stresses for inner cylinder under only operating pressures can be calculated as this:

$$\sigma_{r12} = \frac{E_1}{1-\mu_1^2}\left(C_{1ss}(1+\mu_1) - C_{2ss}\frac{1-\mu_1}{r^2}\right) \tag{3.54.}$$

$$\sigma_{t12} = \frac{E_1}{1-\mu_1^2}\left(C_{1ss}(1+\mu_1) + C_{2ss}\frac{1-\mu_1}{r^2}\right) \tag{3.55.}$$

And for outer cylinder, the equations are:

$$\sigma_{r22} = \frac{E_2}{1-\mu_2^2}\left(C_{3ss}(1+\mu_2) - C_{4ss}\frac{1-\mu_2}{r^2}\right) \tag{3.56.}$$

$$\sigma_{t22} = \frac{E_2}{1-\mu_2^2}\left(C_{3ss}(1+\mu_2) + C_{4ss}\frac{1-\mu_2}{r^2}\right) \tag{3.57.}$$

3.1.3. Calculation of Radial Displacement and Interface Pressure

Substituting equations (3.20.), (3.49.), (3.50.), and (3.29.), into (3.24.) gives:

$$-\frac{p\,(X2 + X3)\,(R + \delta 1)\,(R + t1 + \delta 1)^2}{E1\,t1\,(2R + t1 + 2\delta 1)}$$

In pretty form:

$$\delta_1 = -\frac{p(X_2 + X_3)(R + \delta_1)(R + t_1 + \delta_1)^2}{E_1 t_1 (t_1 + 2R + 2\delta_1)} \tag{3.58.}$$

So, δ_2, δ_3, and δ_4 can be calculated similarly.

It is an expression between δ_1 and p, one equation and two unknowns. To solve this, it is required to find another expression between them. For example equation 3.28. can be used. If δ_1 and δ_2 is substituted into this equation, another equation will be obtained. The solution of this two equations is analytically hard to solve (it is extremely time consuming even today's computation technology). But if constants are substituted for a specific situation. The initial parameters of this situation are shown below in Table 3.1..

Table3.1. The parameters set by programmer to obtain a specific result

Parameter	Value	Parameter	Value	Parameter	Value
p_o	0	μ_1	0,292	S_{y1}	1570×10^6
p_i	30×10^7	μ_2	0,292	S_{y2}	1620×10^6
R	0,016	E_1	207×10^9	α_1	11×10^{-6}
δT	7×10^{-5}	E_2	207×10^9	S_{ep1}	700×10^6
$t1$	0,022	S_{ut1}	1720×10^6	S_{ep2}	700×10^6
$t2$	0,040	S_{ut2}	1760×10^6		

The output of the Mathematica is shown below:

```
{{p → -1.72856×10^11, δ1 → -0.024621},
 {p → -2.99675×10^10, δ1 → 0.0750851},
 {p → 2.58353×10^8, δ1 → -0.0000483616},
 {p → 3.88124×10^11, δ1 → -0.0613505},
 {p → 4.7696×10^16, δ1 → -0.0379575}}
```

This is a real problem. There must be only one solution in used pressure interval. But there are six. The rest are redundant. But which is true? To solve this problem, a numerical approach is used in the study. The result of the numeric calculation is:

$\{\delta 1 \to -0.0000483616, p \to 2.58353 \times 10^8\}$

As seen in output, numerical solution is correct because numerical solution exists in analytical solution list.

3.2. Temperature Calculations on Shrink Fits

As it is given previously, to produce a shrink fit, outer cylinder must be heated to a certain level for expansion. The inner radius of the outer cylinder increases and rises above the outer radius of the inner cylinder. Then inner cylinder is fixed to the inner hole of the outer cylinder. The assembly then cools and inner hole of the outer cylinder shrinks. The contraction applies a contact pressure to the outer surface of the inner cylinder. Temperature change produces a strain, called thermal strain, even the absence of stress. Although thermal strain is not exactly linear with temperature change, for temperature changes of 30°C or 100°C, the actual variation can be closely described by a linear approximation. According to this linear relationship the temperature difference through which the outer component (hub) must be heated to obtain the required expansion over the undeformed solid shaft is:

$$\Delta t_m = \frac{\delta_r}{\bar{a} r_f} \tag{3.59.}$$

Where, $\bar{a}$ is the coefficient of linear thermal expansion it is 11,2x10^{-6} 1/°C for AISI 4140 steel.

Equation (3.59.) can be expressed in terms of radial strain as

$$\varepsilon_r = \frac{\delta_r}{r_f} = \bar{a} \Delta t_m \tag{3.60.}$$

And the total strain is:

$$\delta_r = \varepsilon_r r_f = \bar{a}\Delta t_m r_f \tag{3.61.}$$

To calculate required temperature difference, the δ_T is leaved alone with using equation 3.61. And it is:

$$\Delta t_m = \frac{\delta_T}{c\alpha} \tag{3.62.}$$

3.3. Design for Fatigue Strength

Intensifiers that are used in double acting or phased type water-jet systems operate under fluctuating stresses. This is because as the one side of high pressure cylinder is subjected to high pressure during the compression stage, other side is subjected to low pressure during refilling stage. Continuous operation results in sinusoidal fluctuating stresses. Therefore, the cylinders are subjected to repeated low and high pressures which resulting fluctuating stresses on the walls.

For the design of multi-layer structures, the static failure design and fatigue theories have to be considered respectively. Failure analysis of ductile materials can be realized by means of ductile material failure theories. These theories are; the maximum-shear-stress theory (Tresca's yield criteria) and distortion-energy theory (Von-Misses yield criteria).

Since the distortion energy theory predicts failure most accurately as seen in figure 3.5.

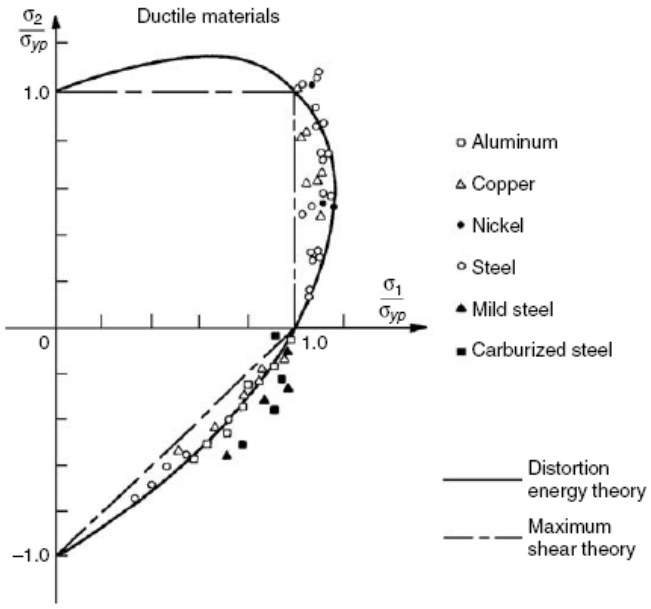

Figure 3.5. Comparison of maximum-shear-stress theory and distortion-energy theory with different materials (Collins, J. 1991, from CRC Handbook of Mechanical Engineering)

The distortion-energy theory states that, yielding begins when the total strain energy stored in the stressed element reaches a critical value, and it becomes:

$$\sigma' = \frac{1}{\sqrt{2}}\sqrt{(\sigma_1 - \sigma_2)^2 + (\sigma_1 - \sigma_3)^2 + (\sigma_2 - \sigma_3)^2} \qquad (3.63.)$$

Designation of the Stresses:

In later sections, some subscript numbers will be used with the stress signs. For example: "σ_{r12}"

Here, "*r*" means radial, in a similar way, "*l*" and "*t*" will represent longitudinal and tangential respectively. Then the first digit represents the inner cylinder or outer cylinder. Subscript "$_1$", and "$_2$" is used to identify inner and outer cylinder respectively. The second digit in the subscript designates whether the stress component is caused by inner and outer pressures or shrink fit situation. In the second subscript, "$_1$" represents interface pressure case, and "$_2$" represents inner case.

3.3.1. Determination of Minimum Stresses on Cylinder Walls

Minimum stresses results from interface pressure when there is no pressure inside cylinders. In other means, this condition occurs during refilled cylinder. Based on static failure theory, minimum values of stresses for inner and outer cylinders can be calculated.

For inner cylinder of the multi-layer intensifier, the radial, tangential, and longitudinal stresses under only interface pressure are called minimum stress components acting on cylinder walls and presented by σ_{r11}, σ_{t11}, σ_{l11}, respectively. Using the distortion-energy theory, minimum stress value is obtained as:

$$\sigma_{1\min} = \frac{1}{\sqrt{2}}\sqrt{(\sigma_{r11}-\sigma_{t11})^2+(\sigma_{r11}-\sigma_{l11})^2+(\sigma_{l11}-\sigma_{t11})^2} \qquad (3.64.)$$

For outer cylinder of the intensifier, the radial, tangential, and longitudinal stresses are presented by σ_{r21}, σ_{t21}, σ_{l21}, respectively. Then the minimum stress value for outer cylinder is:

$$\sigma_{2\min} = \frac{1}{\sqrt{2}}\sqrt{(\sigma_{r21}-\sigma_{t21})^2+(\sigma_{r21}-\sigma_{l21})^2+(\sigma_{l21}-\sigma_{t21})^2} \qquad (3.64.)$$

3.3.2. Determination of Maximum Stresses on Cylinder Walls

In determination of the maximum principal stress acting on the cylinders, all pressures acting on it must be superposed up. These pressures are:

a- Stresses caused by operating pressure.

b- Stresses caused by the shrink fit.

For inner cylinder, the maximum total radial, tangential and longitudinal stress components are:

$$\sigma_{r1} = \sigma_{r11} + \sigma_{r12} \tag{3.65.}$$

$$\sigma_{t1} = \sigma_{t11} + \sigma_{t12} \tag{3.66.}$$

$$\sigma_{l1} = \sigma_{l11} + \sigma_{l12} \tag{3.67.}$$

Using distortion-energy theory, maximum stress can be calculated for inner cylinder:

$$\sigma_{1\max} = \frac{1}{\sqrt{2}}\sqrt{(\sigma_{r1} - \sigma_{t1})^2 + (\sigma_{r1} - \sigma_{l1})^2 + (\sigma_{l1} - \sigma_{t1})^2} \tag{3.68.}$$

For outer cylinder, the maximum radial, longitudinal and tangential stress values are obtained as:

$$\sigma_{r2} = \sigma_{r21} + \sigma_{r22} \tag{3.69.}$$

$$\sigma_{t2} = \sigma_{t21} + \sigma_{t22} \tag{3.70.}$$

$$\sigma_{l2} = \sigma_{l21} + \sigma_{l22} \tag{3.71.}$$

Then the maximum equivalent stress is:

$$\sigma_{2\max} = \frac{1}{\sqrt{2}}\sqrt{(\sigma_{r2} - \sigma_{t2})^2 + (\sigma_{r2} - \sigma_{l2})^2 + (\sigma_{l2} - \sigma_{t2})^2} \tag{3.72.}$$

In fatigue failure analysis, the Modified Goodman Line is the main method (See figure 3.6.). With this diagram, only two of the stress components are used. The endurance limit, fatigue strength, or finite life strength, whichever applies to the particular problem, is the limiting value of the stress amplitude, and so it is plotted on

the ordinate. A straight line from S_e to S_u on the abscissa is also the Modified Goodman Criterion of failure.

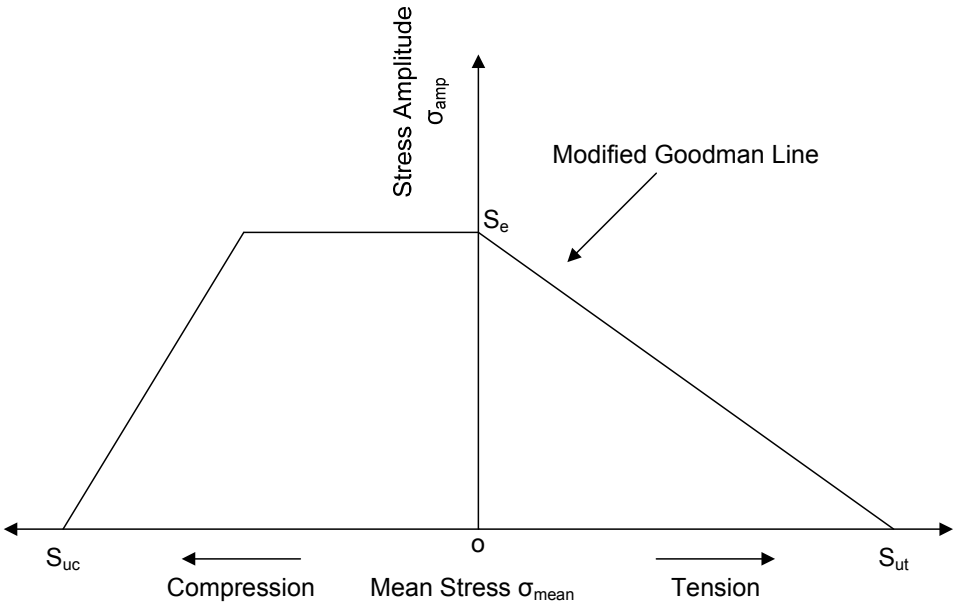

Figure 3.6. Modified Goodman Line (Shigley, 1986)

The amplitude and the mean stress values are calculated based on Shigley, 1986:

$$\sigma_{mean} = \frac{\sigma_{\max} + \sigma_{\min}}{2} \tag{3.73.}$$

$$\sigma_{amp} = \frac{\sigma_{\max} - \sigma_{\min}}{2} \tag{3.74.}$$

And due to this criterion the factor of safety of the each cylinder is:

$$FS = \frac{1}{\frac{\sigma_{mean}}{S_{ut}} + \frac{\sigma_{amp}}{S_e}} \tag{3.75.}$$

Where, S_e is endurance limit and given as a function of some modifiers:

$$S_e = k_a \cdot k_b \cdot k_c \cdot k_d \cdot k_e \cdot k_f \cdot S_{ep} \quad (3.76.)$$

Where

k_a : Surface Factor and equals unity for polished surfaces.

k_b : Size Factor

k_c : Reliability Factor

k_d : Temperature Factor equals unity for the operating conditions below 350^{o}C

k_e : Stress Concentration Factor.

k_f : Miscellaneous Effects Factor

S_{ep} : Endurance Limit of the Rotating Test Specimen

For this condition, S_{ep} can be calculated by this formula (Marghitu, 2005):

$$S_{ep} = 700 \text{ MPa for } S_{ut} > 1400 \text{ MPa} \quad (3.77.)$$

Modifiers that had given by Shigley (1986). are as follows:

$k_a = 1$ Operating surface was honed.

To calculate the size factor, effective diameter of the cylinders must be calculated first. According to Shigley, the effective cylinder must have the 95% area of the stressed region of hollow shaft. The outer cylinder has a stress resource in only one side. So, the effective diameter of the outer cylinder is:

$$d_{e2} = 1000 \cdot \sqrt{0{,}95 \cdot \left((2M)^2 - (2G)^2\right)}$$

And the k_{b2} is

$k_{b2} = 1{,}189 d_{e2}^{-0{,}097}$ for 8mm<d_{e2}<250mm

Beside the outer cylinder, inner cylinder is stressed from both sides and the stressed Area is

$$d_{e1} = 1000 \cdot \sqrt{(2G)^2 - (2R)^2}$$

And,

$k_{b1} = 1{,}189 d_{e1}^{-0{,}097}$ for 8mm<d_{e1}<250mm

$k_c = 1$ The reliability of the endurance limits for two cylinders are taken 50% according to the 8% standard deviation of the endurance limit.

$k_d = 1$ Operating temperature is below 350°C.

$k_e = 1$ There are no stress concentration points such as grooves, notches.

$k_f = 0{,}7$ (There is allowable corrosion on the outer cylinder. Beside this, there is no plating, no cyclic frequency at high temperatures. But there is so much pressure on interface point in elastic range causing frettage.

And endurance limit of the intensifier cylinder was calculated as shown in the following equation. (Shigley, 1986):

$$S_e = k_a \cdot k_b \cdot k_c \cdot k_d \cdot k_e \cdot k_f \cdot S_{ep} \quad (3.78.)$$

3.4. Software Development: Determination of Water Cylinder Dimensions Using Mathematica

A program has been developed by using Mathematica programming language for determining the pre-shrink fit dimensions, interface pressure, all components of stresses acting on both cylinders, and factor of safeties for both cylinders. The program is called as DPro-MLWJI and the program inputs are:

- Post shrink fit dimension of inner cylinders inner radius *R*. If this dimension is known, the required piston dimensions will be predictable for design.
- Total interface displacement δ_T between two cylinders.
- Pre-shrink thicknesses of inner and outer cylinders t_1 and t_2.
- Inner and outer hydraulic pressure P_i and P_o.
- Poisson's Ratio of both inner and outer cylinders μ_1 and μ_2.
- Elasticity Modulus of inner and outer cylinders E_1 and E_2 respectively.
- Ultimate tensile strength of inner and outer cylinders S_{ut1} and S_{ut2}.

3.4.1. Explanation of the Steps of Program DPro-MLWJI

DPro-MLWJI is in the Appendix B and step numbers can be read from there. Here are the steps of program in appendix and meanings respectively:

Step1: Mathematica® gives warning if similar terms are used in the programming. For example μ_1 and μ_2. This command string prevents unnecessary warning messages.

Step2: The inputs about the working conditions and design parameters are expressed. The semicolons are put to prevent the confirmation outputs.

Step3: The inputs about the material property constants are entered. Endurance limits of the test specimens are calculated using equations (3.77.) and (3.78.).

Step4: The "X" values collect the repeating terms in the equations. So it reduces the complexity of the equations. They are calculated based on the equations (3.49.) and (3.50.).

Step5: This step calculates the pre-shrink fit dimensions based on equations (3.29.), (3.30.), (3.31.), and (3.32.).

Step6: This step calculates stress constants that is calculated for the pre-shrink fit situation based on equations (3.16.), (3.17.), (3.18.), (3.19.).

Step7: This step calculates the total deformation values of the inner and outer surfaces of the both cylinders based on the equations (3.25.), (3.26.), (3.27.).

Step8: There are two equations and two unknowns here. Equation at the top is taken from the output 4. from the Appendix A. The second equation is produced from the substitution of the deformation values into equation (3.28.). To solve this simultaneous system, "Solve" command was used. Mathematica solves the system by substituting the numeric constants. The pressure and deformation values are shown in output. One of them is real and the other are redundant.

Step9: "FindRoot" command finds the root of the system by numerically way. Starting the values of:

$\delta_1 = -0{,}0010m$ And $p = 1.000.000Pa$

And the result or output is the subset of the previous output sets with only one element. Thus the solution is correct and accurate.

Step10: This step assigns the last found results for δ_1 and p to them again. "%" means previous result here and "%%" means two times previous.

Step11: This step calculates required heating temperature of the outer cylinder to shrink fit. It is based on the equation (3.62)

Step12: This step calculates the post shrink fit dimensions and the effective diameters of the cylinders for size factor calculations. This will be used in endurance limit calculations.

Step13: The endurance limit modifying factors are calculated and assigned. And the endurance limit of the cylinders are calculated.

Step14: This step calculates the stress constants under only interface pressure based on equations (3.37.), (3.38.), (3.39.), and (3.40.).

Step15: This step calculates the stress constants under only operating pressure.

Step16: This step calculates the radial, tangential, and longitudinal stresses for inner cylinder in only operating pressure and in only interface pressure separately.

Step17: This step calculates the total radial, longitudinal and tangential stresses of the inner cylinder.

Step18: This step calculates the minimum and maximum stresses that is yielded in the inner cylinder; and using these, it calculates the mean and amplitude stresses.

Step19: In this step, the factor of safety of the inner cylinder is calculated.

Step20: This step calculates the radial, tangential, and longitudinal stresses for outer cylinder in only operating pressure and in only interface pressure separately.

Step21: This step calculates the total radial, longitudinal and tangential stresses of the outer cylinder.

Step22: This step calculates the minimum and maximum stresses that is yielded in the inner cylinder; and using these, it calculates the mean and amplitude stresses.

Step23: In this step, the factor of safety of the outer cylinder is calculated.

Step24: This step represents of the all calculated variable in table form. "N" at the beginning of the sentence represents that, results must be numeric, not to be rational or other kinds.

Step25: Is to clear the all saved data to prevent the assignment errors in next iteration.

3.4.2. Flow Diagram of the DPro-MLWJI

The flow diagram of the DPro-MLWJI program is given in figure 3.7. After opening the Mathematica® notebook of DPro-MLWJI, the inputs about P_o, R, P_i, δ_T, t_1, t_2 and material properties are entered into the program. Then, "*Kernel>Evaluation>Evaluate Notebook*" command is entered into the program (or simply press Numpad-Enter, or Shift+Enter). After this command, all of the terms in the notebook will be calculated in a predefined order. The flowchart below shows the main steps of calculation sequence.

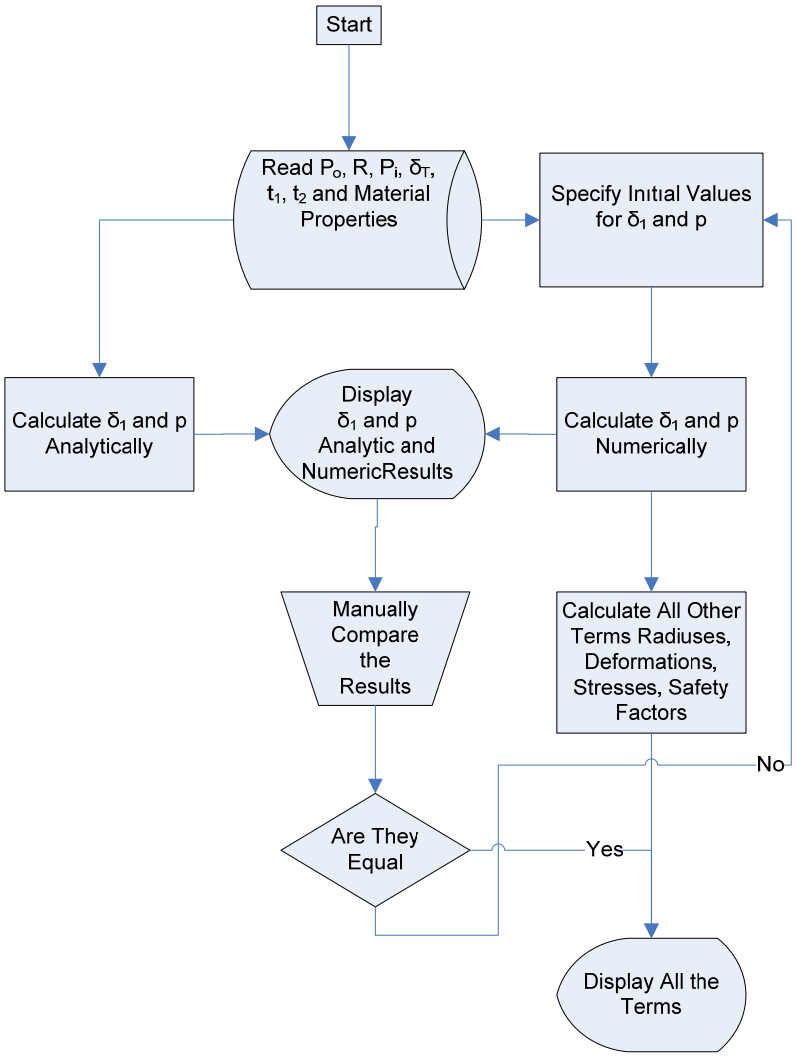

Figure 3.7. The flowchart of the DPro-MLWJI program.

The program firstly reads the values and assigns the basic inputs, and firstly calculate the δ_1 and p analytically as mentioned in Section 3.1.4, after that it calculates them numerically again. Then according to the solution of both parameters, program will calculate the all other parameters. But, the important point in here is, the results will be correct in only and only if numeric solution of the δ_1 and p exists in the analytical solution set.

3.5. Running DPro-MLWJI for Water Jet Intensifier Cylinders Having "n" Layers

DPro-MLWJI program was written for all kinds of cylindrical ultra high pressure two-layer containers those are subject of fluctuating stresses. For containers having more than two layers, the program can also be used. Because in the assumptions accepted before coding the program there is one article. The cylinders are thick and the interface pressure does not affect by the variations in the dimensions due to the other pressures.

The above assumption was used to run DPro-MLWJI in calculation of the safety factors of all layers. This section explains how the program can be run and how the inputs are assigned to reach correct results and avoid the mistakes. Table 4.8. provides the meaning of inputs that are used in the program.

Table 3.2. The program inputs that were changed during the calculation of the one layer of the n layer.

p_i	Operating pressure
R	Post-shrink fit inner radius of inner cylinder
t_1	Inner cylinder thickness
t_2	Outer cylinder thickness
E1	Elasticity modulus of the inner cylinder
E2	Elasticity modulus of the outer cylinder
δ_T	Total interface displacement
μ_1	Poisson's ratio of the inner cylinder
μ_2	Poisson's ratio of the inner cylinder

The n-layer cylinder is assumed to have n different layers concentric with each other. The number of innermost cylinder is "1". As the number increases, the distance of the cylinder to the origin also increases. This number is used as subscript in defining the properties of that cylinder. The innermost cylinder has a radius of r_1, a thickness of t_1, an elasticity modulus of E_1 and a young modulus of μ_1. The number of the cylinders between two are called as "2,3,4,…,n-2,n.-1" The number of the outermost cylinder is "n". r_n is the inner radius and t_n is the thickness, E_n is the

elasticity modulus and μ_n is the Poisson's ratio of this "n'th" cylinder. The number of the cylinders which are inside of the outermost cylinder are going as "n-1", "n-2",…

The DPro-MLWJI calculates the stresses and the factors of safeties for only two cylinders. Thus, firstly the properties of n'th cylinder are assigned to the second cylinder constants as program variables of the outer cylinders. And the constant properties of cylinder numbered as "n-1" is assigned to the inner cylinder properties section in the program. But differently, it must be assumed that the whole cylinders inside are unique. The assignments of the properties of the outermost cylinder are shown in the table 4.9. below. It must not be forgotten in this situation that the operating pressure "p_i" must be kept the same in all of the iterations.

Table 3.3. The program inputs and the values assigned to them for the outermost cylinder.

Assigned Value	Program Input
t_n	t_2
$\sum_{k=1}^{n-1} t_k$	t_1
E_n	E_2
E_{n-1}	E_1
μ_n	μ_2
μ_{n-1}	μ_1
δ_{Tn}	δ_T
S_{epn}	S_{ep2}
S_{epn-1}	S_{ep1}

After giving these values to the program inputs, some of the outputs are used. These are FS2 and p. FS2 is accepted as FSn; the p is accepted as p_n. Namely, the all outputs subscripted with the number 1 represent the properties of the cylinder named as "n-1"; similarly, the all outputs subscripted with the number 2 represent the properties of the cylinder named as "n" the Then the whole process is repeated with taking "n-1" instead of "n" and "n-2" instead of "n-1" till the number "n" reaches to 2. But some point in this problem must not be overlooked. The interface pressure between the shells "n" and "n-1" must be used as the outer pressure p_o as program input. The table 4.10. shows the difference below.

Table 3.4. The program inputs and the values assigned to them for the cylinder “n-1”.

Assigned Value	Program Input
t_{n-1}	t_2
$\sum_{k=1}^{n-2} t_k$	t_1
E_{n-1}	E_2
E_{n-2}	E_1
μ_{n-1}	μ_2
μ_{n-2}	μ_1
$\delta_{T(n-1)}$	δ_T
S_{epn-1}	S_{ep2}
S_{epn-2}	S_{ep1}
p_n	p_o

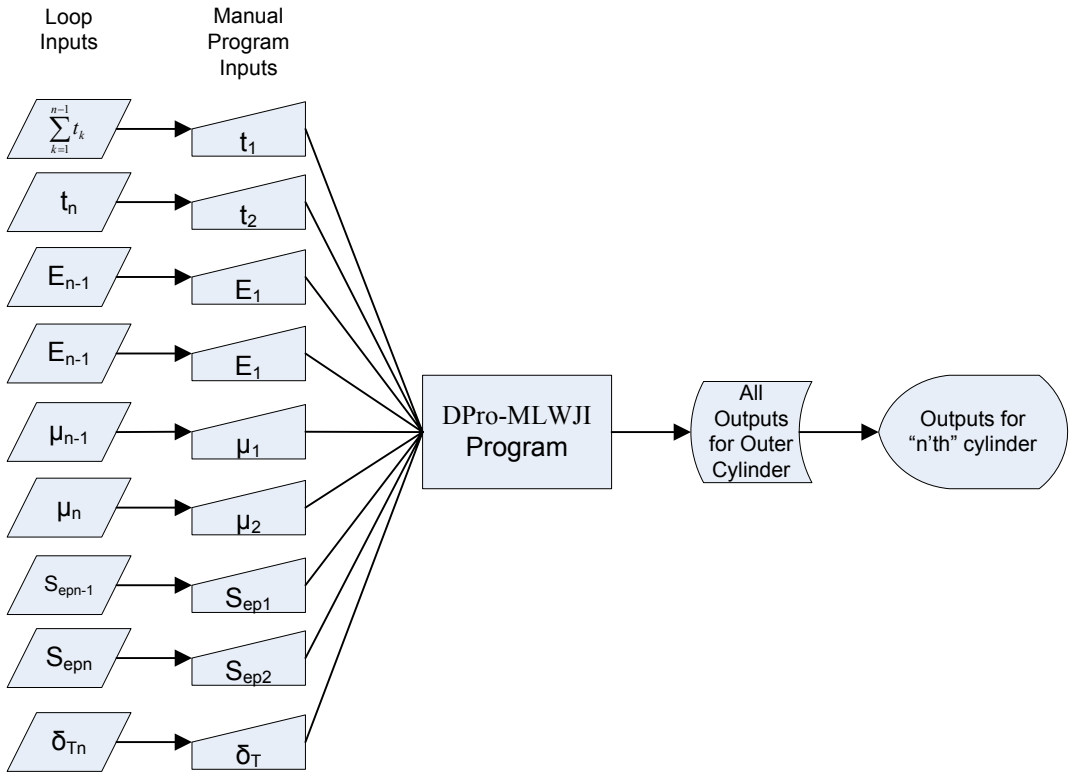

Figure 3.8. The graphical representation of the program input assignment in multi layer condition.

As seen in the figure 4.8., beginning from the outside, assignment of the outermost cylinder pair properties are assigned first. Then program outputs are assigned to the outermost cylinder properties. Then the second cylinder from outside is assumed the outer cylinder of the pair. During these assignments, the thickness of

the inner cylinder is assumed as the single pair with all of the cylinders inside. This process is repeated when the pair selection goes to the innermost cylinder pair.

4. RESULTS AND DISCUSSION

In this study, using the program "DPro-MLWJI", that is written in the previous section, firstly, the optimum design parameters were calculated with discrete optimization process. And an optimum point was calculated roughly. Then, using these results, the relationship between the design parameters and environmental conditions were investigated. Following section provides a methodology for intensifiers having multi layers (more than two layers).

4.1. Methodology of Finding the Optimum Design Parameters of Multi-layer Intensifier

The optimum design parameters for multi-layer intensifier are found in this study. The design program which is called "DPro-MLWJI" was run for different thickness values of the inner and the outer cylinders with changing total interface displacement values systematically. The program inputs about the material properties are given in the Table 4.1.

Table 4.1. The program inputs that is assigned for the specific materials according to the sample in the mechanical Engineering Department Laboratory.

Parameter	Value	Parameter	Value	Parameter	Value
p_o (Pa)	0	E_1 (Pa)	$207x10^9$	S_{y2} (Pa)	$1620x10^6$
p_i (Pa)	$3000x10^5$	E_2 (Pa)	$207x10^9$	α_1 (1/^{o}C)	$11,2x10^{-6}$
R (m)	0,016	S_{ut1} (Pa)	$1720x10^6$	S_{ep1} (Pa)	$700x10^6$
μ_1	0,292	S_{ut2} (Pa)	$1760x10^6$	S_{ep2} (Pa)	$700x10^6$
μ_2	0,292	S_{y1} (Pa)	$1570x10^6$	---	---

The material properties shown in the table 4.1. are the properties of the AISI 4140 steel for outer cylinder, and AISI 4340 steel for the inner cylinder according to the prototype in the laboratory of the Mechanical Engineering Department in University of Çukurova. There are three unknown parameters which are not available in the table left are the optimization parameters. These are δ_T(Total interface displacement), t_1(thickness of the inner cylinder), and t_2(thickness of the outer

cylinder). For the shrink fitting process, the outer cylinder must be heated to expand. The temperature requirement for this process was calculated in the "Material and Method" chapter. Calculations are added to the design programme. The temperature must be a constraint in the calculations for the optimization in order not to produce the morphological deformations on the outer cylinder materials. In other words, the temperature of the outer shell must not exceed the stress annealing temperature of the AISI 4140 steel that will be heated, and that is 200^{o}C.

First of all, 10 mm value was assigned to the thickness values of both the inner and the outer cylinder. Then, total interface displacement δ_T was increased in 10 μm increments starting with zero. It was seen that the inner cylinder is the critical cylinder, because the factor of safety of the inner cylinder was closer to the "0". The rise in the total interface displacement causes an increase in the factor of safety of the inner cylinder and decrease in factor of safety of outer cylinder. After many trial runs, the factor of safety of the inner cylinder began to drop after its optimum point. The maximum factor of safety of the inner cylinder, factor of safety of the outer cylinder and the total interface displacement in which the maximum factor of safety of the inner cylinder value is obtained are written to the excel sheet. Then this process was repeated for the different thickness values of both inner and outer cylinders in 5 mm resolution. The results for FS1 are given in the table 4.2.

Table 4.2. The Factor of safety values for inner cylinders at different thickness combinations.

---		t_2(mm)							
		10		*15*		*20*		*25*	
		FS1	**δ_T**	**FS1**	**δ_T**	**FS1**	**δ_T**	**FS1**	**δ_T**
t_1(mm)	*10*	1,02258	20	1,06389	10	---	---	---	---
	15	1,08994	40	1,11857	20	1,1394	20	---	---
	20	1,12473	60	1,14678	40	1,16291	30	1,17303	30
	25	1,14515	90	1,16152	60	1,17352	50	1,18347	40
	30	1,15461	100	1,16937	80	1,17899	60	---	---
	35	1,15744	110	1,17315	100	---	---	---	---
	40	1,15703	120	---	---	---	---	---	---

Table 4.2. shows the safety factor of the inner cylinder at different thickness combinations of the inner and the outer cylinders. As seen in table 4.2., the first calculation was started from the t_1=10 mm, t_2=10 mm values. Then along the row,

the outer cylinder thickness was increased by 5 mm increments. Along the column, the thickness of the inner cylinder was increased by 5 mm increments. The safety factor values for the inner cylinder and the total interface displacement values at that point were written. There are dark and light rows to follow the constant total thickness $t=t_1+t_2$ diagonals easier on table.

As seen, there is only two calculations for t_1=10 mm. When the third diagonal light cells (t=30 diagonal) are examined, (t_1=20, t_2=10 and t_1=15, t_2=15), the drop of the FS_1 value can be seen. This means that if the calculation was followed, the FS_1 value continues to drop down. So, it is not necessary to calculate the FS_1 anymore. So the required factor of safety value is between 1,1 and 1,2. To balance both the safety and the lightweight product. The safety requirement for this design was taken as 1,15.

Then first row was started to look for required factor of safety. First diagonal (t=20 mm) has the maximum safety of 1,02258 and that is below the requirement. For the second diagonal (t=25) the maximum safety factor is 1,08994. After a few diagonal, t=40 mm diagonal has the acceptable safety factor. When the thickness of the outer cylinder increases in this diagonal, the safety factor increases also, but the total interface displacement decreases and this produces the lack of safety. To balance the enough interface displacement value and safety factor value, t_1=25, t_2=15 box was chosen. The factor of safety of the outer cylinder was FS_2=2,72011

Then the optimum point is obtained as t_1=25 mm, t_2=15 mm, δ_T=60 μm. The resulting safety factors of both inner and the outer cylinders are FS_1=1,16152, FS_2=2,72011. It is the point for calculation that was done for the 5 mm resolution. If this work is repeated for 1 mm resolution to refine the results and make sensitive design, the calculation must be repeated for the boundaries of 5 mm near to the optimum result. As a result of this, the optimization must be repeated for t_1=20-30, t_2=10-20.

4.2. Stress Distributions through Radial Direction of Intensifier Cylinder Wall in Combined Loading

The radial tangential stress distributions along the radial direction are calculated in this section. The inputs are taken from the optimum value that is calculated in Chapter 4.1. Then the graphs of these data are plotted with the graph toolbox of the Mathematica by the program SDRD.

"Design Program for Multi Layer Water Jet Intensifier" DPro-MLWJI program was run using the values which are given in table 4.4. And table 4.5. provides the results of the program.

Table 4.3. The inputs of the DPro-MLWJI.

Parameter	Value	Parameter	Value	Parameter	Value
p_o (Pa)	0	μ_1	0,292	S_{y1} (Pa)	1570×10^6
p_i (Pa)	3000×10^5	μ_2	0,292	S_{y2} (Pa)	1620×10^6
R (m)	0,016	E_1 (Pa)	207×10^9	α_1 (1/°C)	$11{,}2 \times 10^{-6}$
δT (m)	6E-5	E_2 (Pa)	207×10^9	S_{ep1} (Pa)	700×10^6
$t1$ (m)	0,025	S_{ut1} (Pa)	1720×10^6	S_{ep2} (Pa)	700×10^6
$t2$ (m)	0,015	S_{ut2} (Pa)	1760×10^6	---	---

Table 4.4. The outputs of the DPro-MLWJI.

Parameter	Value (mm)	Parameter	Value (MPa)	Parameter	Value (MPa)
a	16,0171	p	93,6388	σ_{t1}	132,337
b	41,0171	p_i	300	σ_{t2}	81,0388
c	40,9571	σ_{r11}	0	σ_{l1}	53,9032
d	55,9571	σ_{r21}	-398,37	σ_{l2}	52,6399
R	16	σ_{r12}	-300	σ_{1min}	220,927
G	40,9973	σ_{r22}	-23,1175	σ_{1max}	398,945
M	56,0334	σ_{t11}	-220,927	σ_{2min}	400,719
δ_1	-0,0170983	σ_{t21}	4,65732	σ_{2max}	488,946
δ_2	-0,0198135	σ_{t12}	353,264	**Parameter**	**Value**
δ_3	0,0798135	σ_{t22}	76,3815	$FS1$	1,16152
δ_4	0,07634	σ_{l12}	53,9032	$FS2$	2,72011
δ_T	0,06	σ_{l22}	52,6399	**Parameter**	**Value (°C)**
t_1	25	σ_{r1}	-300	ΔT	130,799
t_2	15	σ_{r2}	-421,487	---	---

Stress Distribution along Radial Direction (SDRD) is calculated using the outputs by Mathematica language.

And for multi-loading condition (both interface pressure and inner pressure exerted simultaneously) the radial, tangential, and longitudinal stress distributions are calculated in terms of radial direction component "*r*", and these relationships are plotted.

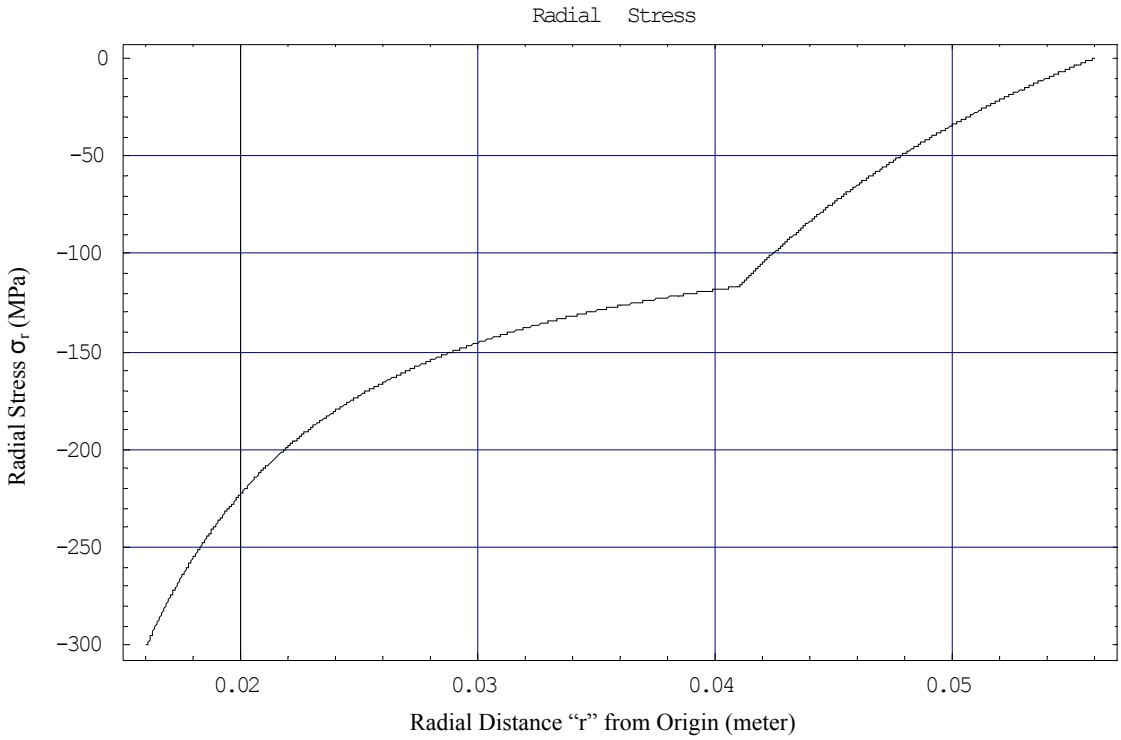

Figure 4.1. The radial stress distribution along radial direction.

Figure 4.1. gives "radial stress" distribution versus radial direction. The horizontal axis represents the radial distance taken from the axis origin of shells; the vertical axis is radial stress acting on the inner and outer parts. The resulting stress distribution has two zones. The zone on the left side is based on the calculations of inner shell; and the right side is based on the calculations of outer shell. The compressive radial stress acting on to the inner cylinder is starting from 300 MPa and decreasing in absolute value down to the 120 MPa level at the interface point. After the interface, this compressive stress decreases to nearly zero. This shows the

efficiency of the outer cylinder thickness. In addition to above, there is no jump in the stress distribution before and after the interface point. It is nearly continuous.

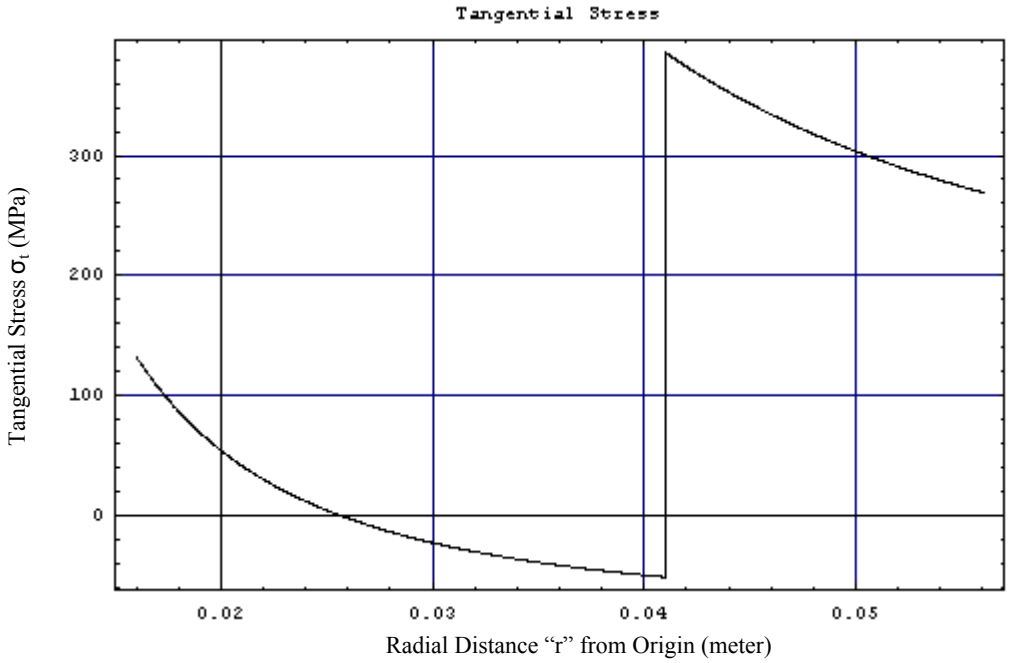

Figure 4.2. The tangential stress distribution along radial direction.

Figure 4.2. shows the distribution of the tangential stress component of the intensifier along the cylinder wall. As seen in figure 4.2. above, there are also two separate zones unlike the previous graph, the lines are in the positive zone. Tangential stress component is tensile and starting from 120 MPa at the inner surface of the inner cylinder and shallowly decreases down to zero at some point in the body of the inner cylinder and passes to the negative (compressive) zone. This means that the tangential component of stress begins tensile at the inner surface of the inner cylinder; but after some point (this point is nearly 24 mm in this situation) it turns to compressive stress up to the interface point. After passing the interface to the outside, there is a drastic change in pressure and tangential stress is positive. This stress gradually reduces down to 280 MPa. The maximum tensile stress is on the outer surface of the outer cylinder and the value of this stress is 380 MPa. This difference creates frettage problem causing the reduction in the endurance limit of the

intensifier unit when the loads are fluctuated. This phenomena is accounted with using the miscellaneous endurance limit modification factor k_f by Shigley, 1986.

The frettage corrosion problem is the result of microscopic motions of tightly fitting parts or structures. Bolted joints, bearing-race fits, wheel hubs, and any set of tightly fitted parts are examples. The process involves surface discoloration, pitting and eventual fatigue (Shigley, 1986). The frettage factor k_f depends upon the material of the mating pairs and ranges from 0,24 to 0,90. The effect of this factor was investigated in section 4.3. in depth.

Briefly, figure 4.1. and 4.2. show that the inner cylinder is subjected to higher radial stress than tangential stress. And the outer cylinder is subjected to higher tangential stress than radial stress.

4.3. Effects of Design Parameters on Factor of Safety for Optimal Dimensions

The effect of adjustable parameters such as "δ_T" the total interface deformation, "t_1" the thickness of the inner shell, "t_2" the thickness of the outer shell are studied in this section. Briefly, an answer given to question of "How do these factors affect the factors of safety of inner and outer cylinders. This chapter introduces to the investigation of mostly how the inner and the outer cylinder are affected from the design parameters by the graphs.

4.3.1. Effect of Total Deformation on Interface Pressure

The effect of total deformation on interface pressure is investigated in this section. While doing this, the parameters are set accordingly based on the optimum point which was found in the chapter 4.1. The program was run and the results are given in the Appendix D in table D1. The figure which is drawn for these data is given in Figure 4.3.

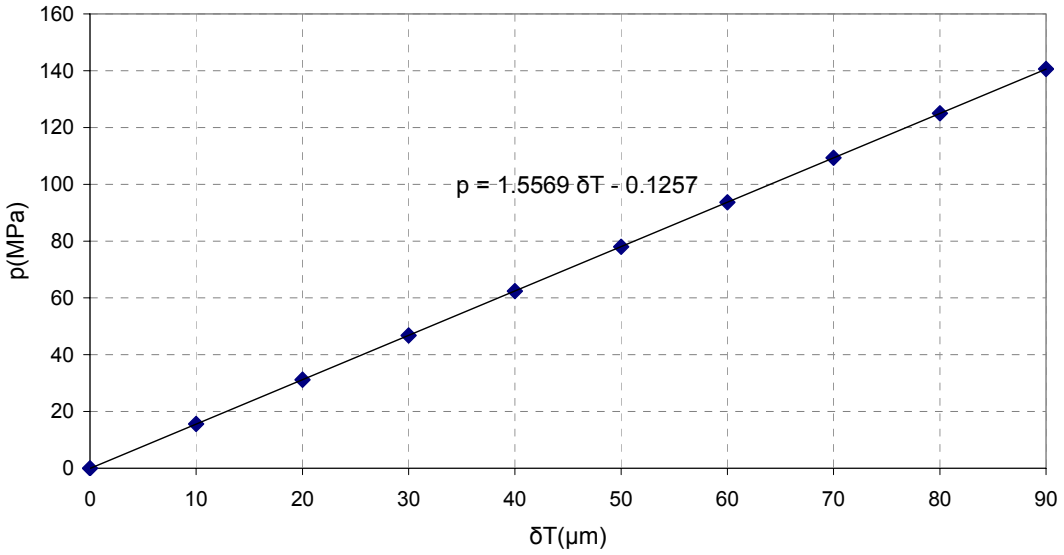

Figure 4.3. Relation between interface pressure and total interface displacement. (p-δ_T relation)

As seen in the figure 4.3., there is a completely linear relationship between total interface displacement and interface pressure. The vertical axis represents the interface pressure values in MPa's. The horizontal axis represents the total interface displacement in microns. The diagonal points are the calculated points. And the line connects the points is the regression line and the formula of this line is given right above in the graph. As a result, interface pressure is directly proportional with the total interface displacement. Thus, the graph of the δ_T-FS1 and p-FS1 will be identical and that is true for FS2.

4.3.2. Effect of Total Interface Displacement on Factors of Safety

It was firstly investigated that what was the relationship is in between the total deformation -an adjustable parameter- and interface pressure -output-. Then, the relation between total interface displacement and factor of safeties are studied. The effect of the interface pressure to the factor of safeties (both will be identical because

there is a linear relationship in between the two, $p=k*\Delta T$) are more important. This section, investigates that the sensitive cylinder to the interface pressure.

The control parameters; the thicknesses t_1 and t_2; are entered into the design program based on the optimal point that is found in previous sections.

These parameters were run in the DPro-MLWJI. And total deformation is increased by 10 points in every calculation. This procedure is repeated by many times and the results are obtained and given in fig. 4.4. The numerical values of the result are provided in the table D1 in the Appendix D.

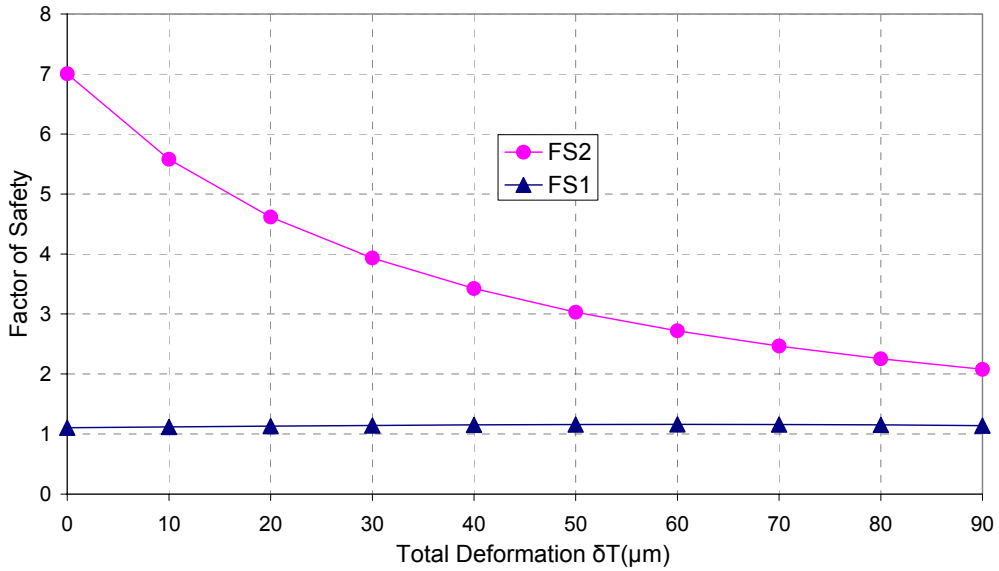

Figure 4.4. Safety Factor-Total Deformation relationship.

As seen clearly in the figure 4.4., horizontal plane representing the total deformation amount in "μm", micrometers. The vertical axis is the scale of safety factor of the both cylinders. The triangular points are representing the coordinate points for the FS1 values. The circular points are representing the coordinate points for FS2 points. The starting point of the FS1 line is in between 1 and 2. As the total deformation rises, the beneficial effect of the outer shell is shown. The safety factor of the inner cylinder begins to increase. But, beside this, the safety factor for the outer shell decreases drastically due to the increase of the interface pressure. But

even in the worst case, the safety factor for the outer cylinder doesn't drop below the value of 1. But the real problem in here is the existence of the optimal point for the safety factor of the inner cylinder. Thus at some point, increase in the shrink fit displacement does not make the inner cylinder more secure, contrarily, makes the inner cylinder less secure by the squeezing effect. After that point, increasing of the interface stringency begins to drop the safety factor of the inner cylinder too. The optimal point for these conditions seems to be near to 60µm.

4.3.3. Effect of Thicknesses of the Inner and Outer Cylinders to Factors of Safety

Now the same inputs are used here and the total interface displacement will be in the optimal point similar with the previous graph. The data about the interpolation points was given in the Table D2 in the Appendix D. However, the results are plotted in figure 4.5. to show the relationship.

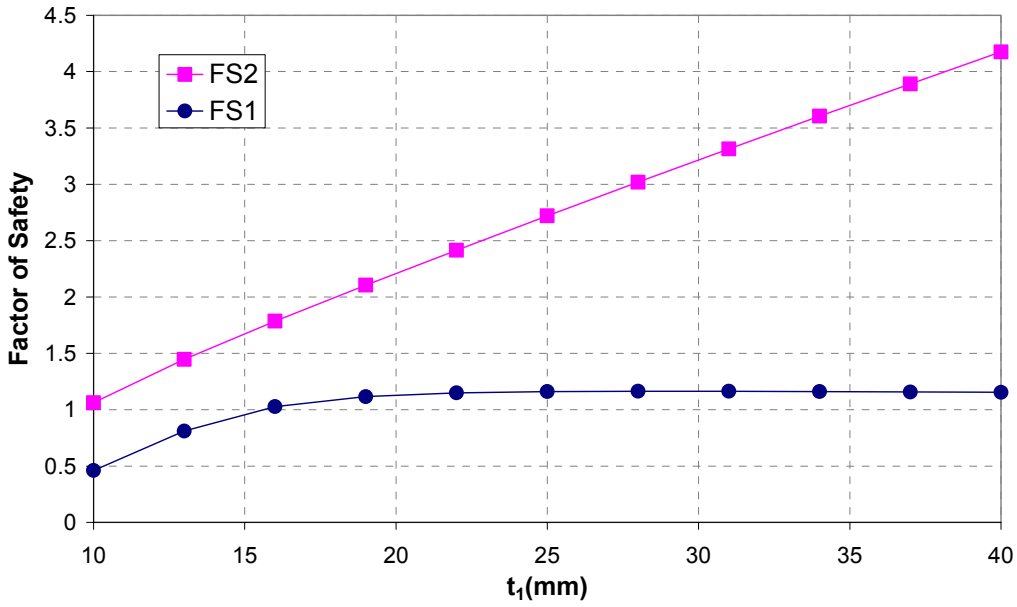

Figure 4.5. The relationship between thickness of the inner cylinder and factor of safeties.

As shown in the figure 4.5., the thickness of the inner cylinder is directly proportional with FS1 and FS2 values and seems like there is a linear relationship

with the factor of the safety of outer cylinder. But after some point (the 13 mm value point for the total deformation δ_T), the slope of factor of safety of the inner cylinder FS_1 begins to decrease. This means, after that point, increase in the thickness of the inner cylinder has no effect on the factor of safety of it.

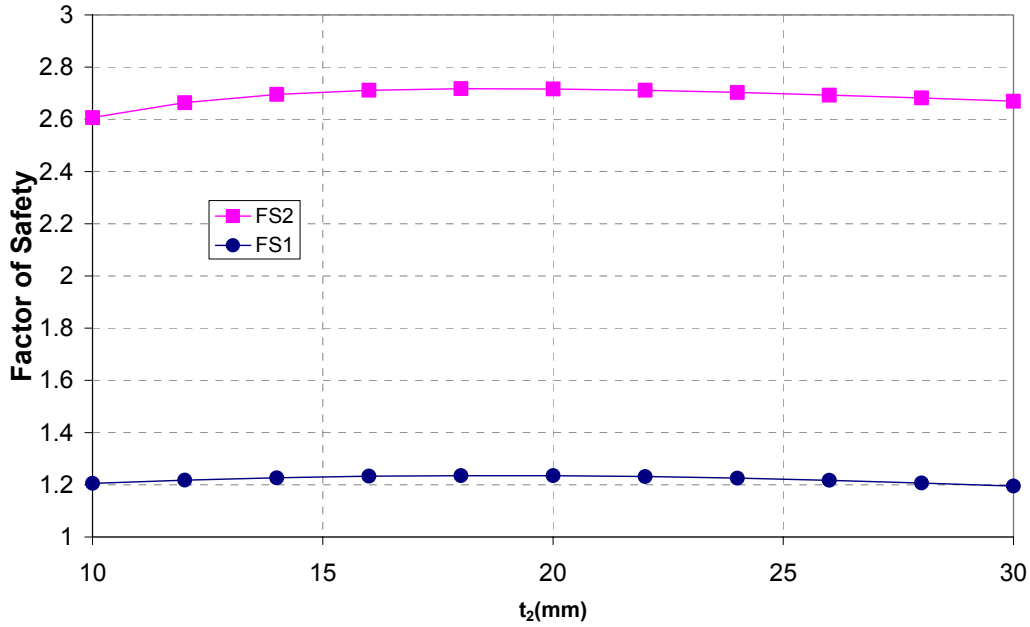

Figure 4.6. The relation between the thickness of the outer cylinder and the factor of safeties of the both cylinders.

As shown in the figure 4.6., vertical axis represents also the factor of safeties of the cylinders, but horizontal axis represents the thickness of the outer cylinder. The effect of the t_2 is smaller than the safety of the inner cylinder. This supports result of the previous interface pressure analysis. Beside this, after some point, increase in the thickness of the outer cylinder causes slight decrease in the factor of safety of the inner cylinder.

4.3.4. Effect of Operating Pressure on Safety Factors of Cylinders

The relations in between the operating pressure and the factors of safety of both inner and outer cylinder are studied in this section. The operating pressure p_i is altered from 2000 Bars and 4000 Bars, and the change in safety factors of inner and

outer cylinders are calculated using DPro-MLWJI according to the optimum data calculated in previous section.

And according to these values given in table D3 in appendix D, the graph of the safety factors is drawn and it is shown in figure 4.7.

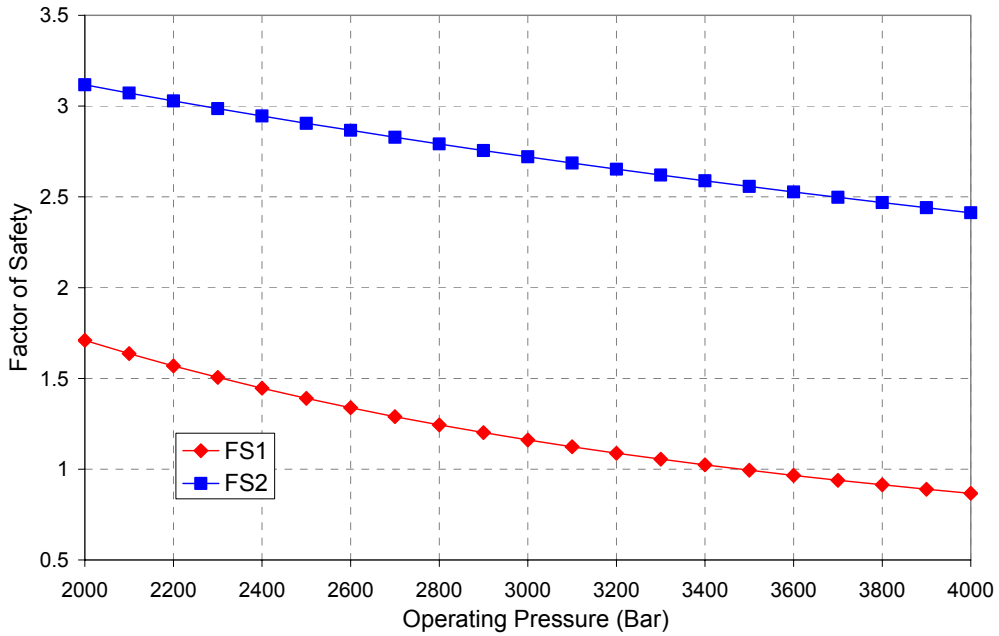

Figure 4.7. The relation between operating pressure and factor of safeties of the both cylinders.

The vertical axis here symbolize the safety factor and the scale of the axis is same for inner cylinder safety factor and the outer cylinder safety factor. For the operating pressure value of 2000 Bars the safety factor of the inner cylinder 1,70. It is very safe value. But as the pressure rises towards 4000 Bars, safety factor reduces and in between 3400 and 3500 Bars, it falls below the unity; the unsafe region. As the pressure rises, outer cylinder safety factor also reduces with nearly linear manner and falls right below the value of 2,5. This means that the system is safe up to the 3400 bar operating pressure.

4.3.5. Effect of Frettage Corrosion on Safety Factors of Cylinders

Fretting can occur when pair of structural elements those are in contact under a normal load while cyclic stress and relative displacement are forced along the contact surface. During fretting the fatigue strength decreases to less than one-third of that without fretting. The strength is reduced because of concentrations of contact stresses such as contact pressure and tangential stress at the contact edge, where fretting fatigue cracks initiate and propagate (Hattori, Watanabe, 2006).

In this study, the miscellaneous endurance limit modifying factor "k_f" was taken a value of 0,7 as a result of fretting affect. But, to examine the one third change mentioned in the previous paragraph, the miscellaneous factor was changed between 0,24 and 0,9 values and changes in the safety factors of both cylinders were calculated using the program. And the results for specific "k_f" values are given in Appendix D, table D4.

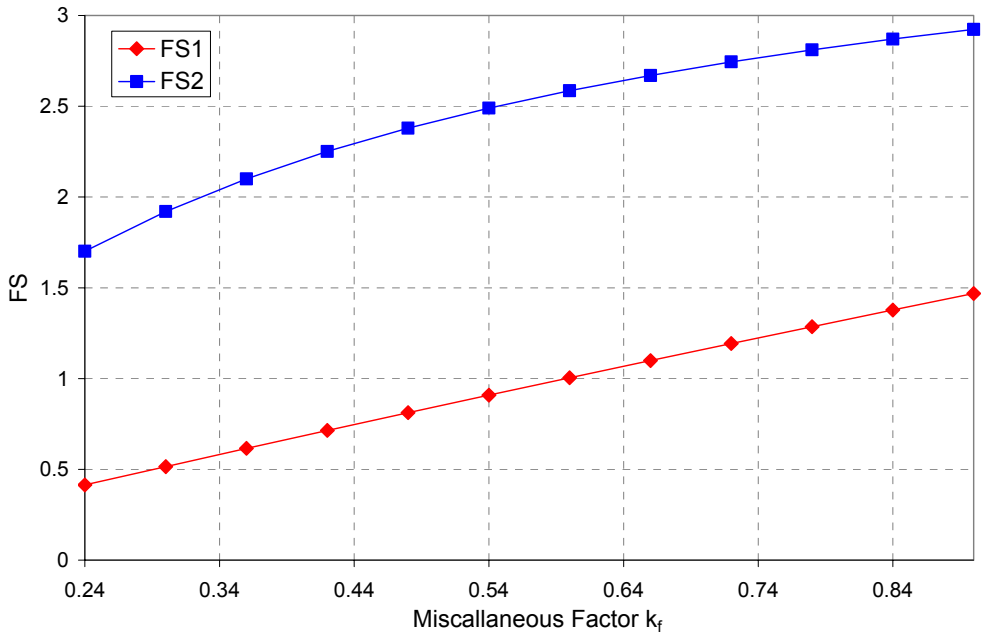

Figure 4.8. The relation between miscellaneous endurance limit modifying factor and factor of safeties of the both cylinders.

The figure above shows the relationship in between the miscellaneous modifying factor "k_f" and safety factors of both cylinders. The horizontal axis

represents the scale for modifying factor. The vertical axis represents the safety factors of both cylinders in the same scale. As seen, the minimum and the maximum values of the safety factor of the inner cylinder are 0,42 and 1,47. Approximately, there is a 3,5 times change in safety factor of the system.

4.4. Safety Calculations for the Prototype in the Mechanical Engineering Laboratory in University of Çukurova.

Same calculations was made with section 4.3.4. for the prototype in the laboratory which has the same materials. But the thickness of the inner cylinder is t_1=18 mm, thickness of the outer cylinder is t_2=40 mm, the inner radius of the inner cylinder is R=20 mm, and the total interface displacement is δ_T=70 µm.

4.4.1. Safety Analysis

The design program ”DPro-MLWJI” was run with the inputs given above. Factor of safety values for inner and outer cylinders were calculated at different operating pressures. Data of this calculation is provided in the Appendix D table D5. The graph which uses the data from the previous calculation is given below.

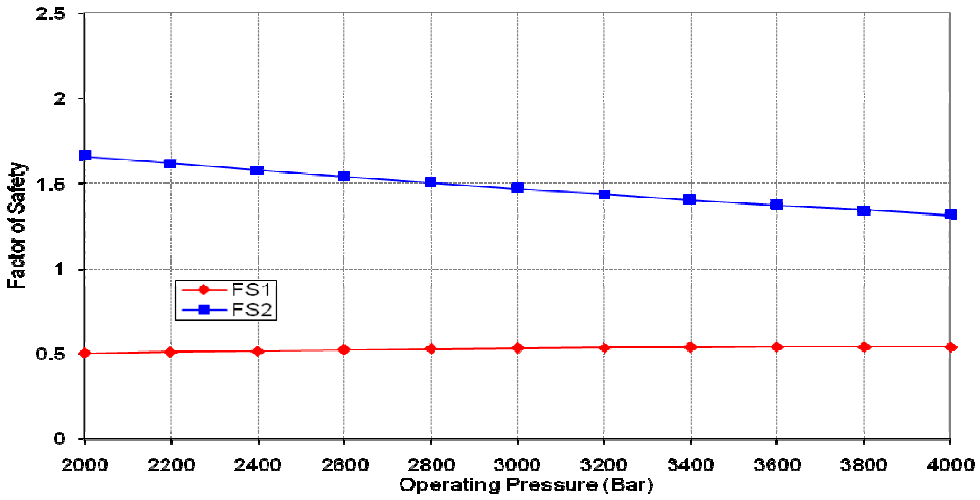

Figure 4.9. The relationship between factor of safeties of cylinders and operating pressure for prototype.

The vertical axis represents the safety factors of inner and the outer cylinders. The factor of safety of the inner cylinder begins from 0,5 and slightly increase when

the pressure rises. This is because; the thickness of the outer cylinder applies higher pressure to the cylinder inside resulting the inner cylinder is crushed from outside resulting the drop in the factor of safety (see fig 4.9. and fig. 4.10.). As the pressure increases, the supply from the outside increases, and the safety factor begins to increase. Beside this, the safety factor of the outer cylinder decreases due to the increase in interface pressure.

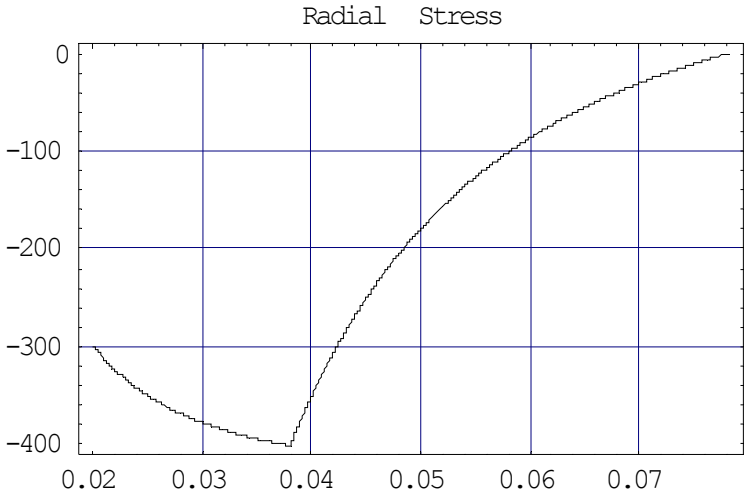

Figure 4.10. The radial stress distribution along the radial direction for 300 MPa operating pressure

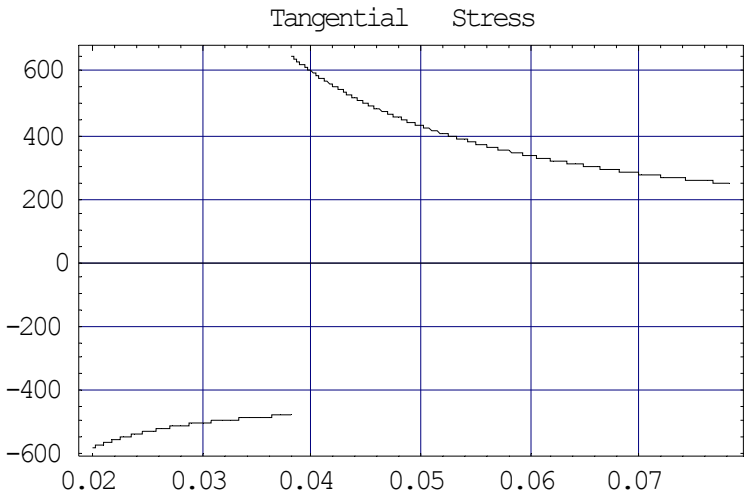

Figure 4.11. The Tangential stress distribution along the radial direction for 300 MPa operating pressure

4.4.2. Double Shrink Fitted Triple Layer Intensifier Solution Trial to the Safety Problem of the Prototype

As shown in the previous section, the prototype is not safe. To overcome this problem, another steel shell which has 25 mm inner diameter after shrink fit can be fitted into the cylinder. Using the calculation method for the multi-layer cylinders mentioned in the Material and Method section, the inner shell is assumed to be monoblock with the inner cylinder of the prototype. But this solution cannot be applied because the safety of the intensifier decreases even the inner pressure is decreased. The problem is in the crushing interface pressure produced by the excessively thick outer cylinder.

To solve this problem, the thickness of the outer shell must be decreased. And the cylinder which has 25 mm diameter again shrink fitted inside the inner cylinder. This study shows the amount of optimum thickness of the outer cylinder which maximizes the safety factor and the dimensions of the cylinder to be shrink-fit inside.

Assuming the innermost cylinder is monoblock with the inner cylinder of the old prototype, the design program DPro-MLWJI gives the optimal safety values at t_2=12 mm.

The interface pressure output of the program is p=158,357 MPa. It will be the outer pressure in the calculations of inner cylinder pairs.

But when the design program was run for these inputs, the factor of safety of the innermost cylinder can not reach over the 0,8.

The problem is formed due to the high interface pressure which exists between the two cylinders. As said before, the cylinder which is inside has a high elasticity modulus, high yield strength and high ultimate tensile strength. That is required for inner cylinder to withstand the ultra-high operating pressure. So it is beneficial for inner cylinder to use high-grade steel up to an acceptable value.

But the case is not so for the outer cylinder. From the interface pressure point of view, a material with higher elasticity modulus reduces the required interface displacement value for shrink-fit strength of the system. Also due to the high cost of the high-grade steels it also increases the total cost of the system.

Another benefit of the low grade steel is to have better shock absorbing characteristics. So the variations in the interface pressure due to the operating pressure will be smaller at that time. That is good for system to work with high fluctuated stresses. So the real solution is to choose softer material for the outer cylinder more than to decrease the thickness. The figure 4.12 is given to show the relationship between safety factors of cylinders and interface pressure of the intensifier cylinder when the outer cylinder is made from softer material which has 100 GPa (nearly the half of the outer shell materials elasticity modulus) elasticity modulus. The program inputs are t_1=18 mm, t_2=40 mm, δ_T=70 µm, E_2=100 GPa. The other inputs are same with the previous runs.

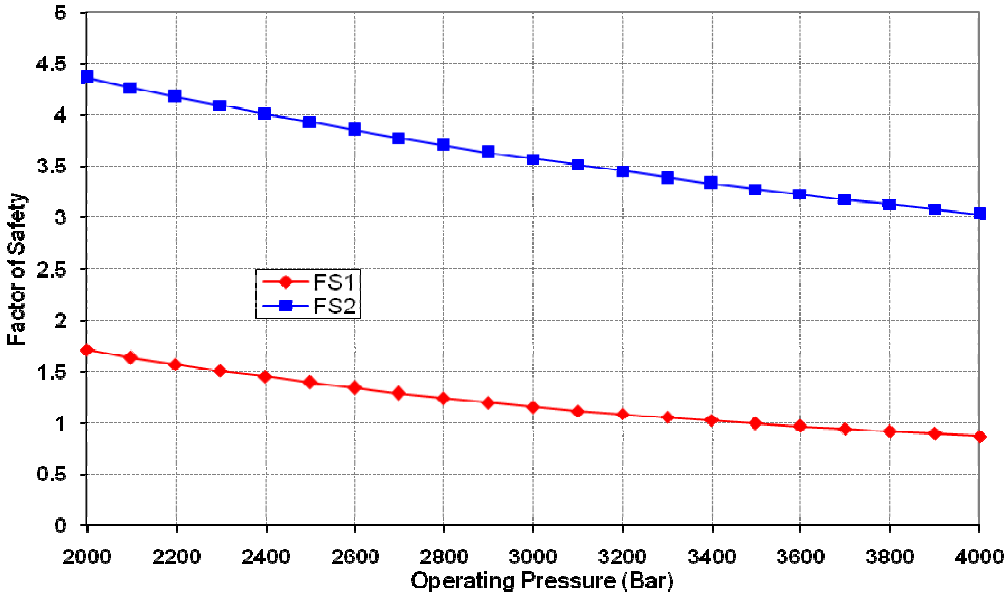

Figure 4.12. Relationship between safety factor cylinders and operating pressure for E_2=100 GPa

It is shown from the Figure 4.12., using softer materials for the outer cylinder increases the factor of safety of the inner cylinder. Wrongly producted prototype can repaired by replacing outer shell with the softer material. The radial and tangential stress distributions of the intensifier at 2400 bar operating pressure is given in the figures 4.13. and 4.14.

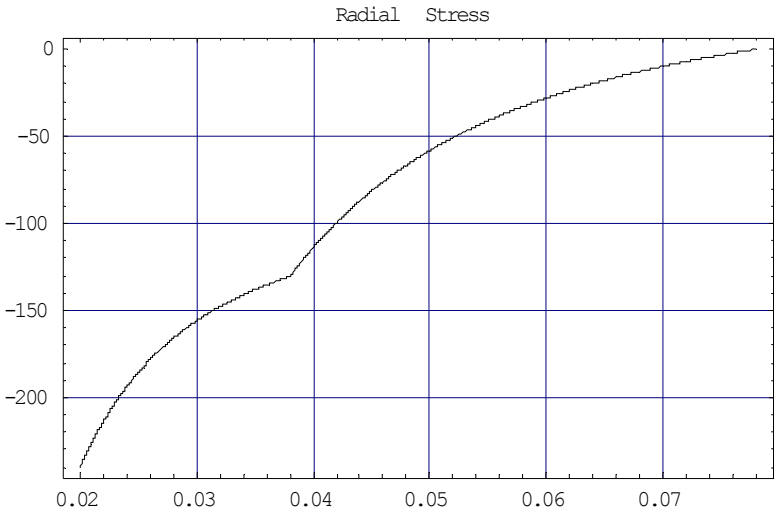

Figure 4.13. The radial stress distribution along radial direction

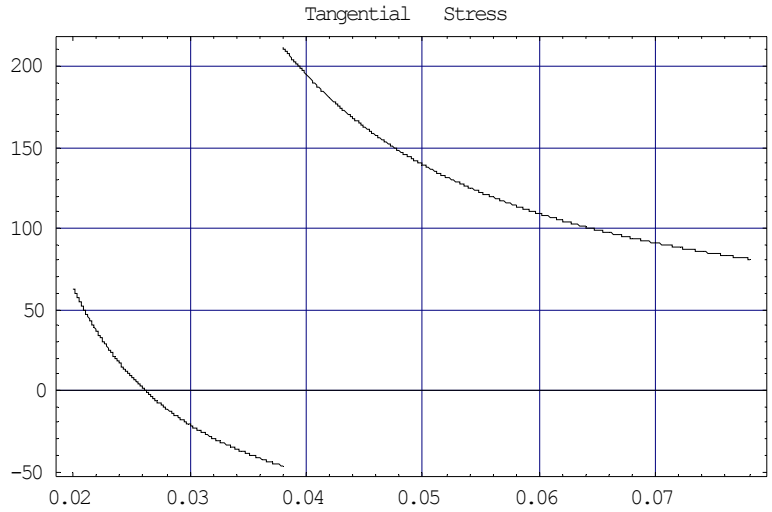

Figure 4.14. The tangential stress distribution along radial direction

The general characteristics of the stress distribution graphics are same with the result found by Güzelbey, Kanber, Eyercioğlu (2005) who use the finite element method with the Boundary Element Method.

5. CONCLUSION

The use of high pressure water-jets as a cutting tool has recently increased in popularity. Most applications have been directed at harder materials and at hose that are more difficult to cut by traditional cutting methods. The popularity of the water-jet cutting comes from its various distinct advantages over the other cutting technologies such as no thermal distortion, high machining versatility, high flexibility, small cutting forces and ability to cut several materials without modifying their mechanical properties.

The most important part of the water-jet cutting system is the pressure intensifier. Single layer thick structures can only sustain pressures up to 1800 bar. Double layer structures are used for ultra high pressure applications which is above 3000 bar operating pressures. The first system was designed for 1800 bar with single layer intensifier which is capable of cutting soft materials. After that a double layer system is designed for 3000 bar operating pressure constituting shrink fitted parts. In this study the objective was to decrease weight and satisfying requirements to sustain high pressures. Selection has been made from the set of the materials. Decision has been made by considering cost, availability, and manufacturability. As a result, AISI 4340 steel for inner cylinder and AISI 4140 steel for outer cylinder had been selected.

In this study, a program was produced in the Mathematica® Programming language and scientific editor using general strength formulas for shrink fitted parts including the distortion energy theory. Then optimization of the inner cylinder thickness, outer cylinder thickness, total interface displacement values were optimized by using this program called “DPro-MLWJI”. At the same time, the stress distributions through inner and the outer cylinder walls in radial direction were drawn using the Mathematica® graph editor by a second program called “SDRD”, lastly the double layer prototype which is made previously in the Mechanical Engineering Laboratory in University of Çukurova is tested using this program. The lack in safety in this prototype is detected and problem is solved suitably. Beside these studies, the relationships between the design parameters such as p-δ_T, δ_T-FS, t_1-

FS, t_2-FS, p_i-FS, k_f-FS are investigated. Stress distributions along the radial direction is drawn using Mathematica.

After these studies, it is shown that excessively thick outer cylinder brings damage more than benefit to the system by excessively pressing to the cylinder inside. This makes the inner cylinder less reliable and safe. To solve this problem, it is shown that the interface pressure is not as high as the operating pressure. So the outer shell can be made from softer material which causes, better shock absorbing characteristic that improves the safety factor of the inner cylinder, reduced cost due to the low prices of the outer cylinder.

It is possible to increase the pressure limit by using the new engineering materials. But cost will be increased at this time.

APPENDIX A:
Mahematica Calculations for Stress Constants

Input1:

```
FullSimplify[
 Solve[{-pi == E1/(1 - μ1^2) (C1 (1 + μ1) - C2 ((1 - μ1)/a^2)), -p1 == E1/(1 - μ1^2) (C1 (1 + μ1) - C2 ((1 - μ1)/b^2)),
   -p2 == E2/(1 - μ2^2) (C3 (1 + μ2) - C4 ((1 - μ2)/c^2)), -po == E2/(1 - μ2^2) (C3 (1 + μ2) - C4 ((1 - μ2)/d^2))},
  {C1, C2, C3, C4}]]
```

Output1:

$$\left\{\left\{C1 \to \frac{(-b^2\,p1 + a^2\,pi)\,(-1+\mu1)}{(a^2-b^2)\,E1},\ C2 \to \frac{a^2\,b^2\,(p1-pi)\,(1+\mu1)}{(a^2-b^2)\,E1},\right.\right.$$
$$\left.\left.C3 \to \frac{(c^2\,p2 - d^2\,po)\,(-1+\mu2)}{(c^2-d^2)\,E2},\ C4 \to -\frac{c^2\,d^2\,(p2-po)\,(1+\mu2)}{(c^2-d^2)\,E2}\right\}\right\}$$

Input2:

```
FullSimplify[
 Solve[{0 == E1/(1 - μ1^2) (C1s (1 + μ1) - C2s ((1 - μ1)/R^2)), -p == E1/(1 - μ1^2) (C1s (1 + μ1) - C2s ((1 - μ1)/G^2)),
   -p == E2/(1 - μ2^2) (C3s (1 + μ2) - C4s ((1 - μ2)/G^2)), 0 == E2/(1 - μ2^2) (C3s (1 + μ2) - C4s ((1 - μ2)/M^2))},
  {C1s, C2s, C3s, C4s}]]
```

Output2:

$$\left\{\left\{C1s \to \frac{G^2\,p\,(-1+\mu1)}{E1\,(G^2-R^2)},\ C2s \to -\frac{G^2\,p\,R^2\,(1+\mu1)}{E1\,(G^2-R^2)},\ C3s \to \frac{G^2\,p\,(-1+\mu2)}{E2\,(G^2-M^2)},\ C4s \to -\frac{G^2\,M^2\,p\,(1+\mu2)}{E2\,(G^2-M^2)}\right\}\right\}$$

Input3:

```
S1 =
 FullSimplify[
  Solve[{-pi == E1/(1 - μ1^2) (C1ss (1 + μ1) - C2ss ((1 - μ1)/R^2)),
    E1/(1 - μ1^2) (C1ss (1 + μ1) - C2ss ((1 - μ1)/G^2)) == E2/(1 - μ2^2) (C3ss (1 + μ2) - C4ss ((1 - μ2)/G^2)), C1ss G + C2ss/G == C3ss G + C4ss/G,
    po == E2/(1 - μ2^2) (C3ss (1 + μ2) - C4ss ((1 - μ2)/M^2))}, {C1ss, C2ss, C3ss, C4ss}]]
```

Output3:

$$\left\{\left\{C1ss \to \frac{(-1+\mu 1)\,(E2\,(G-M)\,(G+M)\,pi\,R^2\,(1+\mu 1)+E1\,(G^2\,(2\,M^2\,po-pi\,R^2\,(-1+\mu 2))+M^2\,pi\,R^2\,(1+\mu 2)))}{E1\,(E2\,(G-M)\,(G+M)\,(-G^2\,(-1+\mu 1)+R^2\,(1+\mu 1))+E1\,(G-R)\,(G+R)\,(G^2\,(-1+\mu 2)-M^2\,(1+\mu 2)))},\right.\right.$$

$$C2ss \to -\frac{G^2\,R^2\,(1+\mu 1)\,(E2\,(G-M)\,(G+M)\,pi\,(-1+\mu 1)+E1\,(G^2\,(pi-pi\,\mu 2)+M^2\,(pi+2\,po+pi\,\mu 2)))}{E1\,(E2\,(G-M)\,(G+M)\,(-G^2\,(-1+\mu 1)+R^2\,(1+\mu 1))+E1\,(G-R)\,(G+R)\,(G^2\,(-1+\mu 2)-M^2\,(1+\mu 2)))},$$

$$C3ss \to \frac{(-1+\mu 2)\,(E2\,(G^2\,(2\,pi\,R^2-M^2\,po\,(-1+\mu 1))+M^2\,po\,R^2\,(1+\mu 1))+E1\,M^2\,po\,(G-R)\,(G+R)\,(1+\mu 2))}{E2\,(E2\,(G-M)\,(G+M)\,(-G^2\,(-1+\mu 1)+R^2\,(1+\mu 1))+E1\,(G-R)\,(G+R)\,(G^2\,(-1+\mu 2)-M^2\,(1+\mu 2)))},$$

$$\left.\left.C4ss \to -\frac{G^2\,M^2\,(E2\,(G^2\,(po-po\,\mu 1)+R^2\,(2\,pi+po+po\,\mu 1))+E1\,po\,(G-R)\,(G+R)\,(-1+\mu 2))\,(1+\mu 2)}{E2\,(E2\,(G-M)\,(G+M)\,(-G^2\,(-1+\mu 1)+R^2\,(1+\mu 1))+E1\,(G-R)\,(G+R)\,(G^2\,(-1+\mu 2)-M^2\,(1+\mu 2)))}\right\}\right\}$$

Input4:

$$S_1 =$$

$$\text{FullSimplify}\left[\text{Solve}\left[\left\{-pi == X1\left(C1ss\,(X2)-C2ss\,\frac{X3}{R^2}\right),\ X1\left(C1ss\,(X2)-C2ss\,\frac{X3}{G^2}\right) == Y1\left(C3ss\,(Y2)-C4ss\,\frac{Y3}{G^2}\right),\right.\right.\right.$$

$$\left.\left.\left.C1ss\,G+\frac{C2ss}{G} == C3ss\,G+\frac{C4ss}{G},\ po == Y1\left(C3ss\,(Y2)-C4ss\,\frac{Y3}{M^2}\right)\right\},\{C1ss, C2ss, C3ss, C4ss\}\right]\right]$$

Output4:

$$\left\{\left\{C1ss \to \frac{M^2\,pi\,R^2\,Y2\,(X1\,X3-Y1\,Y3)+G^2\,(pi\,R^2\,(X1\,X3+Y1\,Y2)\,Y3+M^2\,po\,X1\,X3\,(Y2+Y3))}{X1\,(M^2\,(G-R)\,(G+R)\,X1\,X2\,X3\,Y2+(G^2\,(G-R)\,(G+R)\,X1\,X2\,X3-(G-M)\,(G+M)\,(R^2\,X2+G^2\,X3)\,Y1\,Y2)\,Y3)},\right.\right.$$

$$C2ss \to \frac{G^2\,R^2\,(G^2\,pi\,(X1\,X2-Y1\,Y2)\,Y3+M^2\,(po\,X1\,X2\,(Y2+Y3)+pi\,Y2\,(X1\,X2+Y1\,Y3)))}{X1\,(M^2\,(G-R)\,(G+R)\,X1\,X2\,X3\,Y2+(G^2\,(G-R)\,(G+R)\,X1\,X2\,X3-(G-M)\,(G+M)\,(R^2\,X2+G^2\,X3)\,Y1\,Y2)\,Y3)},$$

$$C3ss \to \frac{M^2\,po\,R^2\,X2\,(-X1\,X3+Y1\,Y3)+G^2\,(pi\,R^2\,(X2+X3)\,Y1\,Y3+M^2\,po\,X3\,(X1\,X2+Y1\,Y3))}{M^2\,(G-R)\,(G+R)\,X1\,X2\,X3\,Y1\,Y2-Y1\,(-G^2\,(G-R)\,(G+R)\,X1\,X2\,X3+(G-M)\,(G+M)\,(R^2\,X2+G^2\,X3)\,Y1\,Y2)\,Y3},$$

$$\left.\left.C4ss \to \frac{G^2\,M^2\,(G^2\,po\,X3\,(-X1\,X2+Y1\,Y2)+R^2\,(pi\,(X2+X3)\,Y1\,Y2+po\,X2\,(X1\,X3+Y1\,Y2)))}{M^2\,(G-R)\,(G+R)\,X1\,X2\,X3\,Y1\,Y2-Y1\,(-G^2\,(G-R)\,(G+R)\,X1\,X2\,X3+(G-M)\,(G+M)\,(R^2\,X2+G^2\,X3)\,Y1\,Y2)\,Y3}\right\}\right\}$$

Input4:

$$\text{FullSimplify}\left[\text{ReplaceAll}\left[\text{ReplaceAll}\left[C1\,a+\frac{C2}{a},\ \left\{C1 \to \frac{b^2\,p\,X3}{(a^2-b^2)\,E1},\ C2 \to \frac{a^2\,b^2\,p\,X2}{(a^2-b^2)\,E1}\right\}\right],\right.\right.$$

$$\left.\left.\{a \to R-\delta 1,\ b \to R-\delta 1+t1\}\right]\right]$$

Output4:

$$-\frac{p\,(X2+X3)\,(R-\delta 1)\,(R+t1-\delta 1)^2}{E1\,t1\,(2\,R+t1-2\,\delta 1)}$$

Input5:

$$\text{Solve}\left[\left\{\delta 1 == -\frac{p\,(X2+X3)\,(R+\delta 1)\,(R+t1+\delta 1)^2}{E1\,t1\,(t1+2\,(R+\delta 1))},\right.\right.$$
$$\delta T == \frac{p\,X2\,(R+\delta 1)^2\,(R+t1+\delta 1)}{E1\,((R+\delta 1)^2-(R+t1+\delta 1)^2)}+\frac{p\,X3\,(R+t1+\delta 1)^3}{E1\,((R+\delta 1)^2-(R+t1+\delta 1)^2)}-$$
$$\frac{p\,Y2\,(R+t1+\delta 1-\delta T)\,(R+t1+t2+\delta 1-\delta T)^2}{E2\,((R+t1+\delta 1-\delta T)^2-(R+t1+t2+\delta 1-\delta T)^2)}-$$
$$\left.\left.\frac{p\,Y3\,(R+t1+\delta 1-\delta T)\,(R+t1+t2+\delta 1-\delta T)^2}{E2\,((R+t1+\delta 1-\delta T)^2-(R+t1+t2+\delta 1-\delta T)^2)}\right\},\{\delta 1,p\}\right]$$

Output5:

$$\{\{p\to -1.72856\times 10^{11},\ \delta 1\to -0.024621\},$$
$$\{p\to -2.99675\times 10^{10},\ \delta 1\to 0.0750851\},$$
$$\{p\to 0.,\ \delta 1\to -0.027\},$$
$$\{p\to 2.58353\times 10^{8},\ \delta 1\to -0.0000483616\},$$
$$\{p\to 3.88124\times 10^{11},\ \delta 1\to -0.0613505\},$$
$$\{p\to 4.7696\times 10^{16},\ \delta 1\to -0.0379575\}\}$$

Input6:

$$\text{FindRoot}\left[\left\{\delta 1 == -\frac{p\,(X2+X3)\,(R+\delta 1)\,(R+t1+\delta 1)^2}{E1\,t1\,(t1+2\,(R+\delta 1))},\right.\right.$$
$$\delta T == \frac{p\,X2\,(R+\delta 1)^2\,(R+t1+\delta 1)}{E1\,((R+\delta 1)^2-(R+t1+\delta 1)^2)}+\frac{p\,X3\,(R+t1+\delta 1)^3}{E1\,((R+\delta 1)^2-(R+t1+\delta 1)^2)}-$$
$$\frac{p\,Y2\,(R+t1+\delta 1-\delta T)\,(R+t1+t2+\delta 1-\delta T)^2}{E2\,((R+t1+\delta 1-\delta T)^2-(R+t1+t2+\delta 1-\delta T)^2)}-$$
$$\left.\left.\frac{p\,Y3\,(R+t1+\delta 1-\delta T)\,(R+t1+t2+\delta 1-\delta T)^2}{E2\,((R+t1+\delta 1-\delta T)^2-(R+t1+t2+\delta 1-\delta T)^2)}\right\},\{\delta 1,-0.0010\},\{p,1000000\}\right]$$

Output6:

$$\{\delta 1\to -0.0000483616,\ p\to 2.58353\times 10^{8}\}$$

APPENDIX B:

Steps of the Design Program"DPro-MLWJI"

Step1:

```
Off[General::spelll]
```

Step2:

```
po = 0;
pi = 300 * 10^6;
R = 16 * 10^-3;
δT = 80 * 10^-6;
t1 = 30 * 10^-3;
t2 = 15 * 10^-3;
```

Step3:

```
μ1 = 0.292;
μ2 = 0.292;
E1 = 207 * 10^9;
E2 = 207 * 10^9;
Sut1 = 1720 * 10^6;
Sut2 = 1760 * 10^6;
Sy1 = 1570 * 10^6;
Sy2 = 1620 * 10^6;
α = 11.2 * 10^-6;
Sep1 = 700 * 10^6 ;
Sep2 = 700 * 10^6;
```

Step4:

$$X1 = \frac{E1}{1-\mu 1^2};\ X2 = 1+\mu 1;\ X3 = 1-\mu 1;\ Y1 = \frac{E2}{1-\mu 2^2};\ Y2 = 1+\mu 2;\ Y3 = 1-\mu 2;$$

Step5:

$$a = R - \delta 1;$$
$$b = a + t1;$$
$$c = b - \delta T;$$
$$d = c + t2;$$

Step6:

$$C1 = \frac{b^2\, p\, X3}{(a^2 - b^2)\, E1};\ C2 = \frac{a^2\, b^2\, p\, X2}{(a^2 - b^2)\, E1};\ C3 = -\frac{d^2\, p\, Y3}{(c^2 - d^2)\, E2};\ C4 = -\frac{c^2\, d^2\, p\, Y2}{(c^2 - d^2)\, E2};$$

Step7:

$$\delta 2 = C1\, b + \frac{C2}{b};\ \delta 3 = C3\, c + \frac{C4}{c};\ \delta 4 = C3\, d + \frac{C4}{d};$$

Step8:

$$\text{Solve}\left[\left\{\delta 1 == C1\, a + \frac{C2}{a},\ \delta T == C1\, b + \frac{C2}{b} + C3\, c + \frac{C4}{c}\right\}, \{\delta 1, p\}\right]$$

Step9:

$$\text{FindRoot}\left[\left\{\delta 1 == C1\, a + \frac{C2}{a},\ \delta T == C1\, b + \frac{C2}{b} + C3\, c + \frac{C4}{c}\right\}, \{\delta 1, -0.0010\}, \{p, 1000000\}\right]$$

Step10:

$$p = p\ /.\ \%;$$
$$\delta 1 = \delta 1\ /.\ \%\%;$$

Step11:

$$\Delta t_m = \frac{\delta T}{c\,\alpha};$$

Step12:

$$G = b + \delta 2;$$
$$M = d + \delta 4;$$
$$de1 = 1000 * \sqrt{(2*G)^2 - (2*R)^2};$$
$$de2 = 1000 * \sqrt{0.95 * ((2*G)^2 - (2*R)^2)};$$

Step13:

```
ka = 1;
kb1 = 1.189 * de1^-0.097; kb2 = 1.189 * de2^-0.097;
kc = 1;
kd = 1;
ke = 1;
kf = 0.7;
Se1 = ka * kb1 * kc * kd * ke * kf * Sep1;
Se2 = ka * kb2 * kc * kd * ke * kf * Sep2;
```

Step14:

$$C1s = \frac{\mu 1 - 1}{E1} \frac{G^2 p}{(G^2 - R^2)};$$

$$C2s = -\frac{\mu 1 + 1}{E1} \frac{G^2 R^2 p}{(G^2 - R^2)};$$

$$C3s = \frac{\mu 2 + 1}{E2} \frac{G^2 p}{(G^2 - M^2)};$$

$$C4s = -\frac{\mu 2 + 1}{E2} \frac{G^2 M^2 p}{(G^2 - M^2)};$$

Step15:

```
C1ss = (M^2 pi R^2 Y2 (X1 X3 - Y1 Y3) + G^2 (pi R^2 (X1 X3 + Y1 Y2) Y3 + M^2 po X1 X3 (Y2 + Y3))) /
    (X1 (M^2 (G - R) (G + R) X1 X2 X3 Y2 +
        (G^2 (G - R) (G + R) X1 X2 X3 - (G - M) (G + M) (R^2 X2 + G^2 X3) Y1 Y2) Y3));
C2ss = (G^2 R^2 (G^2 pi (X1 X2 - Y1 Y2) Y3 + M^2 (po X1 X2 (Y2 + Y3) + pi Y2 (X1 X2 + Y1 Y3)))) /
    (X1 (M^2 (G - R) (G + R) X1 X2 X3 Y2 +
        (G^2 (G - R) (G + R) X1 X2 X3 - (G - M) (G + M) (R^2 X2 + G^2 X3) Y1 Y2) Y3));
C3ss = (M^2 po R^2 X2 (-X1 X3 + Y1 Y3) + G^2 (pi R^2 (X2 + X3) Y1 Y3 + M^2 po X3 (X1 X2 + Y1 Y3))) /
    (M^2 (G - R) (G + R) X1 X2 X3 Y1 Y2 -
      Y1 (-G^2 (G - R) (G + R) X1 X2 X3 + (G - M) (G + M) (R^2 X2 + G^2 X3) Y1 Y2) Y3);
C4ss = (G^2 M^2 (G^2 po X3 (-X1 X2 + Y1 Y2) + R^2 (pi (X2 + X3) Y1 Y2 + po X2 (X1 X3 + Y1 Y2)))) /
    (M^2 (G - R) (G + R) X1 X2 X3 Y1 Y2 -
      Y1 (-G^2 (G - R) (G + R) X1 X2 X3 + (G - M) (G + M) (R^2 X2 + G^2 X3) Y1 Y2) Y3);
```

Step16:

$$\sigma r11 = X1\left(C1s\,X2 - \frac{C2s\,X3}{R^2}\right);$$

$$\sigma t11 = X1\left(C1s\,X2 + \frac{C2s\,X3}{R^2}\right);$$

$$\sigma r12 = X1\left(C1ss\,X2 - \frac{C2ss\,X3}{R^2}\right);$$

$$\sigma t12 = X1\left(C1ss\,X2 + \frac{C2ss\,X3}{R^2}\right);$$

$$\sigma l12 = pi\,\frac{R^2}{G^2 - R^2};$$

Step17:

$$\sigma r1 = \sigma r11 + \sigma r12;$$

$$\sigma t1 = \sigma t11 + \sigma t12;$$

$$\sigma l1 = \sigma l12;$$

Step18:

$$\sigma 1min = \sqrt{\sigma r11^2 + \sigma t11^2 - \sigma r11\,\sigma t11};$$

$$\sigma 1max = \sqrt{\frac{(\sigma r1 - \sigma t1)^2 + (\sigma t1 - \sigma l1)^2 + (\sigma l1 - \sigma r1)^2}{2}};$$

$$\sigma 1mean = \frac{\sigma 1max - \sigma 1min}{2};$$

$$\sigma 1ampl = \frac{\sigma 1max + \sigma 1min}{2};$$

Step19:

$$FS1 = \frac{1}{\frac{\sigma 1mean}{Sut1} + \frac{\sigma 1ampl}{Se1}};$$

Step20:

$$\sigma r21 = Y1\left(C3s\,Y2 - \frac{C4s\,Y3}{G^2}\right);$$

$$\sigma t21 = Y1\left(C3s\,Y2 + \frac{C4s\,Y3}{G^2}\right);$$

$$\sigma r22 = Y1\left(C3ss\,Y2 - \frac{C4ss\,Y3}{G^2}\right);$$

$$\sigma t22 = Y1\left(C3ss\,Y2 + \frac{C4ss\,Y3}{G^2}\right);$$

$$\sigma l22 = pi\,\frac{R^2}{M^2 - G^2};$$

Step21:

```
σr2 = σr21 + σr22;
σt2 = σt21 + σt22;
σl2 = σl22;
```

Step22:

$$\sigma 2min = \sqrt{\sigma r21^2 + \sigma t21^2 - \sigma r21\,\sigma t21}\;;$$

$$\sigma 2max = \sqrt{\frac{(\sigma r2 - \sigma t2)^2 + (\sigma t2 - \sigma l2)^2 + (\sigma l2 - \sigma r2)^2}{2}}\;;$$

$$\sigma 2mean = \frac{\sigma 2max + \sigma 2min}{2};$$

$$\sigma 2ampl = \frac{\sigma 2max - \sigma 2min}{2};$$

Step23:

$$FS2 = \frac{1}{\frac{\sigma 2mean}{Sut2} + \frac{\sigma 2ampl}{Se2}};$$

Step24:

```
N[TableForm[{{"δ1=", δ1, "              ", "a=", a},
   {"δ2=", δ2, "              ", "b=", b}, {"δ3=", δ3, "              ", "c=", c},
   {"δ4=", δ4, "              ", "d=", d}, {"                          "},
   {"δT=", δT, "              ", "R=", R}, {"t1=", t1, "              ", "G=", G},
   {"t2=", t2, "              ", "M=", M}, {},
   {"p=", p, "              ", "pi=", pi}, {},
   {"σr11=", σr11, "              ", "σr12=", σr12},
   {"σr21=", σr21, "              ", "σr22=", σr22}, {},
   {"σt11=", σt11, "              ", "σt12=", σt12},
   {"σt21=", σt21, "              ", "σt22=", σt22}, {},
   {"σl12=", σl12, "              ", "σl22=", σl22}, {},
   {"σr1=", σr1, "              ", "σr2=", σr2},
   {"σt1=", σt1, "              ", "σt2=", σt2},
   {"σl1=", σl1, "              ", "σl2=", σl2}, {},
   {"σ1min=", σ1min, "              ", "σ1max=", σ1max},
   {"σ2min=", σ2min, "              ", "σ2max=", σ2max},
   {"FS1=", FS1, "              ", "FS2=", FS2}, {"Δtm=", Δtm}}]]
```

Step25:

```
ClearAll[δ1, δ2, δ3, δ4, a, b, c, d, R, G, M, p, pi, po, δT, t1, t2, X1, X2, X3,
 Y1, Y2, Y3, C1s, C2s, C3s, C4s, C1ss, C2ss, C3ss, C4ss, σr11, σr12, σr21, σr22,
 σt11, σt12, σt21, σt22, σl12, σl22, σr1, σr2, σt1, σt2, σl1, σl2, σ1min, σ1max,
 σ2min, σ2max, FS1, FS2]
```

APPENDIX C:

Steps of the program "SDRD" which is calculating the stress distributions along the radial direction and drawing graphics.

Step1:

```
Off[General::spelll]
```

Step2:

```
R = 0.02;
G = 0.037998931671400754;
M = 0.0781872935192976;
p = 3.33923 * 10^8;
```

Step3:

```
po = 0;
pi = 3000 * 10^5;
δT = 70 * 10^-6;
t1 = 18 * 10^-3;
t2 = 40 * 10^-3;
```

Step4:

```
μ1 = 0.292;
μ2 = 0.292;
E1 = 207 * 10^9;
E2 = 207 * 10^9;
Sut1 = 1720 * 10^6;
Sut2 = 1760 * 10^6;
```

Step5:

$$C1s = \frac{G^2\, p\, (-1+\mu 1)}{E1\, (G^2 - R^2)};$$

$$C2s = -\frac{G^2\, p\, R^2\, (1+\mu 1)}{E1\, (G^2 - R^2)};$$

$$C3s = \frac{G^2\, p\, (-1+\mu 2)}{E2\, (G^2 - M^2)};$$

$$C4s = -\frac{G^2\, M^2\, p\, (1+\mu 2)}{E2\, (G^2 - M^2)};$$

Step6:

$$C1ss = \frac{(-1+\mu 1)\left(E2\,(G-M)\,(G+M)\,pi\,R^2\,(1+\mu 1) + E1\left(G^2\left(2M^2\,po - pi\,R^2\,(-1+\mu 2)\right) + M^2\,pi\,R^2\,(1+\mu 2)\right)\right)}{\left(E1\left(E2\,(G-M)\,(G+M)\left(-G^2\,(-1+\mu 1) + R^2\,(1+\mu 1)\right) + E1\,(G-R)\,(G+R)\left(G^2\,(-1+\mu 2) - M^2\,(1+\mu 2)\right)\right)\right)};$$

$$C2ss = -\frac{G^2\, R^2\, (1+\mu 1)\left(E2\,(G-M)\,(G+M)\,pi\,(-1+\mu 1) + E1\left(G^2\,(pi - pi\,\mu 2) + M^2\,(pi + 2\,po + pi\,\mu 2)\right)\right)}{\left(E1\left(E2\,(G-M)\,(G+M)\left(-G^2\,(-1+\mu 1) + R^2\,(1+\mu 1)\right) + E1\,(G-R)\,(G+R)\left(G^2\,(-1+\mu 2) - M^2\,(1+\mu 2)\right)\right)\right)};$$

$$C3ss = \frac{(-1+\mu 2)\left(E2\left(G^2\left(2\,pi\,R^2 - M^2\,po\,(-1+\mu 1)\right) + M^2\,po\,R^2\,(1+\mu 1)\right) + E1\,M^2\,po\,(G-R)\,(G+R)\,(1+\mu 2)\right)}{\left(E2\left(E2\,(G-M)\,(G+M)\left(-G^2\,(-1+\mu 1) + R^2\,(1+\mu 1)\right) + E1\,(G-R)\,(G+R)\left(G^2\,(-1+\mu 2) - M^2\,(1+\mu 2)\right)\right)\right)};$$

$$C4ss = -\frac{G^2\, M^2\left(E2\left(G^2\,(po - po\,\mu 1) + R^2\,(2\,pi + po + po\,\mu 1)\right) + E1\,po\,(G-R)\,(G+R)\,(-1+\mu 2)\right)(1+\mu 2)\right)}{\left(E2\left(E2\,(G-M)\,(G+M)\left(-G^2\,(-1+\mu 1) + R^2\,(1+\mu 1)\right) + E1\,(G-R)\,(G+R)\left(G^2\,(-1+\mu 2) - M^2\,(1+\mu 2)\right)\right)\right)};$$

Step7:

$$\sigma r11 = \frac{E1}{1-\mu 1^2}\left(C1s\,(1+\mu 1) - C2s\,\frac{1-\mu 1}{r^2}\right);$$

$$\sigma r12 = \frac{E1}{1-\mu 1^2}\left(C1ss\,(1+\mu 1) - C2ss\,\frac{1-\mu 1}{r^2}\right);$$

$$\sigma r21 = \frac{E2}{1-\mu 2^2}\left(C3s\,(1+\mu 2) - C4s\,\frac{1-\mu 2}{r^2}\right);$$

$$\sigma r22 = \frac{E2}{1-\mu 2^2}\left(C3ss\,(1+\mu 2) - C4ss\,\frac{1-\mu 2}{r^2}\right);$$

$$\sigma t11 = \frac{E1}{1-\mu 1^2}\left(C1s\,(1+\mu 1) + C2s\,\frac{1-\mu 1}{r^2}\right);$$

$$\sigma t12 = \frac{E1}{1-\mu 1^2}\left(C1ss\,(1+\mu 1) + C2ss\,\frac{1-\mu 1}{r^2}\right);$$

$$\sigma t21 = \frac{E2}{1-\mu 2^2}\left(C3s\,(1+\mu 2) + C4s\,\frac{1-\mu 2}{r^2}\right);$$

$$\sigma t22 = \frac{E2}{1-\mu 2^2}\left(C3ss\,(1+\mu 2) + C4ss\,\frac{1-\mu 2}{r^2}\right);$$

$$\sigma l12 = pi\,\frac{R^2}{G^2-R^2};$$

$$\sigma l22 = pi\,\frac{R^2}{M^2-G^2};$$

Step8:

$$\sigma r1 = \sigma r11 + \sigma r12;$$

$$\sigma t1 = \sigma t11 + \sigma t12;$$

$$\sigma l1 = \sigma l12;$$

Step9:

$$\sigma r2 = \sigma r21 + \sigma r22;$$

$$\sigma t2 = \sigma t21 + \sigma t22;$$

$$\sigma l2 = \sigma l22;$$

Step10:

$$\sigma 1min = \sqrt{\sigma r11^2 + \sigma t11^2 - \sigma r11\,\sigma t11};$$

$$\sigma 1max = \sqrt{\frac{(\sigma r1-\sigma t1)^2 + (\sigma t1-\sigma l1)^2 + (\sigma l1-\sigma r1)^2}{2}};$$

Step11:

$$\sigma 2min = \sqrt{\sigma r21^2 + \sigma t21^2 - \sigma r21\,\sigma t21}\;;$$

$$\sigma 2max = \sqrt{\frac{(\sigma r2 - \sigma t2)^2 + (\sigma t2 - \sigma l2)^2 + (\sigma l2 - \sigma r2)^2}{2}}\;;$$

Step12:

$$\sigma 1mean = \frac{\sigma 1max - \sigma 1min}{2};$$

$$\sigma 1ampl = \frac{\sigma 1max + \sigma 1min}{2};$$

Step13:

$$\sigma 2mean = \frac{\sigma 2max + \sigma 2min}{2};$$

$$\sigma 2ampl = \frac{\sigma 2max - \sigma 2min}{2};$$

Step14:

```
gr1 = Plot[σr1 / 10^6, {r, R, G}, Frame -> True, GridLines → Automatic,
   PlotPoints → 1000, PlotLabel → "Radial Stress"];

gr2 = Plot[σr2 / 10^6, {r, G, M}, Frame -> True, GridLines → Automatic,
   PlotPoints → 1000, PlotLabel → "Radial Stress"];

gr3 = Plot[σt1 / 10^6, {r, R, G}, Frame -> True, GridLines → Automatic,
   PlotPoints → 1000, PlotLabel → "Tangential Stress"];

gr4 = Plot[σt2 / 10^6, {r, G, M}, Frame -> True, GridLines → Automatic,
   PlotPoints → 1000, PlotLabel → "Tangential Stress"];
```

Step15:

```
Show[gr1, gr2]
Show[gr3, gr4]
```

APPENDIX D:
The Tables

Table D1. The data of the relationship in between interface pressure "p" and the total interface displacement for t_1=25 mm, t_2=15 mm.

p(MPa)	δ_T (μm)	FS1	FS2
0	0	1,10603	7,00163
15,57318	10	1,12023	5,57812
31,15967	20	1,13312	4,61672
46,7595	30	1,14426	3,93364
62,3726	40	1,15312	3,42514
77,999	50	1,15911	3,03239
93,6388	60	1,16152	2,72011
109,292	70	1,15958	2,46594
124,958	80	1,15251	2,25509
140,638	90	1,13959	2,07737

Table D2. The data of the relationship in between the thickness of the inner cylinder t_1 and the safety factors of the both cylinders inside and outside for t_2=15 mm, and δ_T=60 μm.

t_1 (mm)	FS1	FS2
10	0,46067	1,06267
13	0,8114	1,44664
16	1,02732	1,78519
19	1,1168	2,10557
22	1,14999	2,41613
25	1,16152	2,72011
28	1,16435	3,01896
31	1,16344	3,31347
34	1,16087	3,60413
37	1,15757	3,89128
40	1,15397	4,17522

Table D3. The data of the relationship in between the operating pressure p_i and the safety factors of the both cylinders inside and outside for t_1=25 mm, t_2=15 mm, and δ_T=60 μm.

p_i (Bar)	p_i (MPa)	FS1	FS2
2000	200	1,70962	3,11662
2100	210	1,63712	3,07189
2200	220	1,5691	3,02841
2300	230	1,50545	2,98614
2400	240	1,44594	2,94502
2500	250	1,39033	2,90501
2600	260	1,33835	2,86606
2700	270	1,28973	2,82814
2800	280	1,24421	2,79119
2900	290	1,20155	2,7552
3000	300	1,16152	2,72011
3100	310	1,12391	2,6859
3200	320	1,08852	2,65253
3300	330	1,05519	2,61998
3400	340	1,02374	2,58821
3500	350	0,994041	2,55719
3600	360	0,965949	2,5269
3700	370	0,939347	2,49732
3800	380	0,914123	2,46842
3900	390	0,890179	2,44017
4000	400	0,867424	2,41256

Table D4. The data of the relationship in between the miscellaneous endurance limit modifying factor "k_f" and the safety factors of the both cylinders inside and outside for t_1=25 mm, t_2=15 mm, and δ_T=60 μm.

k_f	FS1	FS2
0,24	0,414613	1,70117
0,3	0,515501	1,92007
0,36	0,615318	2,10024
0,42	0,714081	2,25112
0,48	0,811807	2,37932
0,54	0,908512	2,48959
0,6	1,00421	2,58545
0,66	1,09892	2,66955
0,72	1,19266	2,74393
0,78	1,28544	2,81018
0,84	1,37727	2,86957
0,9	1,46817	2,92311

Table D3. The data of the relationship in between the operating pressure p_i and the safety factors of the both cylinders inside and outside for t_1=18 mm, t_2=40 mm, R=20 mm, and δ_T=70 μm.

p_i (Bar)	p_i (MPa)	FS1	FS2
1000	100	0,462596	1,91525
1200	120	0,471003	1,85907
1400	140	0,479323	1,80607
1600	160	0,487488	1,75599
1800	180	0,495424	1,70859
2000	200	0,503045	1,66366
2200	220	0,510257	1,62101
2400	240	0,516961	1,58048
2600	260	0,52305	1,54192
2800	280	0,52842	1,50517
3000	300	0,532968	1,47013
3200	320	0,536599	1,43667
3400	340	0,539234	1,40469
3600	360	0,540811	1,37409
3800	380	0,541294	1,34478
4000	400	0,540671	1,31669

REFERENCES

DIETER, G.E., 2000, “Engineering Design”, 3rd Edition, McGraw-Hill, Singapore.

MANNING, W.R.D. LABROW, S., 1971. “High Pressure Engineering”, Leonard Hill, London

SHIGLEY, J.E., 1986, ”Mechanical Engineering Design”, McGraw-Hill, Singapore

SUMMERS, D.A., 1995, “Waterjetting technology”, Chapman & Hall.

BEER, F.B., AND JOHNSTON, R.E., 1992, “Mechanics of Materials”, McGraw-Hill.

ÇENGEL, Y.A., BOLES, M.A., 1990, “Thermodynamics: an Engineering Approach”, McGraw-Hill.

GEREN, N., BAYRAMOĞLU, M., TUNÇ, T., 2004, “Simplified Design and Manufacturing of High Pressure Components for a Low Cost Water Jet Intensifier Using Redesign Methodology”, University of Cukurova, Turkey.

GEREN, N., BAYRAMOĞLU, M., EŞME, U., 2007, “Improvement of a Low Cost Water-Jet Machining Intensifier Using Reverse Engineering and Redesign Methodology”, University of Cukurova.

DEAM, R.T., LEMMA, E., AHMED, D.H., 2004, “Modeling of the Abrasive Water Jet Cutting Process”, Swinburne University of Technology, Melbourne, Australia.

MOMBER, A.W., KOVACEVIC, R., KWAK, H., 1995, “Alternative Method for the Evaluation of the Abrasive Water-jet Cutting of Grey Cast Iron”, University of Kentucky.

LİU, H., WANG, J., KELSON, N., BROWN, R.J., 2004, “A Study of Abrasive Water-jet Characteristics by CFD Simulation”, Queensland University of Technology.

CHEN, L., SIORES, E., WONG, W.C.K., 1996, “Optimizing Abrasive Water jet Cutting of Ceramic Materials”, Swinburne University of Technology, Melbourne, Australia.

LEMMA, E., DEAM, R., CHEN, L., 2004, “Maximum Depth of Cut and Mechanics of Erosion in AWJ Oscillation Cutting of Ductile Materials”, 2004, Swinburne University of Technology, Melbourne, Australia.

HOOGSTRATE, A.M., SUSUZLU, T., KARPUCHEVSKI, B., 2006, “High Performance Cutting with Abrasive Waterjets Beyond 400MPa”, Delft University of Technology, Netherlands, University of Magdeburg, Germany.

MIN JOU, 1999, “Analysis of the Stability of Water-Jet Cutting with Linear Theory”, National Lien-Ho Institute of Technology, Taiwan.

FLOWCORP, http://www.flowcorp.com/waterjet-applications.cfm?id=91

HARVEY, J. F., 1974, Theory and Design of Modern High Pressure Vessels, Van Nostrant, Princeton.

MARGHITU, D., 2005, Kinematic Chains and Machine Components Design, Auburn University, Department of Mechanical Engineering, Alabama, USA.

HATTORI, T., WATANABE, T., “Fretting fatigue strength estimation considering the fretting wear process”, 2006, Gifu University, Japan, Hitachi Ltd., Japan.

CADARIO, A., ALFREDSSON, B., “Influence of residual stresses from shot peening on fretting fatigue crack growth”, 2007, Royal Institute of Technology (KTH), SE-100 44 Stockholm, Sweden.

HANSSON, T and CLEVFORS, O (2001), “Fretting fatigue tests at room temperature and 200^{o}C”, Volvo Aero Corporation.

HILL, R, “The mathematical theory of plasticity”, 1950, Oxford University Press, New York.

BROWN, J., “Advanced machining technology handbook”, 1998, Mc Graw Hill press.

CADAVID, R, WÜSTENBERG, D, 2002, “Enhancing the coherent length of cutting water-jets”, Proc of 16th Int Conf Water Jetting. Aix en Provence, France.

CADAVID, R, WÜSTENBERG, D., LOUIS, H., PUDE, F., SENNE, T., 2005, “Effect of helium atmospheres on abrasive suspension water-jets”, Advanced Manufacturing Tecnologies.

CURRICULUM VITAE

The author was born in Seyhan/ADANA in 1982. He graduated from the Mechanical Engineering Department of University of Çukurova in ADANA.He registered to have education of English at foreign languages learning center YADIM in 2000. He graduated from the Mechanical Engineering department which gives the education in English in 2004 and started to his MSc education at same year.